

B. TECH. PROJECT REPORT

On

Effect of process parameters of grit blasting on low carbon steel substrates in different environments

BY
Prathamesh Tawade (180005019)
&
Suyog Shembale (180003057)



DISCIPLINE OF MECHANICAL ENGINEERING
INDIAN INSTITUTE OF TECHNOLOGY INDORE
May 2022

Effect of process parameters of grit blasting on low carbon steel substrates in different environments

A PROJECT REPORT

*Submitted in partial fulfillment of the
requirements for the award of the degrees*

of
BACHELOR OF TECHNOLOGY
in

MECHANICAL ENGINEERING

Submitted by:
Prathamesh Tawade (180005019)
&
Suyog Shembale (180003057)

Guided by:
Dr. Kazi Sabiruddin



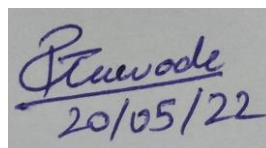
INDIAN INSTITUTE OF TECHNOLOGY INDORE

May 2022

CANDIDATE’S DECLARATION

We hereby declare that the project entitled “**Effect of process parameters of grit blasting on low carbon steel substrates in different environments**” submitted in partial fulfillment for the award of the degree of Bachelor of Technology in ‘Mechanical Engineering’ completed under the supervision of **Dr. Kazi Sabiruddin**, Associate Professor, Department of Mechanical Engineering, IIT Indore is an authentic work.

Further, I/we declare that I/we have not submitted this work for the award of any other degree elsewhere.



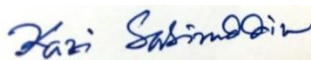

Prathamesh Tawade
(180005019)

Suyog Shembale
(180003057)

Signature and name of the student(s) with date

CERTIFICATE by BTP Guide(s)

It is certified that the above statement made by the students is correct to the best of my/our knowledge.



20/05/2022

Dr. Kazi Sabiruddin (Associate Professor, ME)

Signature of BTP Guide(s) with dates and their designation

Preface

This report on “Effect of process parameters of grit blasting on low carbon steel substrates in different environments” is prepared under the guidance of Dr. Kazi Sabiruddin.

The research work presented in this thesis aims to study the effects of grit blasting on the surface & sub-surface characteristics of mild steel substrates under dry & wet environments. Characterization of grit blasted samples was carried out using contact & non-contact type profilometry, Vickers micro-indentation hardness testing, X-Ray Diffraction (XRD), Field Emission Scanning Electron Microscopy (FESEM) and Energy Dispersive Spectroscopy (EDS).

Prathamesh Tawade & Suyog Shembale

B. Tech. IV Year

Discipline of Mechanical Engineering

IIT Indore

Acknowledgements

We wish to convey our gratitude to our supervisor, Dr. Kazi Sabiruddin, Associate Professor, Discipline of Mechanical Engineering, Indian Institute of Technology Indore, for the continuous guidance and encouragement that he provided us with throughout this research work. We feel ourselves fortunate to have had the opportunity to pursue our BTP under a supervisor who genuinely cared for our work & responded to our queries & concerns so promptly.

We also wish to express our gratitude to Dr. Satyajit Chatterjee, Faculty Incharge, Metallography & Tribology Lab for providing us the opportunity to pursue our research work using the facilities of the aforementioned lab.

We are sincerely grateful to Prof. Santosh K. Sahu, Head of Department, Mechanical Engineering for funding our research work.

We are thankful to Dr. Anand Petare, Assistant Workshop Superintendent, Central Workshop for allowing the use of workshop facilities for our research work. We are particularly grateful to Mr. Umakant Sharma & Mr. Rishiraj Chouhan, machine operators at Central Workshop, for their extended support in the fabrication work related to our research.

We are thankful to Mr. Mayur Dhake, Junior Superintendent, MEMS, IIT Indore for providing us the access to X-Ray Diffraction (XRD), Field Emission Scanning Electron Microscope (FESEM) & Energy Dispersive Spectroscopy (EDS) facilities of the MEMS department. We are also thankful to Mr. Sandeep Patil, Deputy Manager, Solid Mechanics Lab for allowing the use of Vickers microindentation testing facility of the Solid Mechanics Lab for our research work. We also thank Mr. Santosh Sharma, Deputy Manager, Advanced Machining Processes (AMP) Lab, Centre for Excellence in Gear Engineering (CEGE) for allowing the use of optical surface profiling facilities available in AMP Lab for our research work.

We are indebted to Mr. Shahid Hussain, Mr. Avinandan Khaira & Mr. Vaibhav Nemane, Ph.D. research scholars in the Department of Mechanical Engineering (ME), associated with the Metallography & Tribology Lab, for their consistent support during our research work. We are also grateful to Mr. Sandeep Gour, Deputy Manager, Metallography & Tribology Lab, for addressing other lab related concerns.

Abstract

The adhesion of thermally sprayed coatings to their substrates is crucial to the performance of the coatings. Surface roughness and cleanliness are the most important parameters affecting the adhesion strength of the coatings. Grit blasting is commonly used for surface preparation prior to subsequent coating processes. This study aims to analyse the effect of grit blasting on the surface and sub-surface characteristics of mild steel substrates under dry and wet environments. Three types of wet environments were simulated - water, saline water, alcohol. The variation of surface roughness with grit size, standoff distance (SOD) and time was analysed under dry and wet environments. The nature of variation of roughness with the process parameters is observed to be similar under both dry and wet environments. A mathematical model was developed to estimate the increment in contact area for each surface condition. The optimal set of process parameter levels corresponding to the maximum contact area were determined for each environment. Vickers micro-indentation hardness testing was performed on the cross section of grit blasted samples at various depths. The maximum hardness obtained near the grit blasted surface indicates the highest work hardening effect at the sub-surface zone. The influence of grit blasting on substrate hardening is found to decline with depth. Higher the work hardening occurring at the surface, higher is the estimated depth of the affected layer. Work hardening due to grit blasting is observed to be higher under dry conditions vis-à-vis wet conditions. X-Ray Diffraction (XRD) analysis was carried out over as-received grit blasted surfaces to identify the phases formed on the surface under different environments. Ferrite i.e. α -Fe (mostly observed in bulk steel material) is the dominant phase detected over grit blasted surfaces under both dry and wet environments. Significant surface contamination has been observed to take place in saline water environment. Occurrence of Al_2O_3 peaks in the diffraction patterns of surfaces grit blasted under all four environments suggests entrapment of alumina grit residues within the surface. On the basis of the relative intensity of Al_2O_3 peaks occurring in the diffraction patterns of the substrates, it has been argued that the proportion of grit residues entrapped over the grit blasted surface is the lowest when grit blasting is carried out in the alcoholic environment, suggesting some cleaning action of volatile environments. Sub-surface microstructure of grit blasted samples was evaluated using optical microscopy, Field Emission Scanning Electron Microscopy (FESEM) and Energy Dispersive Spectroscopy (EDS) techniques. Sub-surface cracks are noticed to be substantial for samples grit blasted under dry conditions; sub-surface damage is appreciably lower for samples grit blasted under wet environments. SEM micrographs reveal significant grain elongation in the vicinity of the grit blasted surfaces; deformation effects of grit blasting fade out as one moves away from the grit blasted surfaces. EDS results are consistent with the XRD results i.e. the elements corresponding to the phases detected by XRD were detected by EDS as well.

This research work attempts to determine the suitable combination of process parameter levels for performing grit blasting over low carbon steel substrates in different environments. Additionally, it also attempts to help understand the effect of those process parameters on the surface and sub-surface characteristics of the substrates.

Table of Contents

| | |
|---|------------|
| Candidate's declaration & supervisor's certificate | iii |
| Preface | v |
| Acknowledgements | vii |
| Abstract | ix |
| 1 Introduction | 1 |
| 1.1 Surface preparation processes | 1 |
| 1.1.1 Chemical cleaning | 1 |
| 1.1.2 Mechanical cleaning | 2 |
| • Abrasive blasting | 2 |
| • Tumbling/barrel finishing | 2 |
| • Vibratory finishing | 3 |
| • Other mass finishing processes | 3 |
| 1.2 Abrasive blasting | 4 |
| 1.2.1 Shot peening | 4 |
| 1.2.2 Grit/sand blasting | 4 |
| • Dry blasting | 5 |
| • Wet blasting | 5 |
| 1.3 Equipment for dry blasting | 5 |
| 1.3.1 Airless centrifugal blast wheel | 5 |
| 1.3.2 Direct pressure blast nozzle system | 6 |
| 1.3.3 Indirect suction blast nozzle system | 7 |
| 1.4 Surface topography | 9 |
| 1.4.1 Surface roughness | 9 |
| 2 Literature review & research gap | 11 |
| 2.1 Literature review | 11 |
| 2.2 Research gap | 16 |
| 2.3 Objectives | 16 |

| | | |
|----------|---|-----------|
| 3 | Materials and methods | 17 |
| 3.1 | Experimental setup | 17 |
| 3.1.1 | Grit blasting equipment | 17 |
| | • Reciprocating air compressor | 17 |
| | • Suction blasting machine and dust collector subsystem | 19 |
| 3.1.2 | Setup for holding the substrate and adjusting the standoff distance . | 20 |
| 3.2 | Substrate preparation | 21 |
| 3.3 | Design of experiments | 22 |
| 3.4 | Characterization of grit blasted surface | 24 |
| 3.4.1 | Evaluation of substrate surface profile | 24 |
| | • Estimation of increment in contact area due to roughening | 25 |
| 3.4.2 | Microhardness evaluation | 25 |
| 3.4.3 | X-Ray Diffraction (XRD) analysis | 26 |
| 3.4.4 | Sub-surface microstructure study using optical microscopy, FESEM & EDS | 26 |
| 4 | Results and discussions | 27 |
| 4.1 | Analysis of experimental results for each environment | 27 |
| 4.1.1 | Dry | 27 |
| | • Profilometric data | 27 |
| | • Variation of mean response with process parameters | 29 |
| | • Analysis of variance (ANOVA) | 32 |
| | • Variation of peak density with roughness | 32 |
| | • Estimation of increment in contact area due to roughening | 33 |
| | • Optimal set of process parameter levels | 36 |
| | • Microhardness evaluation | 38 |
| | • X-Ray Diffraction (XRD) analysis | 40 |
| | • Sub-surface microstructure study using optical microscopy & FE- SEM | 41 |
| 4.1.2 | Water | 43 |
| | • Variation of mean response with process parameters | 44 |
| | • Variation of peak density with roughness | 46 |
| | • Estimation of increment in contact area due to roughening | 47 |
| | • Optimal set of process parameter levels | 47 |
| | • Microhardness evaluation | 48 |
| | • X-Ray Diffraction (XRD) analysis | 51 |
| | • Sub-surface microstructure study using optical microscopy, FE- SEM & EDS | 52 |

| | | |
|----------|---|-----------|
| 4.1.3 | Saline water | 54 |
| | • Estimation of increment in contact area due to roughening | 55 |
| | • Optimal set of process parameter levels | 55 |
| | • Microhardness evaluation | 56 |
| | • X-Ray Diffraction (XRD) analysis | 58 |
| | • Sub-surface microstructure study using optical microscopy, FE-SEM & EDS | 59 |
| 4.1.4 | Alcohol | 61 |
| | • Estimation of increment in contact area due to roughening | 62 |
| | • Optimal set of process parameter levels | 63 |
| | • Microhardness evaluation | 65 |
| | • X-Ray Diffraction (XRD) analysis | 68 |
| | • Sub-surface microstructure study using optical microscopy, FE-SEM & EDS | 70 |
| 5 | Conclusions & future scope | 73 |
| 5.1 | Conclusions | 73 |
| 5.1.1 | Variation of mean response with process parameters under dry & wet conditions | 73 |
| 5.1.2 | Relationship between Ra & RPc | 74 |
| 5.1.3 | Optimal set of process parameter levels under each environment | 74 |
| 5.1.4 | Hardness analysis | 75 |
| 5.1.5 | XRD analysis | 75 |
| 5.1.6 | Evaluation of sub-surface microstructure | 76 |
| 5.2 | Future scope | 77 |
| | References | 79 |

List of Figures

| | | |
|------|---|----|
| 1.1 | Tumbling (or Barrel Finishing) | 3 |
| 1.2 | Airless Centrifugal Blast Wheel System - Components & Flow of Abrasive Media across them | 6 |
| 1.3 | Airless Centrifugal Blast Wheel System - Tent Blast Pattern | 6 |
| 1.4 | Portable Direct Pressure Blast Cleaning Machine | 7 |
| 1.5 | Suction Blast Equipment | 8 |
| 1.6 | Descriptive figure showing roughness, waviness, flaws & lay | 9 |
| 3.1 | Reciprocating air compressor | 18 |
| 3.2 | Suction blasting machine and dust collector subsystem | 20 |
| 3.3 | Substrate holding setup | 21 |
| 3.4 | Relationship between grit sizes in mesh & micrometre in BSS standards . . | 22 |
| 4.1 | Arithmetic average roughness | 27 |
| 4.2 | Profilometric surface evaluation | 28 |
| 4.3 | Sample parameter table | 29 |
| 4.4 | Variation of mean response with process parameters under dry conditions . | 30 |
| 4.5 | Variation of peak density (RPc) with Ra under dry conditions | 32 |
| 4.6 | Approximation of a roughened surface | 33 |
| 4.7 | Details of approximating model | 34 |
| 4.8 | Flat contact in between the peaks | 35 |
| 4.9 | Variation of ICA with Ra and RPc | 36 |
| 4.10 | Scatter plot showing the variation of ICA with Ra and RPc for dry blasting trials | 37 |
| 4.11 | 3D surface profile of sample 111D | 38 |
| 4.12 | Vickers indentations on the cross-section of 122D at depths of 40, 100, 150 & 200 μm from the grit blasted surface | 40 |
| 4.13 | Variation of cross-section Vickers hardness with depth from the grit blasted surface for sample 122D | 40 |
| 4.14 | XRD pattern for 133D | 41 |
| 4.15 | Surface & sub-surface regions of sample 111D showing indentation and extrusion | 41 |

| | | |
|------|---|----|
| 4.16 | Sub-surface cracks near the grit-blasted surface of sample 111D | 42 |
| 4.17 | SEM micrograph of a sub-surface region of sample 111D showing sub-surface cracks | 42 |
| 4.18 | Comparison of results obtained for each trial under dry and wet (water) conditions in terms of Ra | 43 |
| 4.19 | Variation of mean response with process parameters under wet conditions (water) | 45 |
| 4.20 | Comparison of variation of mean response with process parameters under dry and wet (water) conditions | 45 |
| 4.21 | Variation of peak density (RPc) with Ra under wet (water) conditions . . . | 47 |
| 4.22 | Comparison of variation of peak density (RPc) with Ra under dry & wet (water) conditions | 47 |
| 4.23 | Scatter plot showing the variation of ICA with Ra and RPc for experiments performed under wet (water) conditions | 49 |
| 4.24 | 3D surface profile of sample 122W | 49 |
| 4.25 | Vickers indentations on the cross-section of 122W at depths of 40, 100, 150 & 200 μm from the grit blasted surface | 50 |
| 4.26 | Variation of cross-section Vickers hardness with depth from the grit blasted surface for sample 122W | 50 |
| 4.27 | Comparison of the variation of microhardness with depth for samples 122D & 122W | 51 |
| 4.28 | XRD pattern for 133W | 51 |
| 4.29 | Sub-surface cracks near the grit-blasted surface of sample 122W | 52 |
| 4.30 | SEM micrographs of sub-surface regions of sample 122W | 52 |
| 4.31 | EDS layered images of sub-surface regions of sample 122W & their corresponding spectra | 53 |
| 4.32 | Comparison of results obtained for each 16 mesh trial performed in dry, water & saline water environments in terms of Ra | 54 |
| 4.33 | Scatter plot showing the variation of ICA with Ra and RPc for 16 mesh experiments performed in a saline water environment | 56 |
| 4.34 | 3D surface profile of sample 133S | 56 |
| 4.35 | Vickers indentations on the cross-section of 122S at depths of 40, 100, 150 & 200 μm from the grit blasted surface | 57 |
| 4.36 | Variation of cross-section Vickers hardness with depth from the grit blasted surface for sample 122S | 57 |
| 4.37 | Comparison of the variation of microhardness with depth for samples 122D, 122W & 122S | 58 |
| 4.38 | XRD pattern for 133S | 58 |

| | | |
|------|---|----|
| 4.39 | Sub-surface cracks near the grit-blasted surface of sample 133S | 59 |
| 4.40 | SEM micrographs of a sub-surface region of sample 133S | 60 |
| 4.41 | EDS layered image of a sub-surface region of sample 133S & its corresponding spectrum | 61 |
| 4.42 | Comparison of results obtained for each 16 mesh trial performed in dry, water, saline water & alcohol environments in terms of Ra | 62 |
| 4.43 | Scatter plot showing the variation of ICA with Ra and RPc for 16 mesh experiments performed in an alcoholic | 63 |
| 4.44 | 3D surface profile of sample 122A | 64 |
| 4.45 | 3D surface profiles of samples 111D, 122W, 133S & 122A | 65 |
| 4.46 | Vickers indentations on the cross-section of 122A at depths of 40, 100, 150 & 200 μm from the grit blasted surface | 66 |
| 4.47 | Variation of cross-section Vickers hardness with depth from the grit blasted surface for sample 122A | 66 |
| 4.48 | Comparison of the variation of microhardness with depth for samples 122D, 122W, 122S & 122A | 66 |
| 4.49 | Relationship between average cross-section hardness near a grit blasted surface & corresponding depth of the affected layer | 68 |
| 4.50 | Correlation between work hardening and roughness induced by grit blasting | 68 |
| 4.51 | XRD pattern for 133S | 69 |
| 4.52 | Comparison of the XRD patterns of samples 133D, 133W, 133S & 133A . . | 70 |
| 4.53 | Sub-surface cracks near the grit-blasted surface of sample 122A | 70 |
| 4.54 | SEM micrographs of a sub-surface region of sample 122A | 71 |
| 4.55 | EDS layered image of a sub-surface region of sample 122A & its corresponding spectrum | 72 |

List of Tables

| | | |
|------|--|----|
| 3.1 | Specifications for reciprocating air compressor | 17 |
| 3.2 | Specifications for suction blasting machine | 19 |
| 3.3 | Substrate composition | 21 |
| 3.4 | Levels of process parameters | 22 |
| 3.5 | Approximate conversion of selected mesh sizes in micrometre & millimetre | 22 |
| 3.6 | Approximate densities of the liquid media used for simulating wet environ- ments during grit blasting | 23 |
| 3.7 | Alpha-numerical coding for process parameter levels (1) | 24 |
| 3.8 | Alpha-numerical coding for process parameter levels (2) | 24 |
| 3.9 | Design of experiments for a particular medium | 24 |
| 4.1 | Profilometric data for dry blasting | 28 |
| 4.2 | Final profilometric results for dry blasting | 29 |
| 4.3 | Variation of mean response with grit size (dry) | 30 |
| 4.4 | Variation of mean response with SOD (dry) | 30 |
| 4.5 | Variation of mean response with time (dry) | 30 |
| 4.6 | ANOVA analysis of the Ra data for dry blasting trials | 32 |
| 4.7 | Increment in contact area for each dry blasting trial | 36 |
| 4.8 | Optimal set of process parameters (dry) | 37 |
| 4.9 | Microhardness data for 122D | 39 |
| 4.10 | Variation of Vickers hardness with depth from grit blasted surface for 122D | 39 |
| 4.11 | Final profilometric results for grit blasting carried out in a wet environment of water | 43 |
| 4.12 | Variation of mean response with grit size (water) | 44 |
| 4.13 | Variation of mean response with SOD (water) | 44 |
| 4.14 | Variation of mean response with time (water) | 44 |
| 4.15 | Increment in contact area for each grit blasting trial carried out in a wet en- vironment of water | 48 |
| 4.16 | Optimal set of process parameters (water) | 48 |
| 4.17 | Variation of Vickers hardness with depth from grit blasted surface for 122W | 49 |
| 4.18 | Final profilometric results for 16 mesh trials carried out in a wet environment of saline water | 54 |

| | | |
|------|--|----|
| 4.19 | Increment in contact area for 16 mesh trials carried out in a wet environment of saline water | 55 |
| 4.20 | Optimal set of process parameters (saline water) | 55 |
| 4.21 | Variation of Vickers hardness with depth from grit blasted surface for 122S | 57 |
| 4.22 | Final profilometric results for 16 mesh trials carried out in a wet environment of alcohol | 61 |
| 4.23 | Increment in contact area for 16 mesh trials carried out in a wet environment of alcohol | 62 |
| 4.24 | Optimal set of process parameters (alcohol) | 63 |
| 4.25 | Optimal set of process parameter levels and corresponding Ra & ICA values under each environment | 64 |
| 4.26 | Variation of Vickers hardness with depth from grit blasted surface for 122A | 65 |
| 4.27 | Correlation between hardness and roughness | 67 |
| 5.1 | Optimal set of process parameter levels and corresponding Ra & ICA values under each environment | 74 |

Chapter 1

Introduction

Coating processes involve applying a layer of material to the surface of a component. While being deposited on the surface, the coating material is either in liquid or organic gas form. Coatings can serve several intended functions. The primary reasons for applying coatings include corrosion resistance, wear resistance & aesthetics; coatings may also be applied to alter the surface electrical properties of the substrates. (Groover 2010)

In all cases, proper adhesion between the coating and the substrate is crucial to the performance of the coatings. The most important parameters affecting adhesion are surface cleanliness and roughness. The surfaces of the substrates must be cleaned from unwanted contaminants that may hamper proper adhesion. In addition to cleanliness, the surfaces must be processed to possess an appropriate level of surface roughness. In addition to creating opportunities for mechanical interlocking, this roughening also enhances the contact area between the substrate and the coating. (Varacalle et al. 2006)

Thus, the substrates to be coated must undergo appropriate surface preparation before coating.

1.1 Surface preparation processes

Surface preparation processes can be broadly classified into the following two categories:

- Chemical cleaning
- Mechanical cleaning

1.1.1 Chemical cleaning

Chemical cleaning processes use chemicals to remove surface contaminants from the substrate. These unwanted surface contaminants may include oils, dirt, scales or oxide layers, and any other foreign particle. Preparing the surface for further operations like coating, spraying and plating, eliminating contaminants that could react chemically to the surface, improving product appearance & performance are some of the main reasons for subjecting

fabricated parts to chemical cleaning. There are a wide variety of chemical cleaning processes. Selection of a particular cleaning process for achieving the desired purpose depends on a number of factors like the contaminants to be removed, degree of cleanliness required, substrate morphology, environmental and production factors. (Groover 2010)

The major concern with the chemical cleaning processes is that they often use hazardous, toxic, or environmentally harmful chemicals and it is difficult to dispose these chemicals safely. Examples include chlorofluorocarbons (CFCs) and carbon tetra-chloride (CCl_4), which are responsible for ozone depletion and are now eliminated from commercial use. (Black & Kohser 2008)

1.1.2 Mechanical cleaning

Mechanical cleaning is a category of processes used to remove surface contaminants from the workpiece by the mechanical action of abrasives. Surface contaminants that are mainly targeted by mechanical cleaning include sand from the mold that may stick to the surface during the casting process, metallic oxides or scales that may be produced as a result of heating at high temperatures and rust which can be produced as a result of storage between the processes. From the point of view of their impact on the environment, the main concern associated with mechanical cleaning processes is the exposure to abrasive dust and other airborne particles, which enter the atmosphere during these processes. (Black & Kohser 2008)

Though the primary purpose of mechanical cleaning is the removal of surface contaminants, it can also be used to roughen surfaces in order to prepare them for subsequent processes like coating. On the other hand, it can also be used to uniformly finish workpiece surfaces. Removing flash, burrs, weld spatter etc. are some of the other uses. (Groover 2010)

A broad classification of mechanical cleaning processes is as follows:

- **Abrasive blasting**

The term ‘abrasive blasting’ encompasses a category of mechanical cleaning and roughening processes in which the substrate surfaces are prepared for subsequent processing by blasting them with abrasive particles moving with high velocities. More details about abrasive blasting will occur in later sections.

- **Tumbling/barrel finishing**

Tumbling or barrel finishing is a mass finishing process used to finish large number of small parts. It can be used to deburr, radius, descale, remove rust, polish, brighten, surface-harden,

or prepare parts for further finishing. In barrel finishing or tumbling, the parts are loaded (with or without any abrasive media) into a horizontally oriented barrel of hexagonal or octagonal cross-section until a predetermined level is reached. Rotation of the barrel causes the material to rise until gravity causes the uppermost layer to slide downward in a “landslide” movement as shown in Fig. 1.1. The sliding motion of parts (&/or contact with abrasive media, if any) produces a rubbing & cutting action that effectively removes burr, scales, rust, etc. (Black & Kohser 2008)

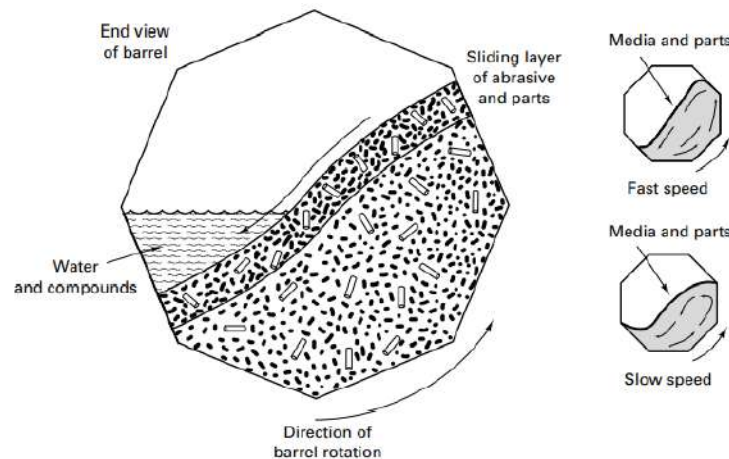


FIGURE 1.1: Tumbling or barrel finishing (adapted from Black & Kohser (2008))

• Vibratory finishing

In late 1950s, vibratory finishing was introduced as an alternative to the tumbling process. Nowadays, it is widely used for removing burrs, scales and also for cleaning, brightening, fine finishing and radiusing. Vibratory finishing is carried out in an open container. The container loaded with work-pieces and media is vibrated at a frequency between 900 and 3600 cycles per minute. Since the entire load is subjected to constant agitation, the cycle times are shorter than that for barrel finishing or tumbling. The process is less noisy, can be easily automated and monitored. (Black & Kohser 2008)

• Other mass finishing processes

Centrifugal disc finishing, spindle finishing and drag finishing are some of the other mass finishing processes.

1.2 Abrasive blasting

Abrasive blasting consists of accelerating the abrasive particulate media to a high velocity and propelling it against the work surface using air, water or a mechanical device. The impact of particulate media on the work surface is responsible for the cleaning and finishing action. The blast cleaning action is mainly performed by the kinetic energy of the abrasive particles.

There are two prominent types of abrasive blasting processes:

- Shot peening
- Grit/sand blasting

1.2.1 Shot peening

In shot peening, small spherical steel pellets called shots are propelled towards the substrate surface to induce compressive residual stresses into the surface layers. These stresses enhance the fatigue strength at the surface by delaying the initiation and propagation of surface cracks. Control over the process parameters is especially important in shot peening to prevent severe surface deformation. Although the primary purpose of shot peening is an improvement in surface fatigue strength, surface cleaning also takes place as a by-product of the process. (Groover (2010); Kalpakjian & Schmid (2010))

1.2.2 Grit/sand blasting

In grit blasting (more broadly, blast cleaning), a high-velocity stream of angular shaped metallic or ceramic grits (or even softer media like plastic beads, crushed nut shells, dry ice) is directed towards the substrate surface with the intention of cleaning and/or roughening to prepare it for subsequent coating processes. The media is propelled towards the surface using pressurized air (dry) or water (wet), or even using a wheel (i.e. utilizing the centrifugal forces of the wheel to propel the media). The primary functions of grit blasting are surface cleaning and roughening (some residual stresses might be induced in the surface layers as a by-product). The blasting productivity in terms of the level of cleanliness & roughness induced depends on several process parameters like abrasive media, grit size, blasting pressure, blasting time, standoff distance & angle of impingement among others. In wet blasting, the composition of the carrier fluid used for propelling the media is also a process parameter. Any further modifications in the process will again increase the number of process parameters to be considered. To achieve the desired surface conditions (&/or cleanliness), it is necessary to select the parameter levels optimally which necessitates prior knowledge regarding how surface topography (&/or cleanliness) is/are affected by each parameter. (Chander et al. 2009)

Grit blasting can be carried out dry (dry blasting) or wet (wet blasting), as discussed below.

- **Dry blasting**

In dry blasting, the abrasive media is accelerated towards the substrate surface using pressurized air. Additionally, it can also be propelled using a blast wheel (this is also known as airless blasting; even then, technically, it would come under dry blasting).

- **Wet blasting**

In wet blasting, the abrasive media is suspended in chemically treated water. The resulting slurry is pumped and continuously agitated (to prevent settling) before being forced towards the substrate surface through one or more nozzles, using pressurized air. The abrasive particles used in wet blasting are usually finer than those used in dry blasting. (ASM International Handbook Committee 1994)

1.3 Equipment for dry blasting

Depending on the substrate size and shape, the equipment used for dry blasting can be classified as cabinet-type machines, continuous-flow machines, blasting tumbling machines, and portable equipment. Three prominent technologies can be employed in these machines to propel the abrasive media towards the substrate surface. These include:

1.3.1 Airless centrifugal blast wheel

Airless centrifugal blast wheels are widely used for propelling abrasive media in dry grit blasting. These blast wheel systems require far less power than the air blast systems to throw equal volumes of abrasive at the same velocity. Friction between the abrasives and the components of the system, along with the interference among those components during operation represent the principal sources of power loss in these systems. Some of these components are shown in the Fig. 1.2.

A controlled flow of abrasive flows into a rotating vaned impeller from an abrasive feed spout. The abrasive is fed to the abrasive feed spout by gravity (through a valve not shown). The impeller has the same number of vanes as the number of wheel blades. The impeller is enclosed by a stationary cylinder (also known as a control cage or impeller case). The control cage is equipped with an opening that can be rotated or locked in a preferred position. While the abrasive is forced out of this opening by the impeller, each blade of the wheel takes up a metered quantity of abrasive at the inner end of the blade, which is then accelerated as it

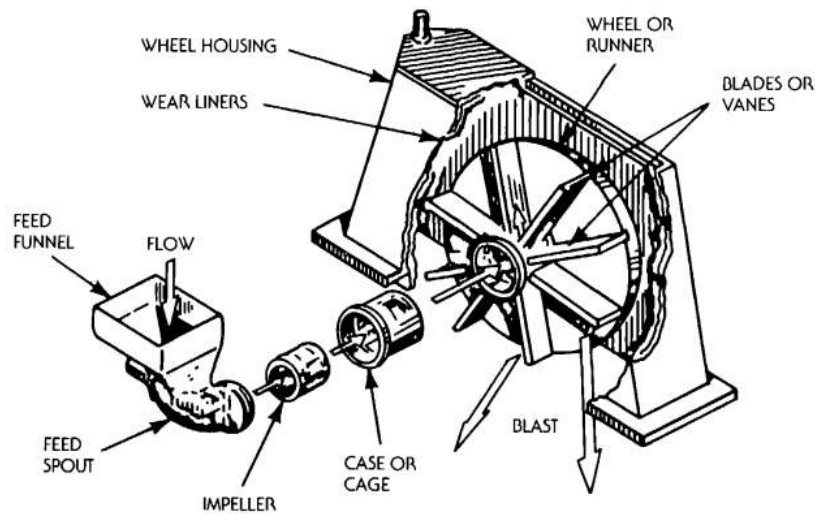


FIGURE 1.2: Airless centrifugal blast wheel system - exploded view of the system depicting its various components and the flow of abrasive media across them (adapted from Enviro-Managament & Research, Inc. (1976))

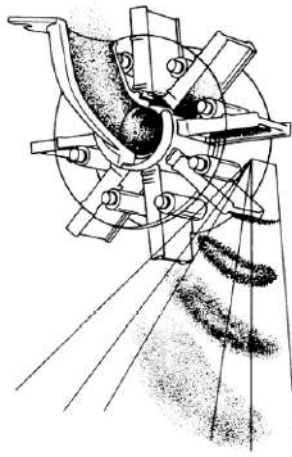


FIGURE 1.3: Abrasive media generating the typical tent blast pattern while exiting the blast wheel (adapted from ASM International Handbook Committee (1994))

moves outwards and finally leaves the wheel (more or less tangentially) towards the substrate surface. This generates the typical tent blast pattern which can be seen in Fig. 1.3. (ASM International Handbook Committee (1994); Enviro-Managament & Research, Inc. (1976))

1.3.2 Direct pressure blast nozzle system

These systems utilize a compressed air supply to propel the abrasive media towards the substrate through a nozzle. Fig. 1.4 depicts a portable blast cleaning machine. The general setup

for larger cabinet-type machines based on the same technology is also very similar.

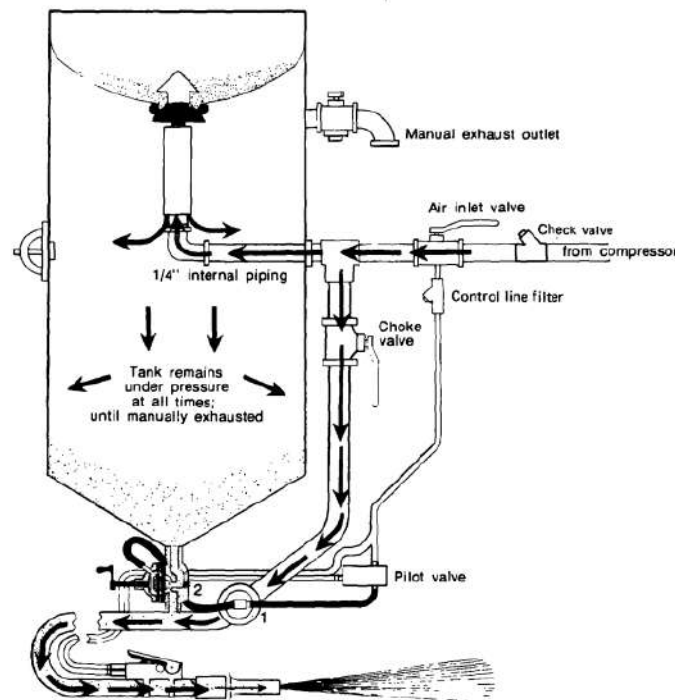


FIGURE 1.4: Portable direct pressure blast cleaning. The general setup for larger machines operating on the same principle is also similar. (Adapted from Enviro-Managament & Research, Inc. (1976))

These systems employ an intermittent pressure tank and a blast hose line; both are connected to a compressed air supply. A metered quantity of abrasive is fed from the pressure tank into the compressed air flowing through the blast hose. This forms an air-abrasive mixture which is then directed towards the substrate surface. The pressure tank is divided into two compartments. The bottom compartment can be replenished by the abrasive in the top compartment by shutting off the air supply and letting open the manual exhaust valve. Without any pressure in the tank, the valve regulating the supply of abrasive from the top compartment to the bottom one opens up by the weight of the abrasive and allows the bottom chamber to be replenished with abrasive media. The flow of abrasive from the pressure tank to the blast hose is regulated by a metering valve fitted at the feed point. (ASM International Handbook Committee (1994); Enviro-Managament & Research, Inc. (1976))

1.3.3 Indirect suction blast nozzle system

Suction blast systems are considered to be one of the simplest abrasive blast systems. Suction blast cabinets are widely used for experimental research purposes in the area of abrasive blasting (The experimental work associated with the present thesis (described in later part) was also conducted using a suction blast cabinet).

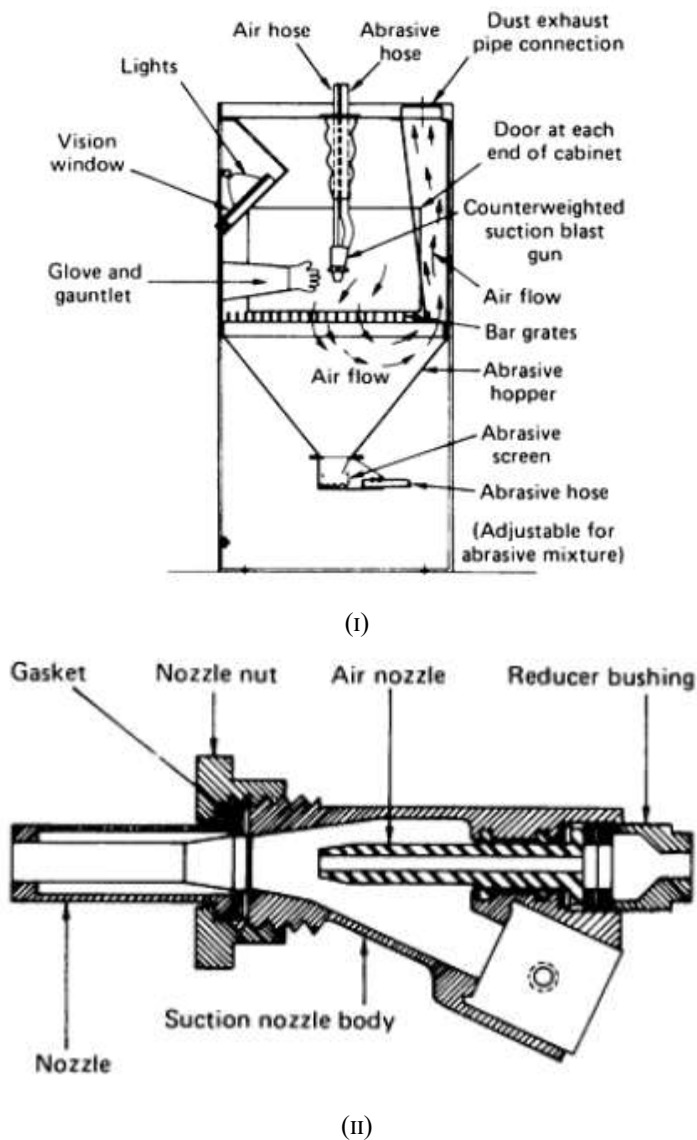


FIGURE 1.5: Suction blast equipment (I) cabinet (II) nozzle assembly (adapted from ASM International Handbook Committee (1994))

These systems utilize an induction nozzle that is connected to a compressed air line and a flexible hose that supplies the abrasive. The induction nozzle generates an air-abrasive blasting mixture by the siphon effect (Venturi effect) of air flowing through the nozzle. The abrasive media is stored in a separate hopper-like container. The blast hose emerging from this container is connected to the induction nozzle. Due to the siphon effect, the abrasive in the container is pulled through the hose and the blasting mixture is formed in the nozzle, which is then directed towards the substrate surface. The proportion of abrasive in the blasting mixture can be controlled by regulating the relative position of the end of the blast hose with respect to the container. (ASM International Handbook Committee (1994); Enviro-Managament & Research, Inc. (1976))

1.4 Surface topography

Each manufacturing process generates a distinct surface pattern. Surface topography refers to the study of geometrical features of a surface which include roughness, waviness, lay, form errors & flaws. The direction of the predominant surface pattern generated by a material removal process is termed as lay. Finely spaced surface irregularities are referred as roughness. Waviness refers to surface irregularity of greater scale. (Black & Kohser (2008))

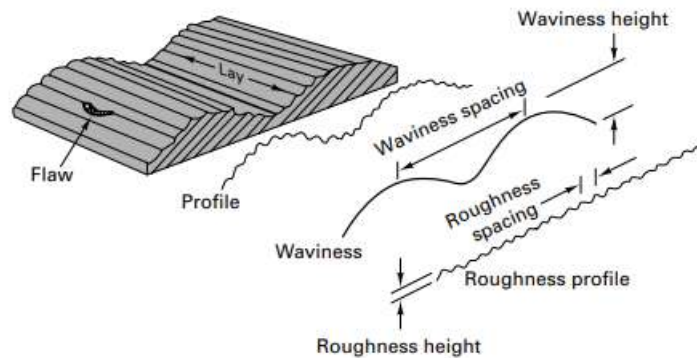


FIGURE 1.6: Descriptive figure showing roughness, waviness, flaws & lay (adapted from Black & Kohser (2008))

1.4.1 Surface roughness

Surface roughness is evaluated by measuring the height of surface irregularities with reference to an average line (or surface). Roughness is usually expressed in micrometres (μm). Surface roughness can be expressed in terms of a number of 2D roughness parameters (R-parameters) like R_a (arithmetic average roughness), R_z (peak-to-valley roughness), R_q (root mean square roughness) among others (Black & Kohser (2008)). The aforementioned parameters are evaluated over a certain evaluation length. Roughness measurements can also be performed over a certain evaluation area. The corresponding parameters are S_a , S_z & S_q respectively.

Substrate surface roughness is crucial to subsequent coating adhesion as it provides opportunities for mechanical interlocking & enhances the contact area between the substrate & the coating. One of the main aims of this research work is to determine the dependence of contact area on roughness and to optimize the grit blasting process parameter levels to maximize the resulting contact area.

Chapter 2

Literature review & research gap

2.1 Literature review

Grit blasting is the most common roughening method for preparing substrates for subsequent coating operations. Traditionally, grit blasting has been performed empirically and qualitatively. Qualitative guidelines like “perform grit blasting until a coarse surface is obtained” could be found in early coating literature. But such descriptions are of little merit in modern manufacturing as they neither indicate what constitutes an acceptable level of coarseness nor how to achieve it. Also, assessment of blasted surfaces based on such qualitative descriptions is subjective and relies on the operator’s skill. Consequently, a considerable amount of research was undertaken at different levels to determine the optimum surface topography for maximum coating adhesion and how can it be achieved by controlling the grit blasting process parameters. In addition to that, attempts were made in the latter half of the last century to develop an inspection procedure for the same, relatable to national and international standards. **Griffiths et al. (1996)** conducted one of the earliest researches on grit blasting as a pre-treatment for plasma spraying. Their research described the online monitoring of grit blasting using 2D roughness parameters. It showed how online monitoring of roughness parameters can help in optimizing the grit blasting conditions to achieve maximum coating adhesion.

Since then, a great deal of research has been carried out on several aspects of grit blasting. Starting from below is a survey of some select recent papers dealing with the topic.

- **Mellali et al. (1997)** conducted a series of experiments on several substrates to examine the effect of grit blasting process parameters on the surface roughness, substrate residual stress, grit residue, and grit erosion. Standoff distance, blasting time, impingement angle & blasting pressure were the process parameters analysed. The substrates that were selected for the study included aluminum alloy, cast iron, and hard steel. The blast media used was white alumina. The surface profiles of the blasted surfaces were characterized by two roughness parameters – Ra (average roughness) & Rt (maximum peak-to-valley depth). The experiments showed that grit size has the highest influence on roughness. Both Ra and Rt were

found to vary linearly with grit size (slope of variation was highest for the materials with lowest Young's modulus). No significant influence of standoff distance on roughness was reported between 80 and 150 mm. However, Ra did not increase much with pressure. Between 60° & 90° , the blasting angle was also found to be insignificant.

- **Varacalle et al. (2006)** conducted a series of experiments to analyse the effect of grit blasting process parameters on surface roughness and the adhesion strength of thermal spray coating applied post roughening. The substrate material chosen was A36/1020 steel. The study consisted of examining the effect of grit blasting process parameters on surface roughness of A36/1020 steel, comparing the effectiveness of metal grits over conventional abrasives (copper slag, coal slag & chilled iron), and assessing the adhesion strength of Twin-Wire Electric Arc (TWEA) sprayed coatings on the blasted surfaces. The grit blasting process parameters that were analysed included grit blast media, blast pressure, and working distance. The process parameters were varied using the Box-type statistical design of experiment (SDE) approach. Initial experiments were carried out with metal grits of four different mesh sizes (HG16, HG18, HG25, HG40). It was reported that the average peak-to-valley surface roughness (Rz) decreases with mesh size (i.e. increases with grit size; blasting with HG16 produced a profile characterized by the highest Rz). The variation of Rz with standoff distance for a given grit size and pressure is increasing initially but becomes decreasing with the passage of time. Rz was reported to increase with blasting pressure for a wide range of pressure; however, a slight drop in Rz was noted at higher pressures. Comparison of the substrate response to blasting with HG16 and that with conventional abrasives showed that HG16 produced surface texture that could be deemed more favorable for subsequent thermal spraying.

- **Chander et al. (2009)** carried out several experiments over low carbon steel substrates to examine the effect of grit blasting process parameters on the surface roughness and surface residual stress. The process parameters that were analysed included blasting pressure, time, angle & standoff distance. Statistical design of experiments (SDE) approach was utilized for varying the same. The mechanism of material removal during grit blasting was also studied using electron microscopy. Correlation between Barkhausen noise signal and residual stress data (measured using X-ray diffraction) was also analysed. It was reported that average surface roughness (Ra) increases with the angle of impingement till the angle is approximately 75° . At low angles, micro-cutting is the dominant mechanism while near 90° , indentation is dominant; between the two extremes, material removal is a mixed-mode phenomenon. At low standoff levels, Ra is low due to greater loss of kinetic energy of impacting abrasives by collision with the ricocheting abrasives. As standoff distance is increased, Ra was reported to increase initially but starts decreasing later due to divergence of the air-abrasive jet. With

blasting time, Ra was reported to increase initially, remain constant for some time, and decrease slightly later. The initial increase in Ra with time was attributed to the attack of grits in previously unaffected areas. Later, there was no appreciable increase for some time due to hardening of the surface layer during initial blasting; as time increased further, Ra reduced slightly due to over-blasting effect. Finally, Ra was reported to increase with grit size and blasting pressure.

- **Sen et al. (2010)** carried out a series of grit blasting experiments to study the influence of blasting pressure and grit size on the roughening of mild steel substrates. The effect of these parameters on the resulting roughness and tensile bond strength of Cu, Al₂O₃, and WC-12Co coatings, deposited subsequently, were also analysed. The blasting media used was gray alumina. Analysis of the experimental results showed that the roughness of the grit-blasted mild steel substrates, as well as the roughness of the subsequently deposited coatings, are critical in determining the coating bond strength. Blasting time was found to have no significant influence on the average surface roughness (Ra). It was argued that grit velocity is a much more fundamental parameter to be correlated with surface roughness. Knowing the fact that grit velocity is a strong function of blasting pressure & grit size and utilizing the experimental results, it was possible to establish the following working relation between surface roughness, blasting pressure & grit size:

$$Ra \propto (PD)^{1/2}$$

where P is the grit-blasting pressure and D is the grit size.

- **Asl & Sohi (2010)**: carried out a series of experiments to investigate the effect of grit blasting parameters on the surface roughness of steel substrates and adhesion strength of plasma spray coatings applied subsequently over the blasted surfaces. The substrate material selected was AISI 4130 steel. Grit blasting was carried out over AISI 4130 steel substrates using Al₂O₃ particles. Standoff distance, blasting time, pressure, and angle were the process parameters analysed. The effect of substrate hardness was also analysed by testing substrates of different heat treatments (annealed, normalized & quenched). The blasted specimens were then plasma spray-coated with 80% ZrO₂ – 20% Y₂O₃ powder and their adhesion strength was correlated with surface roughness. As can be expected, the average roughness (Ra) was reported to decrease with substrate hardness i.e. minimum roughness was induced on quenched surfaces under similar operating conditions (& maximum for annealed). Subsequent experiments to analyse the effect of standoff distance, blasting time, pressure, and angle were carried out on annealed substrates only. With standoff distance, Ra values were reported to increase initially, reach a maximum and then decrease again. Further, Ra was reported to increase with blasting pressure up to a particular level and then remain constant

with pressure. Similar was the variation of Ra with blasting time. Finally, it was also reported that a blasting angle of 90° gave a higher Ra value than a blasting angle of 45° . In subsequent analysis, the adhesion strength of the plasma spray coating was correlated to substrate hardness & roughness.

- **Begg et al. (2015)** performed a parameter study to investigate the effect of blast parameters on surface profile for seven different metallic substrates using a mechanized, robotic blasting system. The study aimed to utilize the findings regarding the effect of the blasting parameters to mechanize the grit blasting process so as to obtain a reproducible surface profile. The blast parameters analysed included blast pressure, standoff distance, media feed rate, blast angle, traverse speed, and media size. The blast media used was brown fused alumina. Results of the above study showed that the blast pressure and media size have the greatest impact on average (areal) surface roughness (Sa) while the blast angle has a lesser influence. Changes in blast angle caused very minor changes in average roughness, but microscopic examinations revealed a change in the material removal process i.e., as blast angle is lowered, the erosion mechanism changes from indentation to micro-cutting. Surface roughness (Sa) of blasted substrates was reported with grit size and blasting pressure. Also, it was observed that Sa initially increases with standoff distance but decreases later.

- **Bobzin et al. (2015)** also conducted a series of experiments to study the effect of grit blasting process parameters on the resulting substrate surface topography. The efficiency and wear behavior of the blasting media were also investigated by comparing the surface roughening created by three different media – alumina, alumina-zirconia, and steel shot. The surface topographies generated by grit blasting are analysed using a number of 2D roughness parameters (Rz, Ra, $R\Delta q$, Rsm, Rvk). Based on these measurements, attempts were made to identify which parameter is more suitable for correlating surface roughness and bond strength of the coating applied post grit blasting. The process parameters that were analysed included grit size, blasting angle, pressure, and standoff distance. The interdependency among the process parameters and its effect on the surface topography is also studied. It was reported that arithmetic average roughness (Ra) increases with blasting pressure up to a certain level, beyond which any increase in pressure has no significant effect on roughness. Interaction between blasting pressure and standoff distance was reported to be significant for Ra. Ra values were reported to increase with grit size. No interdependency is observed between blasting angle and pressure. The effects of blasting pressure and grit size on Ra were also reported to be independent of each other. Minor interdependency between grit size and blasting angle was noticeable. No noticeable difference in Ra was observed by varying blast media i.e. Ra values of surface profiles created by alumina, alumina-zirconia & steel shot were similar. However, alumina-zirconia and steel shot have a longer lifetime than pure

alumina. Finally, preliminary investigation concluded that $R\Delta q$ (root mean square profile slope) & Rvk (reduced valley depth) correlate surface roughness to coating bond strength better than Ra (arithmetic average roughness).

- **Ghara et al. (2020)** carried out a series of experiments to study the effect of grit blasting parameters on a number of surface & near-surface properties of different metal alloys. The surface and near-surface properties that were analysed included surface roughness, surface residual stresses, and surface dislocation density. Blasting pressure, standoff distance, time, and angle of impingement were the process parameters tested. The substrate materials included low carbon steel, Ti-6Al-4V, and Inconel 718. With regards to low carbon steel substrates, it was reported that the average (areal) surface roughness (Sa) initially increases with blasting time, reaches a maximum, and then starts decreasing. Variation of surface compressive residual stress with blasting time was similar. The surface dislocation density increases with blasting time up to a certain duration before attaining a stable value. Both surface roughness (Sa) and residual stress were reported to increase with blasting angle and become maximum at 90° . Micro-cutting and shearing are dominant mechanisms of material removal at low blasting angles while indentation and extrusion dominate at higher angles. The surface dislocation density of low carbon steel substrates was reported to increase monotonically with blasting angle. Both surface roughness (Sa) and residual stress were reported to increase with blasting pressure. Both properties increased with standoff distance (SOD) initially but showed a slight decrease later at higher SODs.

- **Muslimin et al. (2020)** conducted grit blasting experiments on low carbon steel substrates (JIS G3101 SS400) using steel grits (G25) to study the effects on surface characteristics like surface morphology, roughness, and hardness. Grit blasting was carried out with a fixed nozzle pressure and blasting angle while varying nozzle-to-surface distances and blasting times. Surface morphology was examined using a scanning electron microscope (SEM), chemical composition was determined using EDS, surface roughness was measured using profilometry and hardness profiles were inspected using Rockwell and micro-Vickers hardness tests. Experimental results showed that closer nozzle-to-surface distances result in higher average (areal) surface roughness (Sa). This was attributed to the fact that closer distances result in a greater impact on the substrate surface and consequently, induce higher roughness. Further, an increase in blasting duration was also found to contribute to an increase in Sa . It was argued that the longer the substrate surface is exposed to blasting, the greater would be the resulting erosion, as a result of which Sa was found to increase proportionally with blasting time.

2.2 Research gap

Many previous research works have studied the effect of process parameters of grit blasting on steels of different grades. However, all of those were conducted while keeping the substrates in air/dry medium. Performing grit blasting with variable process parameters on steel substrates immersed in any wet medium has not been encountered in the existing literature. Further, a comparative study of steel substrates grit blasted under different environments (dry as well as wet) has not been undertaken before.

2.3 Objectives

The objectives of the presented research work can be summarized as follows:

- To develop a facility for holding the substrate and adjusting the standoff distance (SOD) while blasting
- To determine the effect of grit blasting process parameters (grit size, SOD, time) on the surface and sub-surface characteristics of mild steel substrates under dry conditions
- To determine the effect of grit blasting process parameters (grit size, SOD, time) on the surface and sub-surface characteristics of mild steel substrates in different wet environments simulated for improved heat dissipation
- To determine the optimal set of process parameter levels for performing grit blasting in each environment based on the maximum contact area generated, which is beneficial for achieving strong coating-substrate adhesion
- To perform a comparative study of substrates grit blasted under different environments

Chapter 3

Materials and methods

3.1 Experimental setup

3.1.1 Grit blasting equipment

The grit blasting equipment used for conducting this research consisted of the following components:

- Reciprocating air compressor
- Suction blasting machine and dust collector subsystem

The details and specifications regarding the above components are as follows:

• Reciprocating air compressor

TABLE 3.1: Specifications for reciprocating air compressor

| | |
|----------------------------|-----------------------------|
| Manufacturer | ELGi Equipments Ltd. |
| Model | SS 10 L B – 9 |
| Maximum working pressure | 9 bar |
| No. of cylinders | 2 |
| No. of stages | 1 |
| Main drive rating | 10 hp (7.5 kW) |
| Rated speed of drive | 1430 rpm |
| Type of starter for motor | DOL (Direct online starter) |
| Type of drive transmission | Belt driven |

The compressed air supply in our setup is furnished by a two-cylinder reciprocating air compressor of the above specifications. Reciprocating air compressors are positive displacement compressors. Positive displacement compressors build pressure by compressing gas within a closed chamber. The atmospheric air is aspirated through the two air filters which supply the two cylinders within which it is compressed by reciprocating piston cylinders powered by the motor fixed on the receiver. Some amount of air aspirated through one of

the filters is bypassed to the central cooler unit for heat transfer. The compressed air within the cylinders is then supplied to the receiver via the after-cooler pipe. A non-return valve at the exit of the aftercooler pipe prevents the backflow of compressed air from the receiver. The non-return valve is also accompanied by a safety valve. As compressed air enters the receiver, pressure builds up. A pressure gauge is arranged on the receiver for measurement and visualization of built pressure. The compressed air supply for the desired purpose is established by turning on the ball valve (outlet) at the bottom right of the receiver.



FIGURE 3.1: ELGi Equipments' SS 10 L B - 9 reciprocating air compressor
(Courtesy: Metallography & Tribology Lab, IIT Indore)

Feedback measurements are carried out at the inlet of the receiver. A fraction of the compressed air supply is bypassed to a pressure switch. The pressure switch employs feedback control to prevent the pressure in the receiver to rise beyond a permissible level by turning off the power supply. Further, the feedback control is implemented at both higher and lower levels i.e. in addition to preventing pressure within the receiver to rise beyond a permissible level. Feedback control is also implemented at the lower level to prevent the pressure in the receiver to drop below the desired level. This is implemented by a direct online (DOL) starter. The direct online starter is connected in series with the electric motor. The DOL starter monitors the pressure in the receiver by feedback measurements. If the pressure in the receiver drops below the desired level, it is detected by the DOL. The DOL then establishes a connection between the (3-phase) power supply and the motor, which drives the driver pulley. A V-belt drive is used to transmit power to the driven pulley which drives the crankshaft that runs the reciprocating cylinders as well as the exhaust fan at the back.

Throughout our experiments, the pressure switch and DOL settings were adjusted so that pressure was maintained between 3 to 6 bar (gauge).

• **Suction blasting machine and dust collector subsystem**

TABLE 3.2: Specifications for suction blasting machine

| | |
|--------------------|-----------------------|
| Manufacturer | Synco Industries Ltd. |
| Model | SSB-606060 |
| Cabinet dimensions | 600 x 600 x 600 (mm) |
| Nozzle diameter | 8 mm |
| Input range | 60-90 psi |

The main blast machine consists of an air-line at the bottom of the chamber. This line consists of several components such as non-return valve, solenoid valve, moisture filter, air regulator, pressure gauge, etc. This air-line is connected to the compressed air supply coming out of the reciprocating air compressor via a hose. The air-line is connected to the air nipple of the blast gun via another flexible hose. The blast facility consists of an abrasive storage tank at the back for holding the abrasive media. Another flexible hose connects the storage tank to the abrasive nipple of the blast gun. Passage of air through the blast gun creates a partial vacuum which results in the abrasive media being drawn from the storage tank through the hose connecting it to the blast gun. The interior of the blast cabinet can be accessed by using the cabinet doors on either side. Blasting of substrates can be observed through the vision glass in the front. Beneath the vision glass, there are gloved holes through which the operator can hold the substrate while it is being blasted. The interior of the cabinet is lit by an illumination bulb. A small tank with a spray pipe emerging out of it is attached to one of the cabinet doors. The tank is filled with an anti-corrosion solution. The tank-spray setup is used for occasional cleaning of the interior of the cabinet. The control switches for blasting, dust collector, illumination bulb, and emergency stop can be found on the top of the cabinet. Blasting can be started &/or terminated either by using the switch at the top or by using a foot pedal. The bottom of the cabinet extends into a hopper-like arrangement within which the blasted media fall through the perforated metal base. This hopper is then connected via pipeline to the reclaimer situated just above the abrasive storage tank at the back. The reclaimer returns the abrasive to the storage tank while the dust is separated towards the dust collector subsystem.

Dust collector subsystem: The dust collector subsystem working in conjunction with the suction blasting machine is a fabric filter (baghouse). It consists of 4 filter bags. These bags can either be made up of woven or felted cotton, glass-fiber or some other synthetic material.

These bags are usually coated with a filter enhancer (which can be a chemically inert substance like limestone) to improve the efficiency of dust collection and also, to increase the usage life of the bags. These bags are connected to a shaking handle. This handle is powered by a motor fitted on the top. Generally, the shaking is executed in the horizontal direction. The shaking motion of the handle is transmitted to the fabric bags and the dust collected on the inside of the bag is released. The dust then settles down in the dust tray at the bottom and can be collected post-operation. Clean air devoid of dust is then released through the exhaust fan at the top (also powered by the motor).

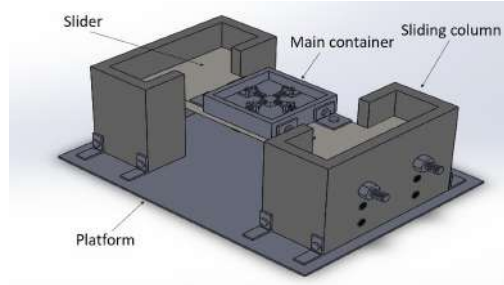


FIGURE 3.2: Synco Industries' SSB-606060 suction blasting machine (Courtesy: Metallography & Tribology Lab, IIT Indore)

3.1.2 Setup for holding the substrate and adjusting the standoff distance

The interior of the suction blast cabinet used for the presented research work lacks an in-built facility for holding the substrate fixedly under the nozzle at various standoff levels. A dedicated setup was, therefore, made for the same. Fig. 3.3 depicts the CAD model of the setup and the corresponding real-life counterpart that was manufactured based on the CAD design. The setup consists of a container with a vise-like arrangement assembled within it

for holding the substrate fixedly. This container is welded over an I-shaped sliding platform that slides within two guiding columns and can be fixed at pre-planned locations using stud supports.



(I)



(II)

FIGURE 3.3: Substrate holding setup (I) CAD model (II) Real-life counterpart

3.2 Substrate preparation

Low carbon steel substrates were chosen for the experiments. These were retrieved from long plates of 5 mm thickness. Substrate preparation involved rust removal using used polishing paper followed by sectioning into final substrate dimensions of 20 mm x 20 mm x 5 mm using a high-speed cut-off machine (Struers Secotom-15).

TABLE 3.3: Substrate composition

| Low carbon steel (Chander et al. 2009) | | | | | |
|--|------|------|------|------|---------|
| Elements | C | Mn | S | P | Fe |
| wt. % | 0.20 | 0.30 | 0.05 | 0.04 | Balance |

3.3 Design of experiments

The process parameters that are varied in the experiments include: grit size, standoff distance (SOD), blasting time and the surrounding medium. The levels of the process parameters involved are tabulated in Table 3.4.

TABLE 3.4: Levels of process parameters

| Grit size (mesh) | SOD (mm) | Time (s) | Medium |
|------------------|----------|----------|---------------|
| 16 | 60 | 30 | Dry |
| 24 | 80 | 45 | Water |
| 36 | 100 | 60 | Saline water |
| - | 120 | 75 | Ethyl alcohol |

The term 'mesh' or 'mesh count' is used to refer to the number of openings per linear inch (or mm) of screen. Higher the mesh count, smaller is the particle size. The relationship between grit sizes in mesh & those in micrometre as per BSS (British Standards in Surveying) standards is visualized in Fig. 3.4.

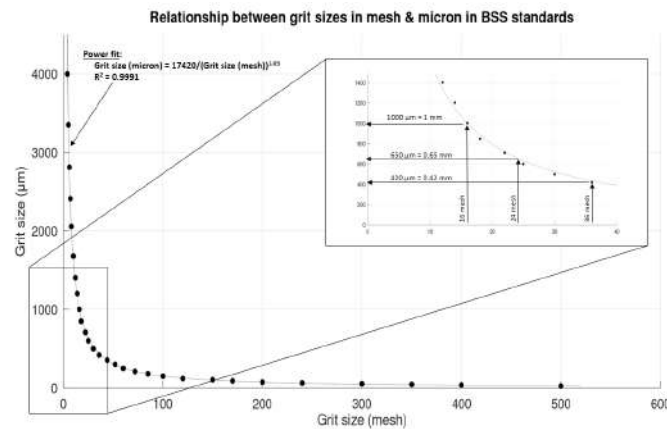


FIGURE 3.4: Relationship between grit sizes in mesh & micrometre in BSS standards

According to BSS standards, 16 mesh corresponds to a particle size of 1 mm, 24 mesh corresponds to that of 0.65 mm & 36 mesh corresponds to 0.42 mm. Gray alumina (Al_2O_3) grits were used for grit blasting.

TABLE 3.5: Approximate conversion of selected mesh sizes in micrometre & millimetre

| mesh | μm | mm |
|------|---------------|------|
| 16 | 1000 | 1 |
| 24 | 650 | 0.65 |
| 36 | 420 | 0.42 |

Water used for the wet experiments was demineralised (DM water). Saline water used for the concerned experiments was prepared by mixing 37.5 g iodised salt with 1 L (i.e. 1 kg) of DM water to emulate the average seawater concentration which varies between 3.5-3.7% wt. Ethyl alcohol used for the concerned experiments is diluted to 50% (vol.) concentration using DM water.

The approximate densities of the aforementioned liquid media at 25 °C & atmospheric pressure are tabulated in Table 3.6.

TABLE 3.6: Approximate densities of the liquid media used for simulating wet environments during grit blasting

| Medium | Density |
|---|-------------------|
| - | kg/m ³ |
| Water (DM) | 997.05 |
| Saline water (\approx 3.6% wt. NaCl) | 1034.55 |
| Ethyl alcohol (50% (vol.) conc.) | 891.13 |

The density of air under similar conditions is approximately 1.18 kg/m³.

For the experiments performed under wet conditions, the perforated metal base of the cabinet is sealed using polythene & cardboard to prevent wet grits from being reclaimed to the hopper. The wet grits are disposed after each experiment. As the grits are not reclaimed under these conditions, these experiments were performed with a starting quantity of grits in the hopper greater than that under dry conditions. Further, during the wet experiments, splashing of the medium during grit blasting makes it necessary to continuously supply the medium through some arrangement. This was made possible by making use of the tank-spray system attached to one of the cabinet doors for occasional cleaning of the interior of the cabinet. Instead of the anti-corrosion solution used for cleaning, the tank was filled with the concerned medium at the start of each experiment and the medium was sprayed into substrate holding container during grit blasting using one hand. The capacity of the cleaning tank is such that the wet experiments of time periods: 30 s & 45 s could be conducted in one go. However, the wet experiments of time periods: 60 s & 75 s experiments were required to be performed in an intermittent manner to replenish the tank with the medium. Wet experiments of time period 60 s are performed in two steps of 30 s each while those of time period 75 s were performed in steps of 30 s & 45 s respectively.

The levels of the process parameters are coded using the alpha-numerical terminology tabulated in Table 3.7 & Table 3.8. Partially mixed design of experiments was implemented for varying the process parameters. While keeping the medium constant, the other three process parameters were varied in the manner shown in Table 3.9.

Pressure varied continuously between 3-6 bar during each experiment. To be consistent, all experiments were started from the highest pressure (6 bar), allowing it to fall to 3 bar

TABLE 3.7: Alpha-numerical coding for process parameter levels (1)

| Grit size (mesh) | SOD (mm) | Time (s) | CODE |
|------------------|----------|----------|------|
| 16 | 60 | 30 | 1 |
| 24 | 80 | 45 | 2 |
| 36 | 100 | 60 | 3 |
| - | 120 | 75 | 4 |

TABLE 3.8: Alpha-numerical coding for process parameter levels (2)

| Medium | CODE |
|---------------|------|
| Dry | D |
| Water | W |
| Saline water | S |
| Ethyl alcohol | A |

TABLE 3.9: Design of experiments for a particular medium

| Trial | Grit size | SOD | Time |
|-------|-----------|-----|------|
| 1 | 1 | 1 | 1 |
| 2 | 1 | 2 | 2 |
| 3 | 1 | 3 | 3 |
| 4 | 1 | 4 | 4 |
| 5 | 2 | 1 | 2 |
| 6 | 2 | 2 | 1 |
| 7 | 2 | 3 | 4 |
| 8 | 2 | 4 | 3 |
| 9 | 3 | 1 | 3 |
| 10 | 3 | 2 | 4 |
| 11 | 3 | 3 | 1 |
| 12 | 3 | 4 | 2 |

and rise again to 6 bar during blasting due to the DOL & pressure switch settings of the reciprocating air compressor. Angle of impingement was maintained constant at 80° . The grit blasted substrates were subjected to air blast cleaning using a blow gun for few seconds before storing in a desiccator.

3.4 Characterization of grit blasted surface

3.4.1 Evaluation of substrate surface profile

Two dimensional visualization of substrate surface profile and measurements related to it were obtained using a contact type stylus profilometer (Taylor Hobson – Surtronic 25). Six measurements were performed on each surface (3 in horizontal direction, 3 in vertical). For each measurement, the profilometer supplies three plots (surface profile, waviness profile,

roughness profile) and a parameter table containing a list of roughness parameters and their corresponding values reported for that measurement. Based on the average data, it was possible to estimate the average surface profile generated by grit blasting for a given set of process parameters.

• Estimation of increment in contact area due to roughening

A mathematical model was developed to estimate the increment in contact area due to roughening resulting from grit blasting. The surface asperities on a roughened surface can be modelled as conical peaks with an average height of twice the average roughness (R_a). The average number of peaks per unit length of the profile can be estimated from the peak density (RPc). The average base diameter of the conical asperities is mathematically equivalent to the reciprocal of RPc. Knowing the number, height and base diameter of the conical asperities enabled us to calculate the curved surface area of the surface asperities generated due to grit blasting over a unit base area (reference area). The increment in the area of the roughened surface with respect to the reference surface was then estimated.

Based on the increment in contact area, the optimal set of process parameter levels under each environment were estimated & the corresponding surface profile was three dimensionally visualized using an optical surface profiler (Veeco, NT 9080).

3.4.2 Microhardness evaluation

The variation of cross-section hardness with depth from the grit blasted surface was studied for samples grit blasted under a particular setting of mesh size, SOD & time but under different environments using Vickers microindentation hardness testing. With the help of the data obtained, the thickness of the affected layer was estimated under dry & wet conditions. Mitutoyo's manual hardness testing system (HM-200: System A) was used for the same. Hardness measurements were carried out at a load of 50 gf (dwell time = 10 s). Five to six indentations were made at each depth and the lengths of the diagonals of the indentations were measured. Based on the average diagonal length, Vickers hardness is estimated using the formula:

$$HV = 1.854 \frac{P}{d^2} \quad (3.1)$$

where $d = \frac{d_1 + d_2}{2}$, d_1 & d_2 being the lengths of the diagonals of the indentation in mm while P being the load applied in kgf.

The best four readings were considered for estimating the average Vickers hardness at a particular depth from the grit blasted surface.

3.4.3 X-Ray Diffraction (XRD) analysis

XRD analysis of the grit blasted surfaces were carried out using PANalytical EMPYREAN X-ray diffractometer by Anton Paar, operating at 35 kV & 30 mA. The diffractometer utilises a copper anode to generate the Cu K- α radiation (1.54060 \AA) used for diffraction. XRD data was analysed using X'Pert High score Plus© (Phillips) analysis package to identify the possible surface phases and formations (if any on the surface) post grit blasting.

3.4.4 Sub-surface microstructure study using optical microscopy, FE-SEM & EDS

Analysis of the sub-surface microstructure of grit blasted substrates was carried out using both optical microscopy & electron microscopy. Leica DM IL LED inverted microscope was used for optical microscopy while electron microscopy was carried out using a field emission scanning electron microscope (FESEM) facility by JEOL (JSM-7610FPlus). Sub-surface microstructure study was performed for the samples grit blasted under the optimal set of process parameter levels found for each environment. The grit blasted samples were sectioned and their cross sections are polished to reveal the cross-sectional microstructure. Polishing was first carried out using silicon carbide (SiC) polishing papers on Struers LaboPol-25 polishing machine in the proper metallographic sequence of increasing mesh size i.e. beginning from 220 mesh to 2500 mesh. Final polishing was done using $1 \text{ }\mu\text{m}$ diamond polishing paste on selvyt polishing cloth. Polishing using SiC polishing papers was carried out at 350 rpm while diamond polishing was carried out at 150 rpm. The surface and sub-surface regions of the polished specimens were then observed at 1000X magnification under the inverted microscope to assess the level of sub-surface damage occurring under different conditions and other features of interest, if any. The polished surfaces of the samples were then etched using Nital solution (3 mL 60% HNO_3 + 900 mL 96% $\text{C}_2\text{H}_5\text{OH}$) for 30 s and observed again using FESEM. EDS analysis was carried out over selected sub-surface regions to obtain information about the presence of elements in that region. EDS was performed in parallel with electron microscopy using the same system (JEOL, JSM7610FPlus).

Chapter 4

Results and discussions

4.1 Analysis of experimental results for each environment

4.1.1 Dry

• Profilometric data

As mentioned in chapter 3, profilometric data related to the surface profiles of grit-blasted substrates were collected using Taylor Hobson's Surtronic 25 contact type stylus profilometer. Six measurements were performed on each surface (3 in horizontal direction, 3 in vertical). For each measurement, the profilometer supplies three plots pertaining to the surface profile and corresponding waviness & roughness profiles, along with a parameter table containing the numerical values of roughness parameters corresponding to the measured profile. The aforementioned plots and parameter table for a sample measurement are shown in Fig. 4.2 & Fig. 4.3 respectively

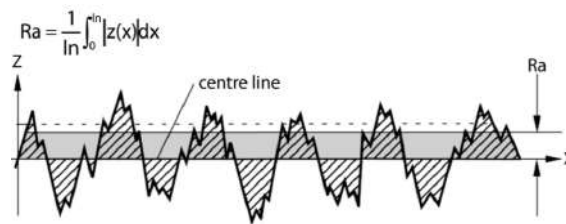
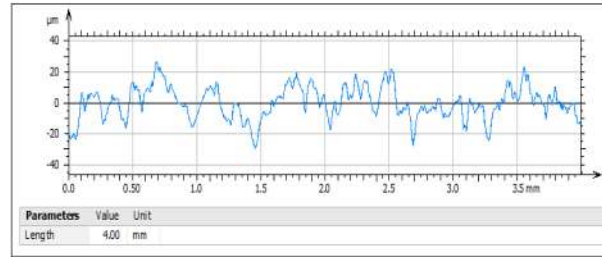
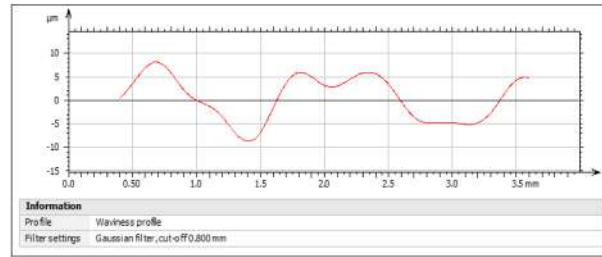


FIGURE 4.1: Arithmetic average roughness (adapted from Bobzin et al. (2015))

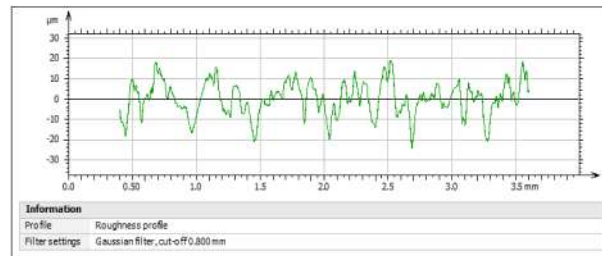
Arithmetic average roughness (Ra) is a well-established parameter used to evaluate substrate surface roughness in thermal spray industry (Bobzin et al. 2015). Consequently, Ra is also the main parameter of interest used in the presented research work for evaluating substrate surface roughness post grit blasting under different levels of process parameters. Ra is mathematically the arithmetic average of all the ordinate values of the roughness profile within the evaluation length. Another parameter of interest for the research work presented in this thesis is the peak density of roughness profile (RPc). It will be used later in estimating the increment in contact area due to roughening.



(I)



(II)



(III)

FIGURE 4.2: Profilometric surface evaluation (I) Sample surface profile (II) Corresponding waviness profile (III) Corresponding roughness profile

The R_a and RP_c values corresponding to each measurement for all the 12 experiments performed under dry conditions are tabulated in Table 4.1. For each experiment, the average value of R_a is calculated. The surface profile whose R_a value is closest to the average is chosen to represent the average surface profile and is differently highlighted within the same table.

TABLE 4.1: Profilometric data for dry blasting

| Trial | CODE | Run 1 | | Run 2 | | Run 3 | | Run 4 | | Run 5 | | Run 6 | | Average |
|-------|------|---------|--------|---------|--------|---------|--------|---------|--------|---------|--------|---------|--------|---------|
| | | R_a | RP_c | R_a | RP_c | R_a | RP_c | R_a | RP_c | R_a | RP_c | R_a | RP_c | |
| - | - | μm | 1/mm | μm | 1/mm | μm | 1/mm | μm | 1/mm | μm | 1/mm | μm | 1/mm | μm |
| 1 | 111D | 7.22 | 41.4 | 7.89 | 37.4 | 8 | 47.2 | 6.83 | 30.8 | 7.92 | 36.2 | 7.44 | 47.6 | 7.55 |
| 2 | 122D | 6.85 | 38.4 | 8.14 | 38.9 | 8.9 | 39 | 7.5 | 36.2 | 7.42 | 40.9 | 6.97 | 39.8 | 7.63 |
| 3 | 133D | 7.66 | 35.7 | 7.43 | 36.3 | 7.27 | 38.9 | 7.33 | 43.1 | 6.89 | 39.8 | 7.72 | 38.8 | 7.38 |
| 4 | 144D | 7.65 | 34.6 | 7.24 | 45.6 | 7.7 | 39.5 | 5.68 | 39.8 | 7.68 | 34 | 6.87 | 40.8 | 7.14 |
| 5 | 212D | 4.22 | 49.5 | 3.91 | 51.8 | 5.82 | 51.8 | 5.23 | 45.7 | 5.93 | 41.1 | 4.91 | 56.1 | 4.91 |
| 6 | 221D | 4.95 | 36.9 | 5.92 | 48 | 4.66 | 44.5 | 4.95 | 42 | 6.11 | 38.6 | 4.66 | 45.3 | 5.21 |
| 7 | 234D | 4.12 | 47.4 | 3.58 | 44.8 | 4.05 | 56.1 | 4.78 | 43.1 | 4.73 | 41.5 | 4.29 | 49 | 4.26 |
| 8 | 243D | 6.48 | 38.1 | 4.76 | 41.6 | 4.97 | 45.7 | 4.46 | 43.9 | 4.15 | 52.4 | 6.22 | 49 | 5.17 |
| 9 | 313D | 3.15 | 31.6 | 3.18 | 45.5 | 3.7 | 44.8 | 3.91 | 41.2 | 3.27 | 45.8 | 4.67 | 36 | 3.65 |
| 10 | 324D | 3.89 | 39 | 3.81 | 44.7 | 3.53 | 45.6 | 3.3 | 41.9 | 3.4 | 48.3 | 4.14 | 32.9 | 3.68 |
| 11 | 331D | 4.31 | 39.8 | 4.5 | 36.8 | 5.14 | 33.3 | 4.25 | 33 | 5.35 | 35.7 | 3.94 | 45.9 | 4.58 |
| 12 | 342D | 3.36 | 35 | 3.85 | 40.8 | 3.69 | 34.6 | 3.89 | 47.5 | 3.88 | 36.6 | 3.97 | 29.1 | 3.77 |

The final results for dry blasting in terms of roughness (R_a) and peak density (RP_c) are tabulated in Table 4.2.

| ISO 4287 | | |
|---|--------------------|---|
| Amplitude parameters - Roughness profile | | |
| Rp | 16.8 μm | Gaussian filter, 0.8 mm |
| Rv | 21.5 μm | Gaussian filter, 0.8 mm |
| Rz | 38.2 μm | Gaussian filter, 0.8 mm |
| Rc | 26.6 μm | Gaussian filter, 0.8 mm |
| Rt | 43.4 μm | Gaussian filter, 0.8 mm |
| Ra | 6.90 μm | Gaussian filter, 0.8 mm |
| Rq | 8.50 μm | Gaussian filter, 0.8 mm |
| Rsk | -0.349 | Gaussian filter, 0.8 mm |
| Rku | 2.68 | Gaussian filter, 0.8 mm |
| Material Ratio parameters - Roughness profile | | |
| Rmr | 0.783 % | c = 1 μm under the highest peak, Gaussian filter, 0.8 mm |
| Rdc | 13.9 μm | p = 20%, q = 80%, Gaussian filter, 0.8 mm |
| Amplitude parameters - Primary profile | | |
| Pp | 26.2 μm | |
| Pv | 29.5 μm | |
| Pz | 55.8 μm | |
| Pc | 34.1 μm | |
| Pt | 55.8 μm | |
| Pa | 8.15 μm | |
| Pq | 10.3 μm | |
| Psk | -0.151 | |
| Pku | 2.91 | |
| Spacing parameters - Primary profile | | |
| PSm | 0.401 mm | |
| Pdq | 24.7 ° | |
| Peak parameters - Primary profile | | |
| PPc | 24.9 1/mm | +/-500 μm |
| Spacing parameters - Roughness profile | | |
| RSm | 0.265 mm | Gaussian filter, 0.8 mm |
| Rdq | 23.7 ° | Gaussian filter, 0.8 mm |
| Peak parameters - Roughness profile | | |
| RPc | 37.7 1/mm | +/-500 μm , Gaussian filter, 0.8 mm |

FIGURE 4.3: Sample parameter table

TABLE 4.2: Final profilometric results for dry blasting

| Trial | CODE | Ra | RPc |
|-------|------|---------------|------|
| - | - | μm | 1/mm |
| 1 | 111D | 7.44 | 47.6 |
| 2 | 122D | 7.5 | 36.2 |
| 3 | 133D | 7.43 | 36.3 |
| 4 | 144D | 7.24 | 45.6 |
| 5 | 212D | 4.91 | 56.1 |
| 6 | 221D | 4.95 | 42 |
| 7 | 234D | 4.29 | 49 |
| 8 | 243D | 4.97 | 45.7 |
| 9 | 313D | 3.7 | 44.8 |
| 10 | 324D | 3.81 | 44.7 |
| 11 | 331D | 4.5 | 36.8 |
| 12 | 342D | 3.85 | 40.8 |

• Variation of mean response with process parameters

The variation of the mean response (mean Ra) with the process parameters - grit size, standoff distance (SOD) & time - under dry conditions is tabulated in Tables 4.3, 4.4 & 4.5.

TABLE 4.3: Variation of mean response with grit size (dry)

| Grit size | | Mean response |
|-----------|--------|----------------------|
| CODE | (mesh) | Ra (μm) |
| 1 | 16 | 7.40 |
| 2 | 24 | 4.78 |
| 3 | 36 | 3.97 |

TABLE 4.4: Variation of mean response with SOD (dry)

| Standoff distance | | Mean response |
|-------------------|------|----------------------|
| CODE | (mm) | Ra (μm) |
| 1 | 60 | 5.35 |
| 2 | 80 | 5.42 |
| 3 | 100 | 5.41 |
| 4 | 120 | 5.35 |

TABLE 4.5: Variation of mean response with time (dry)

| Time | | Mean response |
|------|-----|----------------------|
| CODE | (s) | Ra (μm) |
| 1 | 30 | 5.63 |
| 2 | 45 | 5.42 |
| 3 | 60 | 5.37 |
| 4 | 75 | 5.11 |

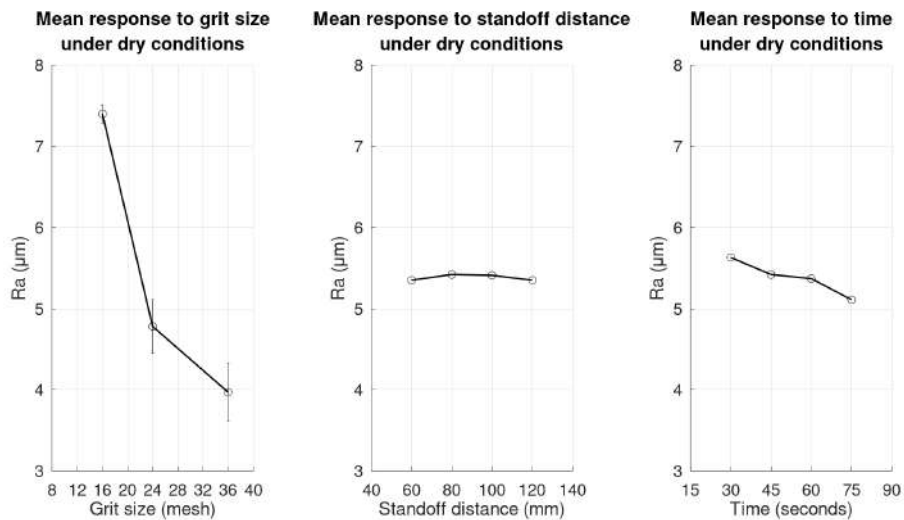


FIGURE 4.4: Variation of mean response with process parameters under dry conditions

Variation of mean response with grit size: Ra can be seen to decrease with mesh size. Higher the mesh size, lower is the grit size. Ra is maximum for 16 mesh (≈ 1 mm) and

then decreases monotonously for 24 mesh (≈ 0.65 mm) and 36 mesh (≈ 0.42 mm). Increase in grit size would be accompanied by a slight decrease in the number as well as the velocity of the abrasives striking the substrate surface but this would be overshadowed by the increase in the mass of abrasive particles. Consequently, abrasive particles of higher grit size are able to produce greater impact when they strike the substrate surface. This results in generation of deeper peaks and valleys and consequently, greater deviation from the nominal surface which is reflected in higher Ra values. The increase in Ra with grit size is consistent with the variation reported in the existing literature.

Variation of mean response with SOD: The variation of mean Ra with SOD is initially increasing up to SOD = 80 mm. At this point, Ra reaches its maximum. Further, with increase in SOD, Ra is reported to decrease slightly for SOD = 100 mm and then decrease further for SOD = 120 mm. This trend of Ra with SOD is consistent with that reported in the existing literature. Existing literature suggests Ra increases with SOD between 5D to 10D (D being the nozzle diameter) and then starts decreasing. The diameter of the induction nozzle used in our suction blasting machine is $D = 8$ mm. Consequently, 5D-10D corresponds to 40-80 mm. Ra is increasing with SOD from 60-80 mm, reaches maximum at 80 mm and then decreases with SOD, which is perfectly consistent with the existing literature.

At very low SOD, collisions between the impinging grits and the grits rebounding from the surface is high. This reduces the velocity and hence, subsequent impact of the impinging particles when they strike the substrate surface. Further, at low SODs, the impinging particles do not get enough room for accelerating to a certain velocity before they strike the substrate surface. As a result, Ra values are lower at lower SODs. With increase in SOD, the number of collisions between the impinging and rebounding grits reduce; also, the impinging grits get enough time to attain sufficiently high velocities. As a result, Ra values are reported to increase. However, at very high SODs, divergence of abrasive jet due to flaring within the atmosphere reduces the average grit velocity at impact, which is again reflected by a decrease in Ra.

Variation of mean response with time: The general trend for the variation of Ra with time is found to be a decreasing one, though the decrease is slight. Ra decreases with time from 30 to 45 s, then remains, more or less, constant from 45 to 60 s, and then decreases again for 75 s. In the existing literature, the general trend has been reported to be initially increasing, then decreasing before reaching a stable value. The initial phase of Ra increasing with time was attributed to attack of grits on previously unaffected areas. This depends on the substrate dimensions chosen. The initially increasing trend of Ra with time might be found if the experiments are repeated with substrates of greater dimensions. The absence of such an initial trend in our plot suggests that the entire substrate area was attacked by grit at or before

30 s. Subsequent decrease of Ra with time was due to the over-blasting effect coming into play. The initial decrease in Ra from 30 to 45 s might be due to the impinging grits cutting the previously generated surface asperities; thus reducing the roughness. Between 45 to 60 s, there is no significant variation in Ra with time which might be attributed to work hardening. Further decrease in Ra from 60 to 75 seconds can again be attributed to elimination of the remaining surface asperities by the impinging grits. This decrease is not likely to continue and Ra can be expected to reach a, more or less, stable value within 100-120 s, based on the existing literature.

• Analysis of variance (ANOVA)

ANOVA analysis of the Ra data for dry blasting trials was carried out to investigate the significance of each factor on Ra, taking p-value < 0.05 or F > 4 as significant. Further, percentage contributions of each parameter were calculated to determine the relative importance of each parameter. The results of ANOVA analysis are tabulated in Table 4.6.

TABLE 4.6: ANOVA analysis of the Ra data for dry blasting trials

| Sr. No. | Parameter | Degrees of freedom | Sum of squares | Mean squares | F-ratio | p-value | Contribution (%) |
|---------|-----------|--------------------|----------------|--------------|----------|----------|------------------|
| 1 | Grit size | 2 | 25.82067 | 12.91034 | 30.54913 | 0.010125 | 93.80491 |
| 2 | SOD | 3 | 0.02152 | 0.00717 | 0.01697 | 0.99635 | 0.07816 |
| 3 | Time | 3 | 0.41592 | 0.13864 | 0.32805 | 0.80781 | 1.51099 |
| 4 | Error | 3 | 1.26783 | 0.42261 | - | - | 4.60594 |
| Total | - | 11 | 27.52593 | - | - | - | 100 |

The above results suggest that grit size is a considerable parameter affecting surface roughness; further, its effect on surface roughness is far more influential than that of standoff distance and blasting time, which is consistent with the existing literature.

• Variation of peak density with roughness

Fig. 4.5 depicts the variation of peak density (RPc) with roughness (Ra) under dry conditions.

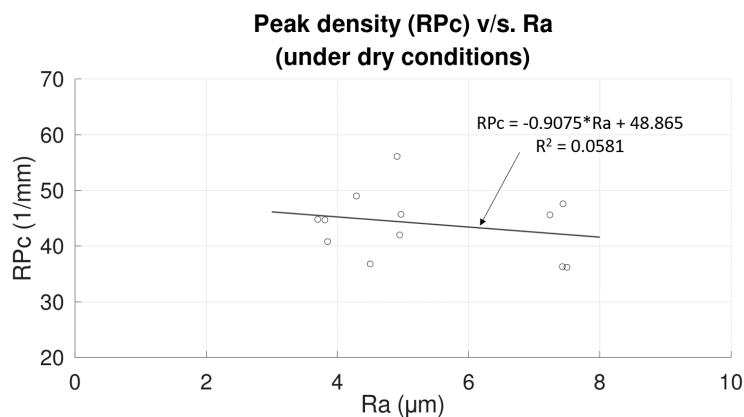


FIGURE 4.5: Variation of peak density (RPc) with Ra under dry conditions

Though the general trend observed based on the data collected is decreasing, the scatter of the data is huge, as a result of which, the correlation between RP_c & R_a is poor ($R^2 = 0.0581$). It can be concluded that RP_c and R_a vary, more or less, independently.

• Estimation of increment in contact area due to roughening

As mentioned in chapter 3, a mathematical model can be developed to estimate the increment in contact area due to roughening resulting from grit blasting. The surface asperities on a roughened surface can be modelled as conical peaks with an average height of twice R_a . The average number of peaks per unit length of the profile is equivalent to the peak density (RP_c) while the average base diameter of the conical asperities is mathematically equivalent to the reciprocal of peak density (RP_c). Having information about the number, height & base diameter of the conical asperities will enable us to estimate the approximate increment in contact area due to roughening. The approximation of an actual roughened surface using the above model is visualized in Fig. 4.6. The details of the model are presented in Fig. 4.7.

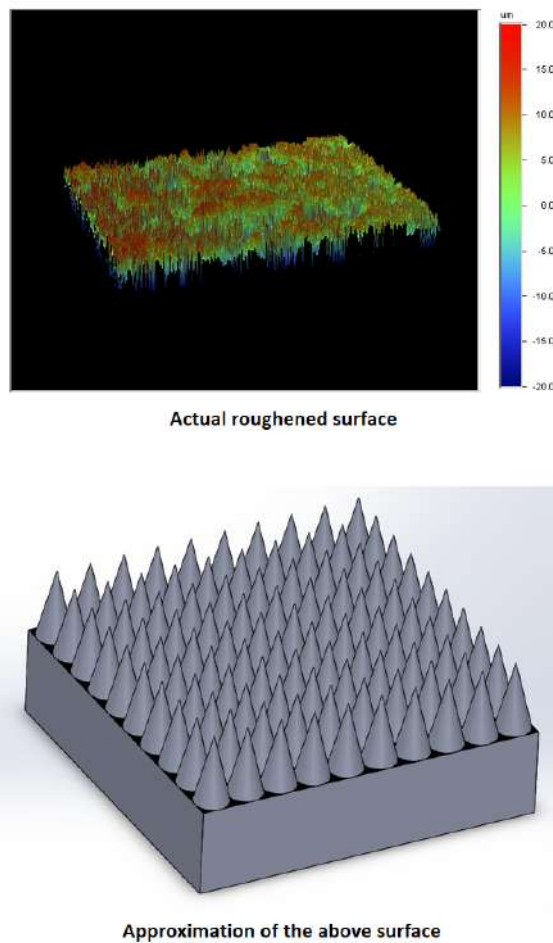


FIGURE 4.6: Approximation of a roughened surface

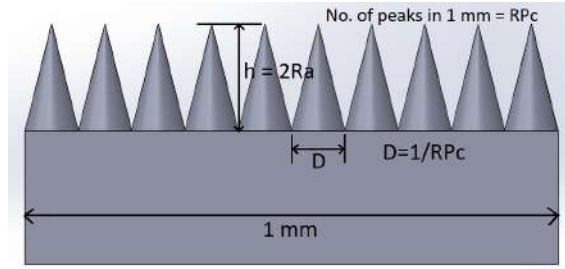


FIGURE 4.7: Details of approximating model

The contact area calculations are performed on a reference area of 1 mm^2 . Considering Ra to be in mm, D to be in mm & RPc to be in $1/\text{mm}$, the curved surface area (CSA) of a single conical asperity can be calculated as follows:

$$CSA = \pi r l \quad (4.1)$$

where

$$l = \sqrt{h^2 + r^2} \quad (4.2)$$

$$r = D/2 \text{ \& } D = 1/RPc \quad (4.3)$$

$$h = 2Ra \quad (4.4)$$

The total curved surface area (TCSA) of all conical asperities in a reference area of 1 mm^2 can be calculated as follows:

$$TCSA = RPc \times RPc \times CSA \quad (4.5)$$

Simplifying eqⁿ 4.5 using eqⁿs 4.1, 4.2, 4.3, & 4.4 gives:

$$TCSA = \frac{\pi}{2} \sqrt{(2RaRPc)^2 + \frac{1}{4}} \quad (4.6)$$

The flat contact area (FCA) in between the peaks (shown in black in Fig. 4.8) can be calculated as follows:

$$FCA = 1 - \left[RPc \times RPc \times \frac{\pi}{4} \times D^2 \right] \text{ mm}^2 \quad (4.7)$$

which simplifies to

$$FCA = 1 - \frac{\pi}{4} = \text{constant} \quad (4.8)$$

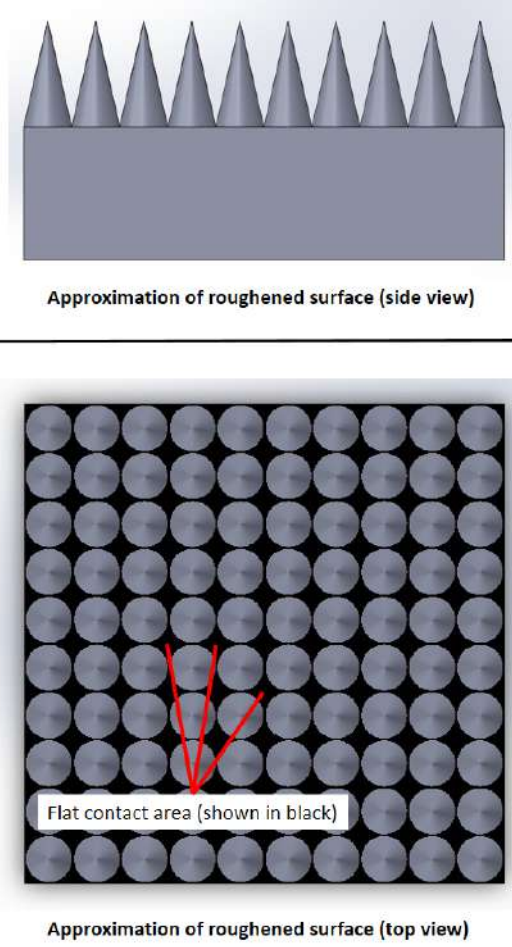


FIGURE 4.8: Flat contact area in between the peaks (shown in black in the top view)

The total contact area (TCA) provided by a roughened surface is equal to:

$$TCA = TCSA + FCA \quad (4.9)$$

The increment in contact area (ICA) per unit reference area due to roughening is, therefore, equal to:

$$ICA = TCSA + FCA - 1 \quad \text{mm}^2 \quad (4.10)$$

Simplifying eqⁿ 4.10 using eqⁿs 4.6 & 4.8 gives:

$$ICA = \frac{\pi}{2} \sqrt{(2RaRPc)^2 + \frac{1}{4}} - \frac{\pi}{4} \quad \text{mm}^2 \quad (4.11)$$

It was concluded earlier that Ra and RPc vary almost independently of each other. As a result, eqⁿ 4.11 suggests that the increment in contact area (ICA) due to roughening is a function of two independent variables: Ra and RPc . The variation of ICA with Ra and RPc is visualized in the Fig. 4.9. It can be seen that ICA increases with both Ra and RPc .

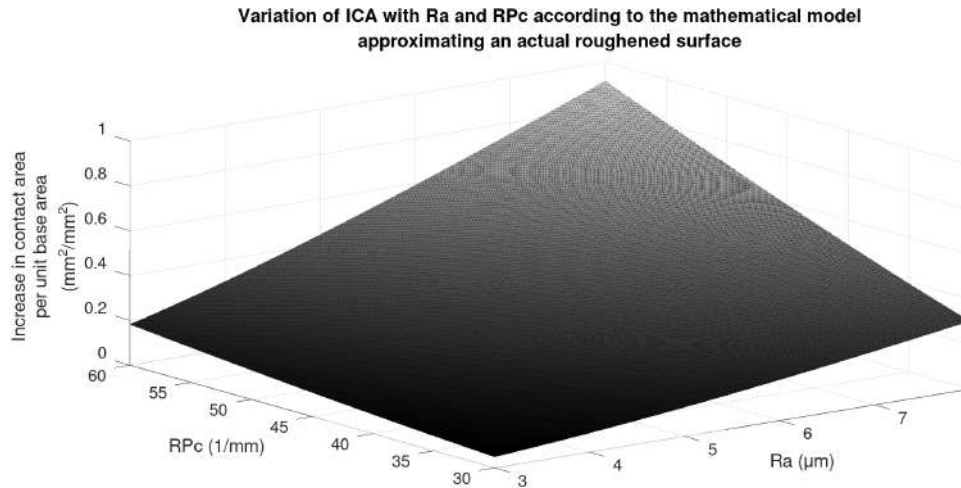


FIGURE 4.9: Variation of ICA with Ra and RPc

The increment in contact area per unit reference area is calculated for each of the 12 dry blasting experiments, based on the Ra and RPc data finalised for the same. The results are tabulated in Table 4.7.

TABLE 4.7: Increment in contact area for each dry blasting trial

| Trial | CODE | Ra | RPc | ICA |
|-------|------|---------------|---------------|---------------------------|
| - | - | μm | $1/\text{mm}$ | mm^2/mm^2 |
| 1 | 111D | 7.44 | 47.6 | 0.5765 |
| 2 | 122D | 7.5 | 36.2 | 0.3741 |
| 3 | 133D | 7.43 | 36.3 | 0.3699 |
| 4 | 144D | 7.24 | 45.6 | 0.5156 |
| 5 | 212D | 4.91 | 56.1 | 0.3832 |
| 6 | 221D | 4.95 | 42 | 0.2361 |
| 7 | 234D | 4.29 | 49 | 0.2407 |
| 8 | 243D | 4.97 | 45.7 | 0.2757 |
| 9 | 313D | 3.7 | 44.8 | 0.1570 |
| 10 | 324D | 3.81 | 44.7 | 0.1649 |
| 11 | 331D | 4.5 | 36.8 | 0.1567 |
| 12 | 342D | 3.85 | 40.8 | 0.1422 |

• Optimal set of process parameter levels

The final results for the dry blasting experiments are tabulated in Table 4.8. Maximum Ra is obtained for **trial 122D: grit size = 16 mesh, SOD = 80 mm, time = 45 s**. On the other hand, maximum contact area is obtained for **trial 111D: grit size = 16 mesh, SOD = 60 mm, time = 30 s**. Consequently, the optimal set of parameter levels for dry blasting trials is: **grit size = 16 mesh, SOD = 60 mm, time = 30 s**. A scatter plot showing the variation of ICA

with Ra & RPc for dry blasting trials is shown in Fig. 4.10. Fig. 4.11 shows the 3D surface profile of sample 111D.

TABLE 4.8: Optimal set of process parameters (dry)

| Trial | CODE | Ra μm | RPc 1/mm | ICA mm^2/mm^2 |
|-------|------|---------------------|-------------|----------------------------------|
| - | - | | | |
| 1 | 111D | 7.44 | 47.6 | 0.5765 |
| 2 | 122D | 7.5 | 36.2 | 0.3741 |
| 3 | 133D | 7.43 | 36.3 | 0.3699 |
| 4 | 144D | 7.24 | 45.6 | 0.5156 |
| 5 | 212D | 4.91 | 56.1 | 0.3832 |
| 6 | 221D | 4.95 | 42 | 0.2361 |
| 7 | 234D | 4.29 | 49 | 0.2407 |
| 8 | 243D | 4.97 | 45.7 | 0.2757 |
| 9 | 313D | 3.7 | 44.8 | 0.1570 |
| 10 | 324D | 3.81 | 44.7 | 0.1649 |
| 11 | 331D | 4.5 | 36.8 | 0.1567 |
| 12 | 342D | 3.85 | 40.8 | 0.1422 |

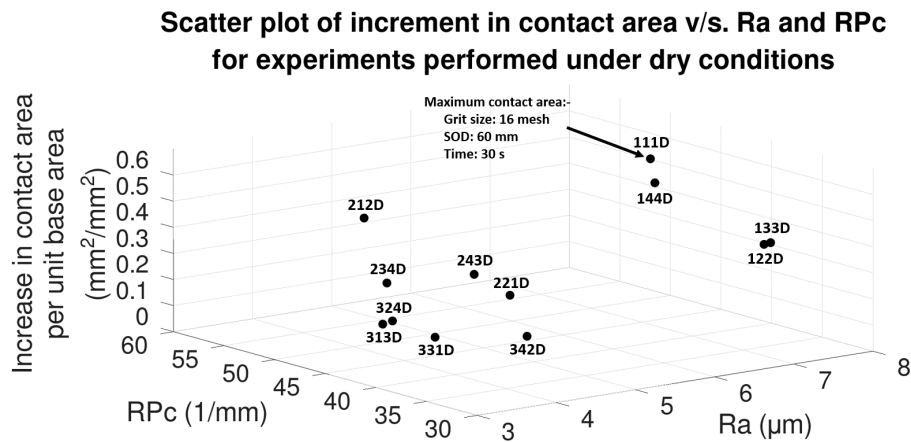


FIGURE 4.10: Scatter plot showing the variation of ICA with Ra and RPc for dry blasting trials

Different sets of parameter levels corresponding to maximum Ra and maximum ICA are possible because ICA depends on both Ra and RPc according to the mathematical model developed for approximating a roughened surface and as such, RPc was found to vary almost independently of Ra.

The existing literature on surface preparation using grit blasting has so far interpreted roughness only in terms of Ra which gives an estimation of the average deviation from the nominal surface. The interpretation of roughness in terms of the number of surface asperities

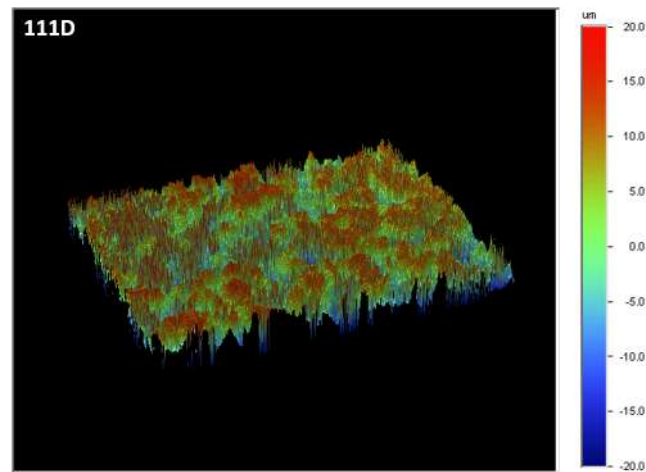


FIGURE 4.11: 3D surface profile of sample 111D

has been mostly ignored. Surface asperities, in addition to increasing contact area, also create opportunities for mechanical interlocking. Further, they act as activation sites for chemisorption and physisorption interactions responsible for coating adhesion.

In trial 122D, maximum Ra of 7.5 μm was achieved with a peak density of 36.2 1/mm. Ra obtained for trial 111D was lower (7.44 μm) but the decrease in Ra was overshadowed by an increase in peak density (RPc = 47.6 1/mm for trial 111D), leading to a higher contact area. Consequently, the optimal parameter levels obtained with respect to maximum Ra were different with those obtained with respect to maximum contact area. This highlights the need for future work on determining the parameters affecting the number of surface asperities i.e. peak density. It is possible that peak density is affected by the same process parameters that affect Ra. In that case, as Ra and RPc were found to vary nearly independently, the variation of RPc with the process parameters may not be in sync with that of Ra. In that case, a compromise in selection of optimal parameter levels is necessary. Further, it is also possible that there are some additional parameters which affect RPc but have not been known to affect Ra. In that case, it is necessary to find such parameters. This forms one of the potential areas for future research on the topic.

• Microhardness evaluation

Vickers hardness measurements were carried out at a load of 50 gf (dwell time: 10 s) and at depths of 40, 100, 150 & 200 μm from the grit blasted surface of sample 122D. The Vickers indentations made at various depths on sample 122D are visible in Fig. 4.12. The microhardness calculations for sample 122D (grit size: 16 mesh, SOD: 80 mm, time: 45 s, environment: dry) are detailed in Table 4.9.

TABLE 4.9: Microhardness data for 122D

| Depth from grit blasted surface | d ₁ | d ₂ | HV0.05 | Avg. HV0.05 | Std. dev. HV0.05 |
|---------------------------------|----------------|----------------|-------------------|-------------|------------------|
| μm | μm | μm | kgf/mm^2 | | |
| 40 | 17.85 | 18.57 | 279.6 | 275.5 | 3.2 |
| | 18.16 | 18.6 | 274.5 | | |
| | 18.15 | 18.52 | 275.8 | | |
| | 18.62 | 18.31 | 271.9 | | |
| 100 | 18.54 | 18.63 | 268.4 | 265.4 | 5.2 |
| | 18.22 | 19.28 | 263.7 | | |
| | 18.68 | 19.17 | 258.9 | | |
| | 18.22 | 18.8 | 270.6 | | |
| 150 | 18.18 | 19.08 | 267.1 | 256.9 | 7.7 |
| | 18.85 | 19.52 | 251.9 | | |
| | 19.4 | 19.1 | 250.2 | | |
| | 18.9 | 19 | 258.2 | | |
| 200 | 19.22 | 19.88 | 242.6 | 244.6 | 6.8 |
| | 19.53 | 18.65 | 254.4 | | |
| | 19.28 | 19.84 | 242.3 | | |
| | 19.58 | 19.81 | 239 | | |

The final results showing the variation of average Vickers hardness with depth are summarized in Table 4.10.

TABLE 4.10: Variation of Vickers hardness with depth from grit blasted surface for 122D

| Depth from grit blasted surface | Avg. HV0.05 | Std. dev. HV0.05 |
|---------------------------------|-------------------|------------------|
| μm | kgf/mm^2 | |
| 40 | 275.5 | 3.2 |
| 100 | 265.4 | 5.2 |
| 150 | 256.9 | 7.7 |
| 200 | 244.6 | 6.8 |

The variation of average cross-section Vickers hardness with depth from the grit blasted surface for sample 122D is shown in Fig. 4.13.

Bulk hardness substrate hardness was determined to be 231.4 ± 9.9 HV0.05 (kgf/mm^2). Considerable work hardening of the surface results due to grit blasting which is visible in Fig. 4.13. Maximum hardness is reported near the surface. The influence of work hardening declines with depth; consequently hardness values are found to decrease gradually with depth up to a certain depth where it attains the bulk hardness level. The heat generated during grit blasting is mostly received by the surface & sub-surface regions, while the bulk material doesn't receive any heat. Heat generation influences work hardening and hence, in turn, determines the depth of the affected layer. From the collected data visualized in Fig. 4.13, it is clear that the bulk hardness is attained at a depth near 300 μm . Extrapolation using best fit line ($R^2 = 0.9906$) suggests that bulk hardness would be achieved at a depth of approximately 300.83 μm ; consequently, the depth of the affected layer is around 300.83 μm .

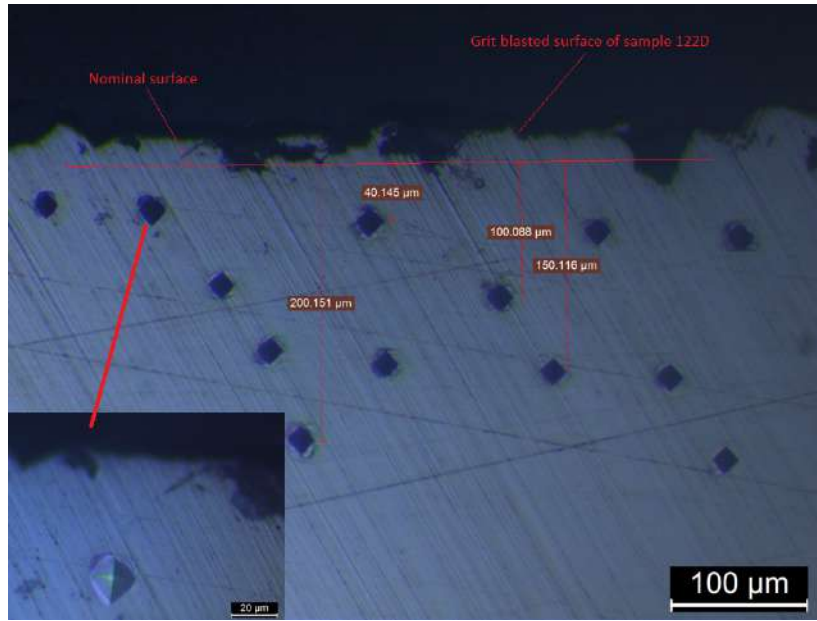


FIGURE 4.12: Vickers indentations on the cross-section of 122D at depths of 40, 100, 150 & 200 μm from the grit blasted surface

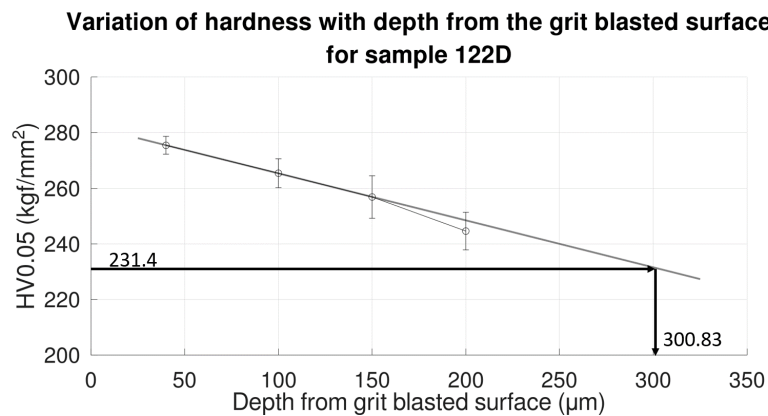


FIGURE 4.13: Variation of cross-section Vickers hardness with depth from the grit blasted surface for sample 122D

• X-Ray Diffraction (XRD) analysis

The XRD pattern for sample 133D (tested under: grit size=16 mesh, SOD = 100 mm, time = 60 s, environment = dry) is shown in Fig. 4.14.

The occurrence of α -Fe on the grit blasted surface indicates that no change in nascent surface metallurgy occurred due to grit blasting, which is consistent with the existing literature. The presence of Al_2O_3 peaks suggests entrapment of grit residues at some locations over the surface.

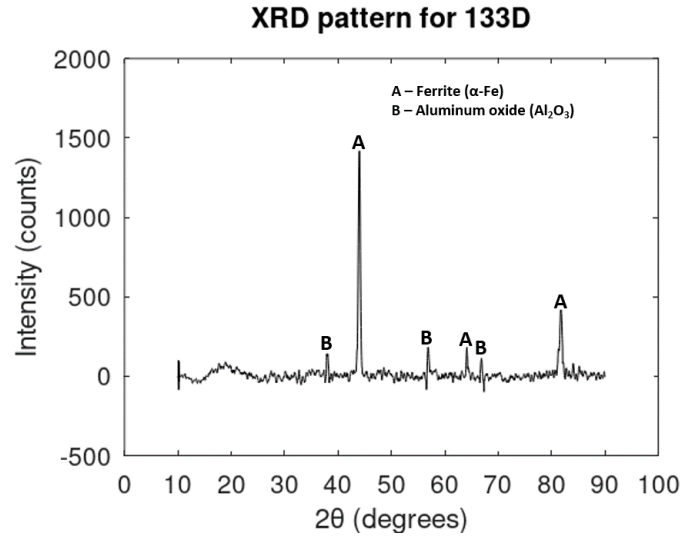


FIGURE 4.14: XRD pattern for 133D

• Sub-surface microstructure study using optical microscopy & FESEM

Figures 4.15 & 4.16 show the surface & sub-surface regions of sample 111D. These images were captured at 1000X magnification using Leica DM IL LED inverted microscope.

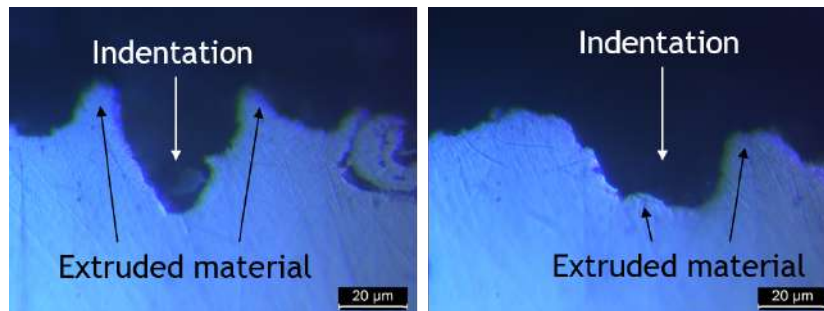


FIGURE 4.15: Surface & sub-surface regions of sample 111D showing indentation and extrusion

Signatures of indentation & extrusion of the area peripheral to the indentation area are visible Fig. 4.15. This suggests that indentation is the dominant mechanism of material removal and roughness generation under the set of conditions maintained during grit blasting of sample 111D. This is as per the expectations. Existing literature suggests that micro-cutting & shearing are dominant at lower angles of impingement while indentation & extrusion are dominant at higher angles (i.e. angles near 90°). The angle of impingement was maintained constant throughout the experiments at 80° ; hence, the aforementioned observations are as per the expectations. At higher impingement angles, the grits tend to indent the substrate surface. This leads to extrusion of the material in the vicinity of the indentation area which is visible in Fig. 4.15.

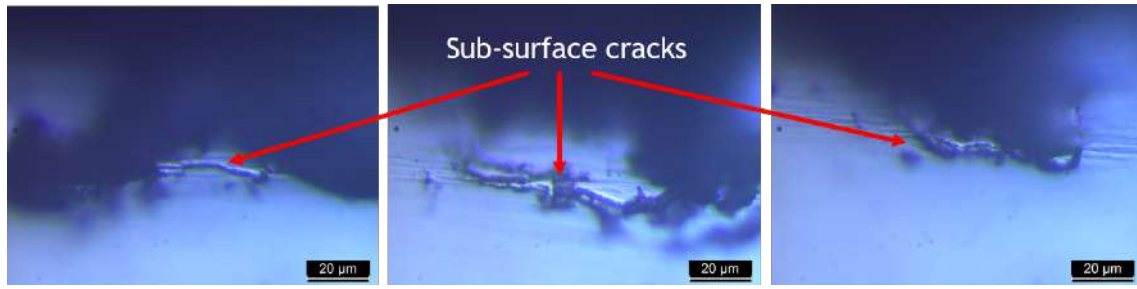


FIGURE 4.16: Sub-surface cracks near the grit-blasted surface of sample 111D

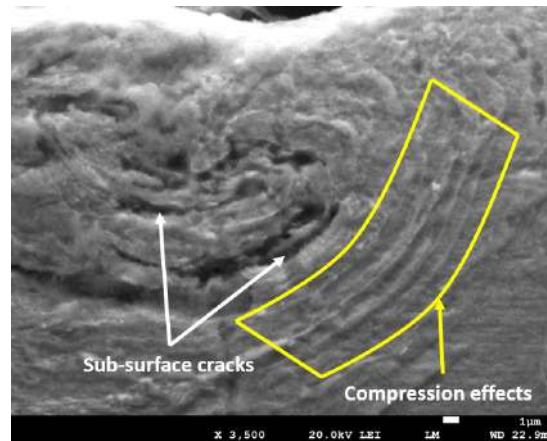


FIGURE 4.17: SEM micrograph of a sub-surface region of sample 111D showing sub-surface cracks

Sub-surface cracks propagating in horizontal direction are visible in Fig. 4.16. These cracks are generated due to compressive residual stresses & thermal stresses and are detrimental to the mechanical properties of the coating-substrate system. Sub-surface damage is quite substantial for sample 111D. Though compressive residual stresses improve surface fatigue strength, they also lead to an appreciable amount of sub-surface damage.

Fig. 4.17 is an SEM micrograph (3500X) of a sub-surface region of sample 111D. Sub-surface cracks have been highlighted in the micrograph. Deformation effects of grit blasting are visible in the regions surrounding the cracks. The microstructure in the vicinity of the grit blasted surface undergoes significant deformation in the form of grain elongation. Grain elongation increases the effective grain boundary perimeter. As grain boundaries act as a barrier to dislocation motion, this results in improvement in the strength & hardness of the sub-surface regions.

4.1.2 Water

The final profilometric results for grit blasting carried out in a wet environment of water are tabulated in Table 4.11:

TABLE 4.11: Final profilometric results for grit blasting carried out in a wet environment of water

| Trial | CODE | Ra | RPc |
|-------|------|---------------|------|
| - | - | μm | 1/mm |
| 1 | 111W | 6.66 | 40.9 |
| 2 | 122W | 7.22 | 47 |
| 3 | 133W | 7.39 | 42.7 |
| 4 | 144W | 6.44 | 45.1 |
| 5 | 212W | 4.58 | 46.1 |
| 6 | 221W | 4.36 | 36.9 |
| 7 | 234W | 4.81 | 41.1 |
| 8 | 243W | 5.06 | 45.2 |
| 9 | 313W | 3.73 | 39.4 |
| 10 | 324W | 3.47 | 50.1 |
| 11 | 331W | 3.5 | 45 |
| 12 | 342W | 3.69 | 41.1 |

A one-to-one comparison of the results in terms of Ra obtained for each trial under dry and wet (water) conditions is visualized in the Fig. 4.18.

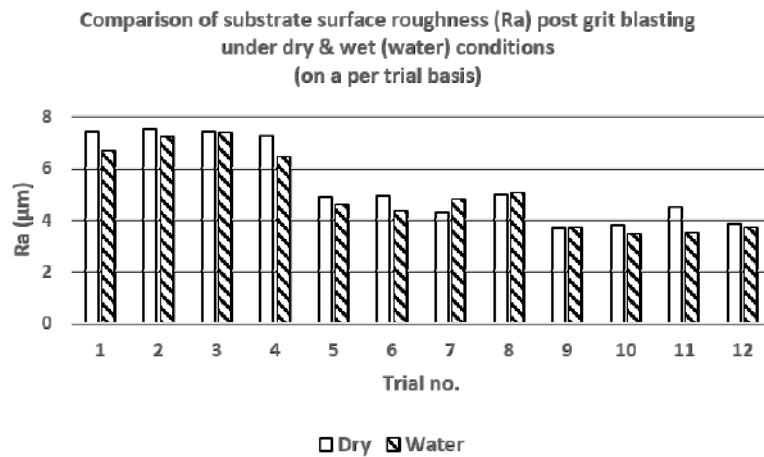


FIGURE 4.18: Comparison of results obtained for each trial under dry and wet (water) conditions in terms of Ra

Majority of the points for the wet (water) trials fall below their dry counterparts. Only three points lie above (234W, 243W, 313W). This can be attributed to pressure variation. Wet experiments for time periods of 60 and 75 s are required to be performed in an intermittent

manner to replenish the medium for supply during blasting. For example, wet experiments of time period 60 s are required to be performed in two steps of 30 s each while those of 75 s are required to be performed in steps of 30 s and 45 s respectively. After the first step, the pressure is raised again to 6 bar and the next step is started again from 6 bar. As a result, the average pressure during wet blasting trials of 60 and 75 s was slightly higher than their dry blasting counterparts. Overall, it can be conveniently concluded that roughness values are lower for wet blasting in comparison to dry blasting. The continuous presence of a layer of water over the substrate surface during blasting creates an environment for greater heat dissipation which prevents any appreciable increase in substrate ductility and diminishes the susceptibility of the surface to greater deformation. Further, the impinging grits are deflected and decelerated due to the density effects of water. As a result, lower Ra values are expected.

• Variation of mean response with process parameters

The variation of the mean response (mean Ra) to the process parameters - grit size, standoff distance (SOD) & time - under wet conditions (water) is tabulated in Tables 4.12, 4.13 & 4.14.

TABLE 4.12: Variation of mean response with grit size (water)

| Grit size | | Mean response |
|-----------|--------|----------------------|
| CODE | (mesh) | Ra (μm) |
| 1 | 16 | 6.93 |
| 2 | 24 | 4.70 |
| 3 | 36 | 3.60 |

TABLE 4.13: Variation of mean response with SOD (water)

| Standoff distance | | Mean response |
|-------------------|------|----------------------|
| CODE | (mm) | Ra (μm) |
| 1 | 60 | 4.99 |
| 2 | 80 | 5.02 |
| 3 | 100 | 5.23 |
| 4 | 120 | 5.06 |

TABLE 4.14: Variation of mean response with time (water)

| Time | | Mean response |
|------|-----|----------------------|
| CODE | (s) | Ra (μm) |
| 1 | 30 | 4.84 |
| 2 | 45 | 5.16 |
| 3 | 60 | 5.39 |
| 4 | 75 | 4.91 |

The variation of mean response with process parameters under wet conditions (water) is shown in Fig. 4.19. A comparison of the variation of mean response with process parameters under dry & wet (water) conditions is visualized in Fig. 4.20.

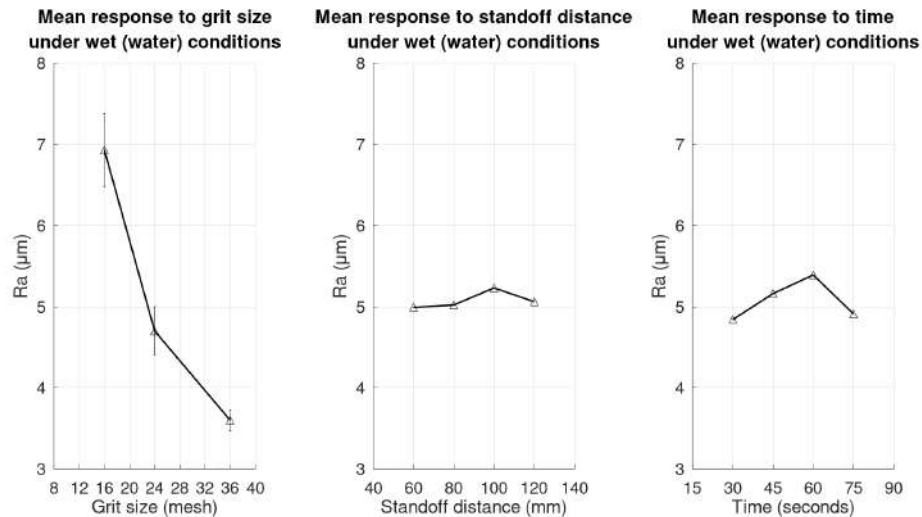


FIGURE 4.19: Variation of mean response with process parameters under wet conditions (water)

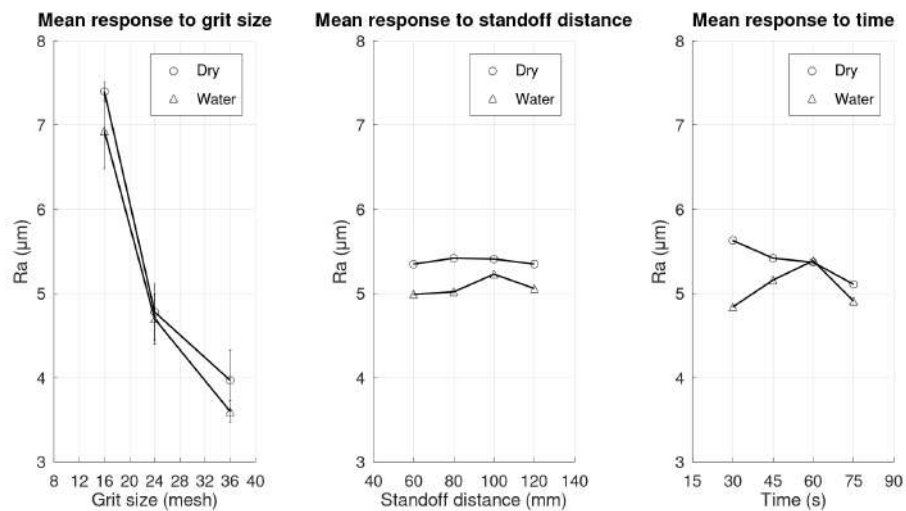


FIGURE 4.20: Comparison of variation of mean response with process parameters under dry and wet (water) conditions

Variation of mean response with grit size: Ra increases with grit size (decreases with mesh size) as was observed under dry conditions. Mean Ra values for each grit size are lower than their counterparts under dry conditions; otherwise, the presence of medium doesn't have an effect on the variation of Ra with grit size.

Variation of mean response with SOD: The variation of mean Ra with SOD is initially increasing up to SOD = 100 mm (where it attains its maximum) and then falls for SOD = 120 mm. In comparison to dry blasting, the location of the maximum has shifted to one level on the higher side i.e. the location of the maximum has shifted from SOD = 80 mm (under dry conditions) to SOD = 100 mm (under wet (water) conditions). Splashing of the medium during grit blasting results in deflection & deceleration of the impinging grits. Higher the density of the medium, greater would be the hindrance to the motion of the impinging grits. Further, these density effects are higher at lower SODs. The presence of a medium over the substrate surface (in this case, water) reduces the effective SOD. This results in the maximum mean response being achieved at slightly higher SODs compared to that observed under dry conditions. Overall, it can be concluded that the nature of variation of Ra with SOD is conserved under wet conditions; only, the location of the maximum shifts towards higher SODs.

Variation of mean response with time: Mean Ra increases with time initially up to time = 60 s and then falls for 75 s.

Existing literature on dry blasting suggests that in dry blasting, Ra initially increases with time and decreases later before it attains a stable value. The initial phase corresponding to increase in Ra with time was attributed to attack of grits on previously unaffected areas. It was reasoned earlier that due to smaller substrate dimensions, the entire surface must have been affected by grits within 30 s and during subsequent blasting, the over-blasting effect came into play which resulted in a slight decrease in Ra; as a result, the initial phase corresponding to an increase in Ra with time was not observed by the authors under dry conditions.

Under wet (water) conditions, it is observed that mean Ra increases with time initially up to 60 s and then falls for 75 s. The initial phase corresponding to an increase in Ra with time is being observed under wet (water) conditions and this can be attributed to the fact that the presence of a medium delays the contact of grits with the substrate surface. It is possible that due to the presence of a medium, some areas of the substrate surface remain unaffected for some time. The proportion of unaffected areas reduce with time as they get attacked by grits due to which Ra is observed to increase initially with time only up to some point. Thus, it can be concluded that the nature of variation of Ra with time is conserved under wet conditions as well; however, the initiation of roughening is delayed to some extent.

• Variation of peak density with roughness

Fig. 4.21 depicts the variation of peak density (RPc) with roughness (Ra) under wet (water) conditions. Comparison of the same with that under dry conditions is shown in Fig. 4.22. Once again, the scatter of RPc v/s. Ra data is very huge. The correlation between RPc & Ra under wet (water) conditions is poorer ($R^2 = 0.0037$). Hence, it can be concluded that RPc and Ra vary, more or less, independently under wet conditions as well.

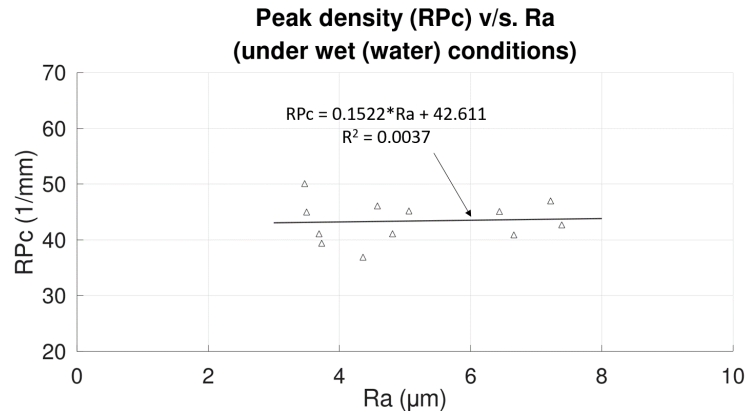


FIGURE 4.21: Variation of peak density (RPc) with Ra under wet (water) conditions

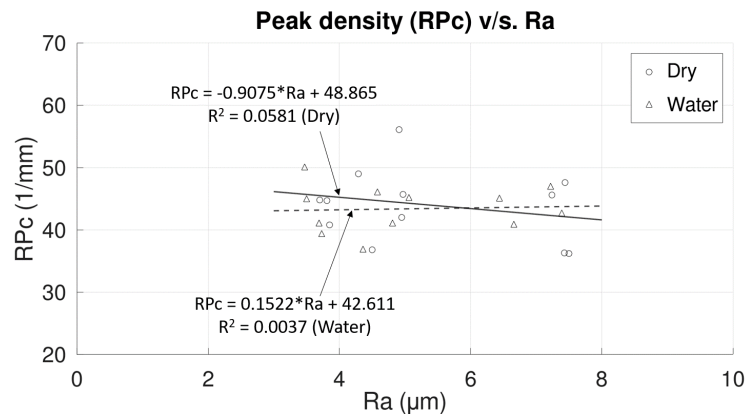


FIGURE 4.22: Comparison of variation of peak density (RPc) with Ra under dry & wet (water) conditions

• Estimation of increment in contact area due to roughening

The increment in contact area per unit reference area is calculated for each of the 12 grit blasting experiments performed under wet (water) conditions, based on the Ra and RPc data finalised for the same. The results are tabulated in Table 4.15.

• Optimal set of process parameter levels

The final results for the grit blasting experiments performed under wet (water) conditions are tabulated in Table 4.16. Maximum Ra is obtained for **trial 133W: grit size = 16 mesh, SOD = 100 mm, time = 60 s, environment = water**. On the other hand, maximum contact area is obtained for **trial 122W: grit size = 16 mesh, SOD = 80 mm, time = 45 s, environment = water**. Consequently, the optimal set of parameter levels for grit blasting trials carried out in an environment of water are: **grit size = 16 mesh, SOD = 80 mm, time = 45 s**. A scatter plot showing the variation of ICA with Ra & RPc for grit blasting trials performed under wet

TABLE 4.15: Increment in contact area for each grit blasting trial carried out in a wet environment of water

| Trial | CODE | Ra | RPc | ICA |
|-------|------|---------------|------|-----------------------------|
| - | - | μm | 1/mm | $\text{mm}^2 / \text{mm}^2$ |
| 1 | 111W | 6.66 | 40.5 | 0.3761 |
| 2 | 122W | 7.22 | 47 | 0.5387 |
| 3 | 133W | 7.39 | 42.7 | 0.4794 |
| 4 | 144W | 6.44 | 45.1 | 0.4185 |
| 5 | 212W | 4.58 | 46.1 | 0.2426 |
| 6 | 221W | 4.36 | 36.9 | 0.1486 |
| 7 | 234W | 4.81 | 41.1 | 0.2159 |
| 8 | 243W | 5.06 | 45.2 | 0.2791 |
| 9 | 313W | 3.73 | 39.4 | 0.1257 |
| 10 | 324W | 3.47 | 50.1 | 0.1712 |
| 11 | 331W | 3.5 | 45 | 0.1429 |
| 12 | 342W | 3.69 | 41.1 | 0.1332 |

(water) conditions is shown in Fig. 4.23. Fig. 4.24 shows the 3D surface profile of sample 122W.

TABLE 4.16: Optimal set of process parameters (water)

| Trial | CODE | Ra | RPc | ICA |
|-------|------|---------------|------|-----------------------------|
| - | - | μm | 1/mm | $\text{mm}^2 / \text{mm}^2$ |
| 1 | 111W | 6.66 | 40.5 | 0.3761 |
| 2 | 122W | 7.22 | 47 | 0.5387 |
| 3 | 133W | 7.39 | 42.7 | 0.4794 |
| 4 | 144W | 6.44 | 45.1 | 0.4185 |
| 5 | 212W | 4.58 | 46.1 | 0.2426 |
| 6 | 221W | 4.36 | 36.9 | 0.1486 |
| 7 | 234W | 4.81 | 41.1 | 0.2159 |
| 8 | 243W | 5.06 | 45.2 | 0.2791 |
| 9 | 313W | 3.73 | 39.4 | 0.1257 |
| 10 | 324W | 3.47 | 50.1 | 0.1712 |
| 11 | 331W | 3.5 | 45 | 0.1429 |
| 12 | 342W | 3.69 | 41.1 | 0.1332 |

• Microhardness evaluation

Vickers hardness measurements were carried out at a load of 50 gf (dwell time: 10 s) and at depths of 40, 100, 150 & 200 μm from the grit blasted surface of sample 122W. The Vickers indentations made at various depths on sample 122W are visible in Fig. 4.25. The final results showing the variation of average Vickers hardness with depth for sample 122W (grit size: 16 mesh, SOD: 80 mm, time: 45 s, environment: water) are summarized in Table 4.17.

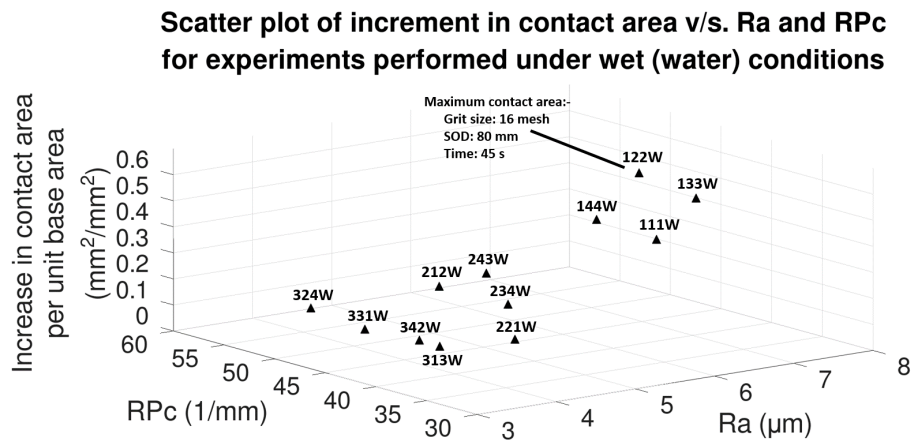


FIGURE 4.23: Scatter plot showing the variation of ICA with Ra and RPc for experiments performed under wet (water) conditions

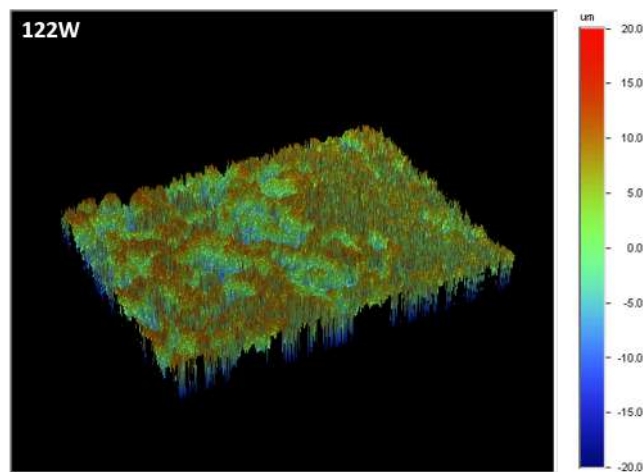


FIGURE 4.24: 3D surface profile of sample 122W

TABLE 4.17: Variation of Vickers hardness with depth from grit blasted surface for 122W

| Depth from grit blasted surface | Avg. HV0.05 | Std. dev. HV0.05 |
|---------------------------------|-------------------|------------------|
| μm | kgf/mm^2 | |
| 40 | 262.3 | 14.2 |
| 100 | 255.2 | 12.5 |
| 150 | 248.4 | 4.4 |
| 200 | 242.6 | 4.6 |

The variation of average cross-section Vickers hardness with depth from the grit blasted surface for sample 122W is shown in Fig. 4.26.

The comparison of the variation of microhardness with depth between samples 122D & 122W is shown in Fig. 4.27.

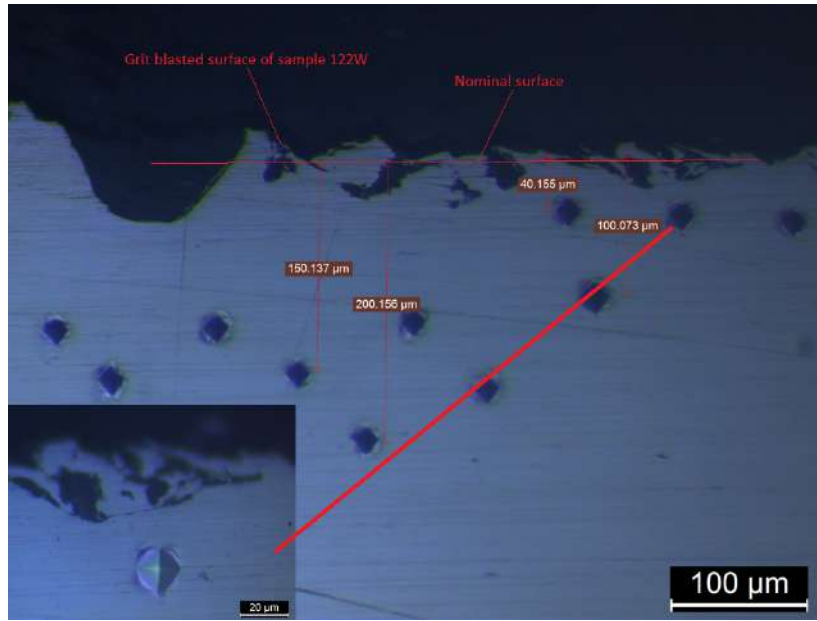


FIGURE 4.25: Vickers indentations on the cross-section of 122W at depths of 40, 100, 150 & 200 μm from the grit blasted surface

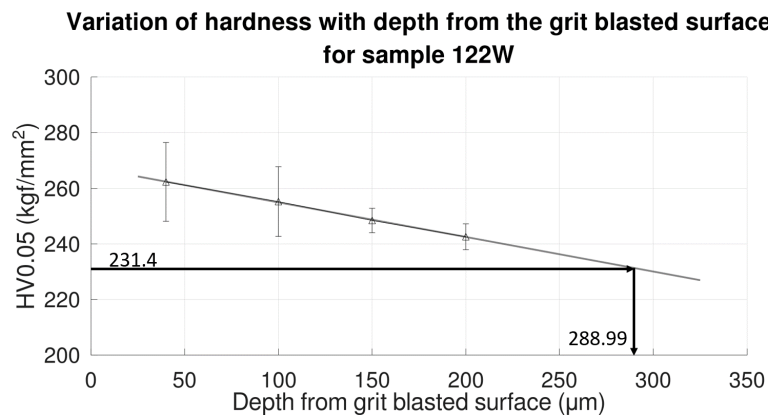


FIGURE 4.26: Variation of cross-section Vickers hardness with depth from the grit blasted surface for sample 122W

Microhardness values at the same depths are consistently lower for 122W as compared to 122D. Further, it is clear from the hardness data for 122W that bulk hardness would be attained between 250-300 μm . Extrapolation using a best fit line ($R^2 = 0.9992$) suggests that bulk hardness would be achieved at a depth of approximately 288.99 μm ; consequently, the depth of the affected layer is around 288.99 μm which is lower than that obtained for 122D. This suggests a decrease in the level of work hardening under wet (water) conditions which is as per the expectations. Supply of water at the surface during grit blasting deflects & decelerates the impinging grits to some extent, slightly reducing the impact they generate on striking the surface. Further, supply of water during grit blasting also improves heat

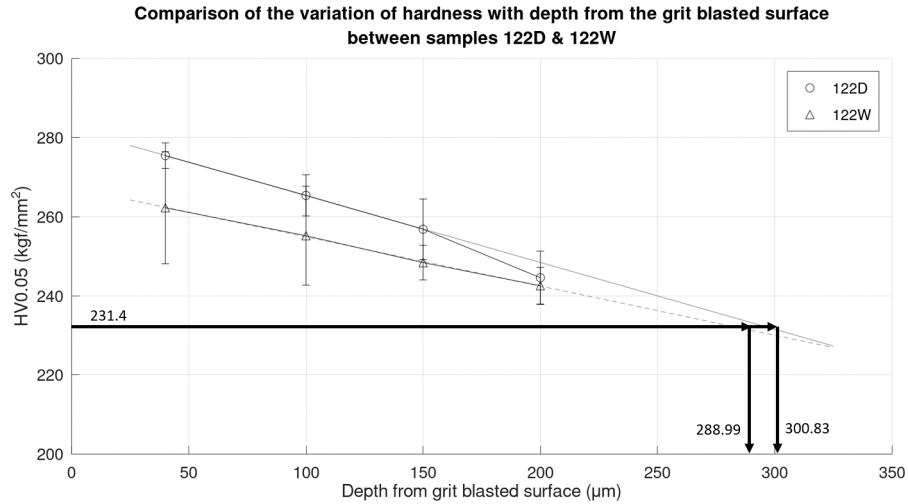


FIGURE 4.27: Comparison of the variation of microhardness with depth for samples 122D & 122W

dissipation from the surface & sub-surface regions. The reduction in the impact produced by the impinging grits on the surface coupled with improved heat dissipation from the surface & sub-surface regions is, thus, reflected in the reduced microhardness values & depth of the affected layer.

• X-Ray Diffraction (XRD) analysis

The XRD pattern for sample 133W (tested under: grit size=16 mesh, SOD = 100 mm, time = 60 s, environment = water) is shown in Fig. 4.28.

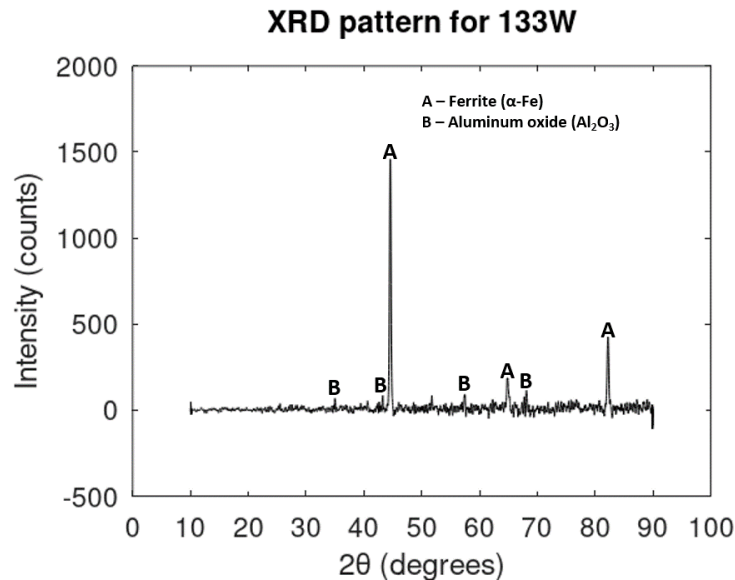


FIGURE 4.28: XRD pattern for 133W

Occurrence of α -Fe peaks in the pattern suggests that there is no change in nascent surface metallurgy post grit blasting under wet conditions as well. Grit residue was once again detected; its presence being validated by occurrence of Al_2O_3 peaks in the XRD pattern. However, Al_2O_3 peaks are less prominent than those observed in the diffraction pattern of sample 133D. This suggests slightly a lower proportion of grit residue being entrapped over the surface when blasting is carried out in the presence of a medium (in this case, water), though this is just a preliminary conclusion. Susceptibility of surface to deformation is lower when blasting is carried out in the presence of water due to better heat dissipation. This results in creation of lesser, smaller craters over the surface - as the number & size of these craters reduce, so do the grit residues entrapped in these surface features. However, as mentioned earlier, the conclusions arrived at by observing the relative intensity of Al_2O_3 peaks under dry & wet (water) conditions are preliminary conclusions & further, research is necessary to validate them.

• Sub-surface microstructure study using optical microscopy, FESEM & EDS

Fig. 4.29 shows the surface & sub-surface regions of sample 122W. These images were captured at 1000X magnification using Leica DM IL LED inverted microscope.

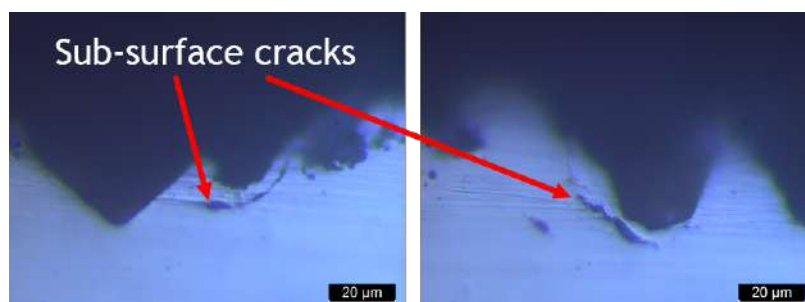


FIGURE 4.29: Sub-surface cracks near the grit-blasted surface of sample 122W

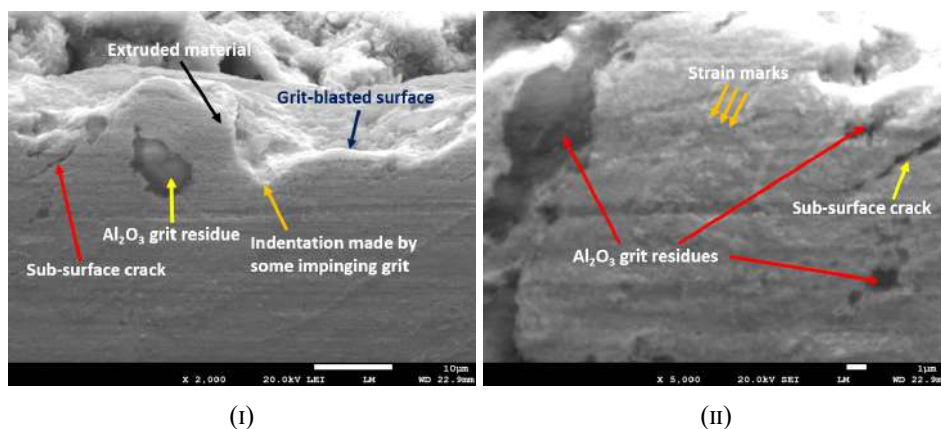


FIGURE 4.30: SEM micrographs of sub-surface regions of sample 122W

Sub-surface cracks can be seen in Fig. 4.29 & also in the SEM micrographs presented in Fig. 4.30. However, evaluation of the sub-surface regions throughout the sample length using optical microscopy revealed a lower level of sub-surface damage in the form of cracks as compared to that observed under dry conditions. This can be attributed mainly to the reduction in the level of thermal stresses generating within the sub-surface regions due to better heat dissipation through the medium (in this case, water). SEM micrographs show Al_2O_3 grit residues entrapped within the surface. The presence of craters near the grit blasted surface & corresponding extrusion of material in the periphery of the craters supports the claim that indentation & extrusion are the dominant mechanisms of material removal & roughness generation at higher impingement angles. Strain marks characteristic of the deformation pattern induced by grit blasting are also visible.

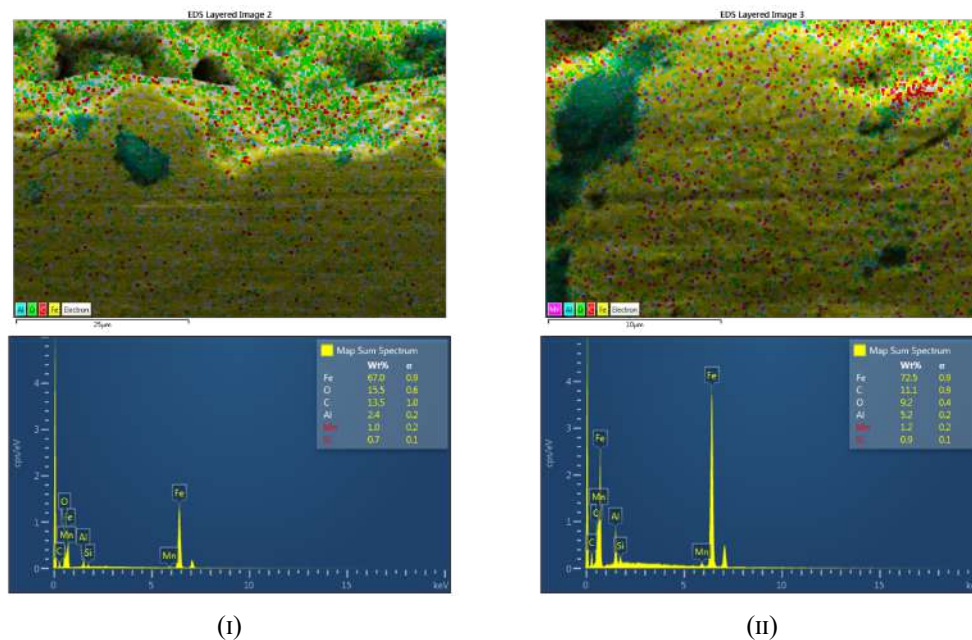


FIGURE 4.31: EDS layered images of sub-surface regions of sample 122W & their corresponding spectra

EDS results are in agreement with the XRD results i.e. only the elements corresponding to ferrite (α -Fe) & Al_2O_3 are detected by EDS.

4.1.3 Saline water

It is known that grit size is the most influential process parameter affecting Ra. Also, all the optimal parameter level sets have fallen within the 16 mesh domain. The variation of mean response with process parameters in saline water environment can be expected to be similar to that obtained under wet (water) conditions. No additional information is expected to be revealed from 24 mesh and 36 mesh experiments. Hence, experiments under saline water & alcoholic environments are performed for 16 mesh only.

The final profilometric results for 16 mesh experiments carried in a wet environment of saline water are tabulated in Table 4.18.

TABLE 4.18: Final profilometric results for 16 mesh trials carried out in a wet environment of saline water

| Trial | CODE | Ra | RPc |
|-------|------|---------------|------|
| - | - | μm | 1/mm |
| 1 | 111S | 6.53 | 41.5 |
| 2 | 122S | 6.63 | 42.8 |
| 3 | 133S | 6.72 | 45.5 |
| 4 | 144S | 6.04 | 46.7 |

A one-to-one comparison of results in terms of Ra obtained for each 16 mesh trial performed in dry, water & saline water environments is visualized in the Fig. 4.32.

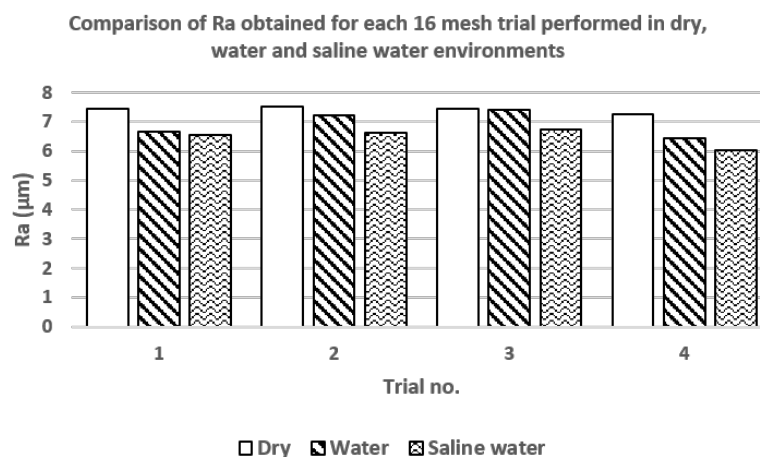


FIGURE 4.32: Comparison of results obtained for each 16 mesh trial performed in dry, water and saline water environments in terms of Ra

Ra values are in the order: Dry > Water > Saline water. It was argued that Ra values for surfaces grit blasted in the presence of water are lower than dry blasted surfaces because better heat dissipation by water reduces the susceptibility of surface to greater deformation; also, supply of water during grit blasting was argued to hinder the motion of grits. Saline

water has a higher heat capacity than water leading to even greater heat dissipation. Further, saline water also has a higher density than water and hence, it will result in greater deflection & deceleration of the impinging grits. This will lead to even lower Ra values as the results suggest.

• Estimation of increment in contact area due to roughening

The increment in contact area per unit reference area is calculated for each of the four 16 mesh experiments performed in a saline water environment, based on the Ra and RPc data finalised for the same. The results are tabulated in Table 4.19.

TABLE 4.19: Increment in contact area for 16 mesh trials carried out in a wet environment of saline water

| Trial | CODE | Ra | RPc | ICA |
|-------|------|---------------|------|---------------------------|
| - | - | μm | 1/mm | mm^2/mm^2 |
| 1 | 111S | 6.53 | 41.5 | 0.3729 |
| 2 | 122S | 6.63 | 42.8 | 0.4027 |
| 3 | 133S | 6.72 | 45.5 | 0.4554 |
| 4 | 144S | 6.04 | 46.7 | 0.3987 |

• Optimal set of process parameter levels

The final results for the grit blasting experiments performed in a saline water environment are tabulated in Table 4.20. In this case, maximum Ra and maximum contact area are both obtained for **trial 133S: grit size = 16 mesh, SOD = 100 mm, time = 60 s**. Consequently, the optimal set of parameter levels for grit blasting trials performed in a saline water environment is: **grit size = 16 mesh, SOD = 100 mm, time = 60 s**. A scatter plot showing the variation of ICA with Ra & RPc for grit blasting trials performed in a saline water environment is shown in Fig. 4.33. Fig. 4.34 shows the 3D surface profile of sample 133S.

TABLE 4.20: Optimal set of process parameters (saline water)

| Trial | CODE | Ra | RPc | ICA |
|-------|------|---------------|------|---------------------------|
| - | - | μm | 1/mm | mm^2/mm^2 |
| 1 | 111S | 6.53 | 41.5 | 0.3729 |
| 2 | 122S | 6.63 | 42.8 | 0.4027 |
| 3 | 133S | 6.72 | 45.5 | 0.4554 |
| 4 | 144S | 6.04 | 46.7 | 0.3987 |

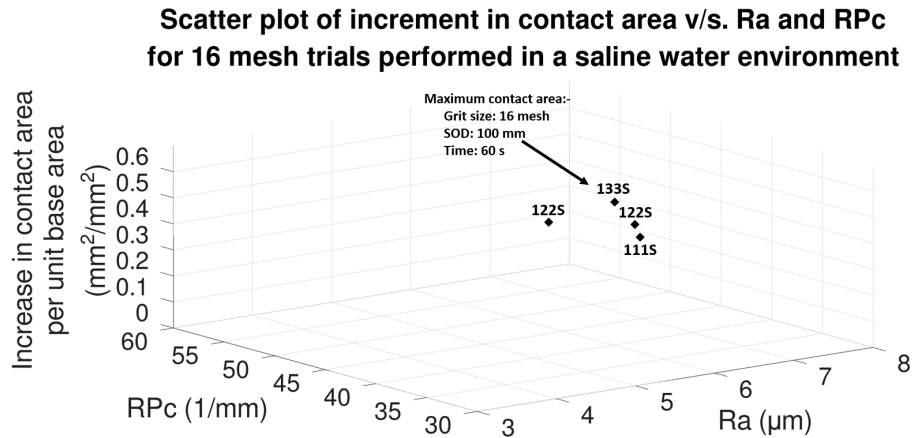


FIGURE 4.33: Scatter plot showing the variation of ICA with Ra and RPc for 16 mesh experiments performed in a saline water environment

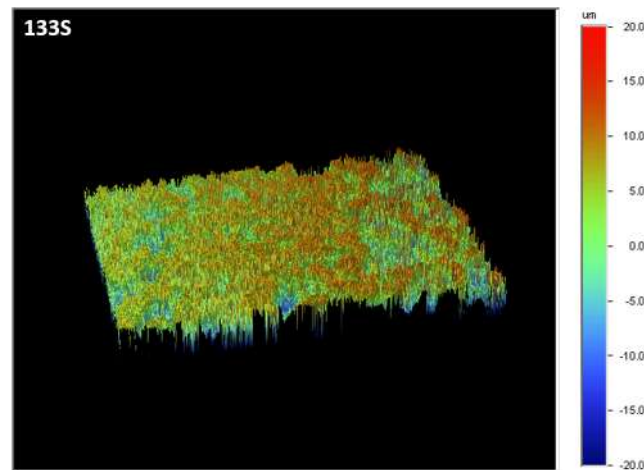


FIGURE 4.34: 3D surface profile of sample 133S

• Microhardness evaluation

Vickers hardness measurements were carried out at a load of 50 gf (dwell time: 10 s) and at depths of 40, 100, 150 & 200 μm from the grit blasted surface of sample 122S. The Vickers indentations made at various depths on sample 122S are visible in Fig. 4.35. The final results showing the variation of average Vickers hardness with depth for sample 122S (grit size: 16 mesh, SOD: 80 mm, time: 45 s, environment: saline water) are summarized in Table 4.21.

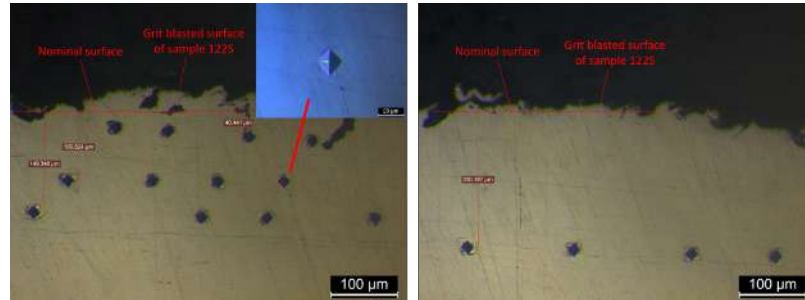
The variation of average cross-section Vickers hardness with depth from the grit blasted surface for sample 122S is shown in Fig. 4.36.

The comparison of the variation of microhardness with depth between samples 122D, 122W & 122S is shown in Fig. 4.37.

Extrapolation using the best fit line ($R^2 = 0.9755$) suggests that bulk hardness would

TABLE 4.21: Variation of Vickers hardness with depth from grit blasted surface for 122S

| Depth from grit blasted surface μm | Avg. HV0.05 kgf/mm^2 | Std. dev. HV0.05 kgf/mm^2 |
|--|----------------------------------|---------------------------------------|
| 40 | 260.2 | 3.6 |
| 100 | 253.5 | 5.7 |
| 150 | 245.2 | 5.1 |
| 200 | 233.9 | 5.2 |

FIGURE 4.35: Vickers indentations on the cross-section of 122S at depths of 40, 100, 150 & 200 μm from the grit blasted surface

Variation of hardness with depth from the grit blasted surface for sample 122S

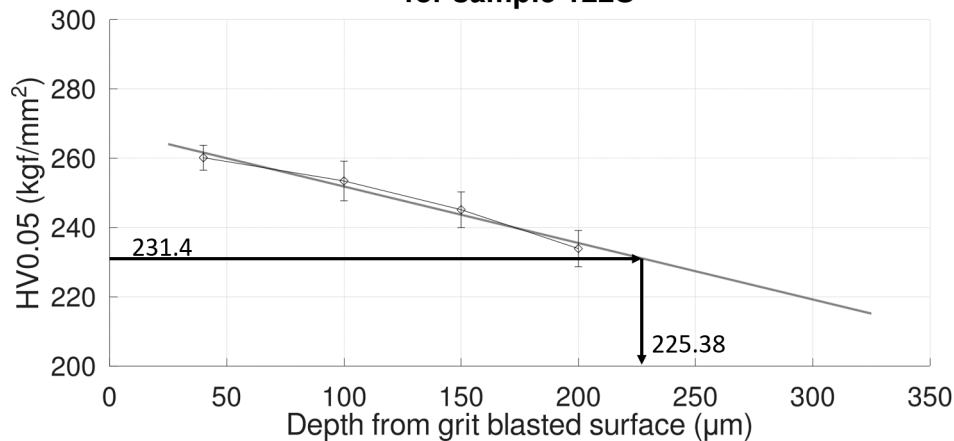


FIGURE 4.36: Variation of cross-section Vickers hardness with depth from the grit blasted surface for sample 122S

be achieved at a depth of approximately 225.38 μm ; consequently, the depth of the affected layer is around 225.38 μm .

Work hardening is less severe in a saline water environment as compared to that for samples grit blasted under dry & wet (water) conditions. This can be attributed to greater density effects of saline water that reduce the impact created by the impinging grits on the surface & sub-surface regions. Slight loss of structural integrity due to contamination resulting from

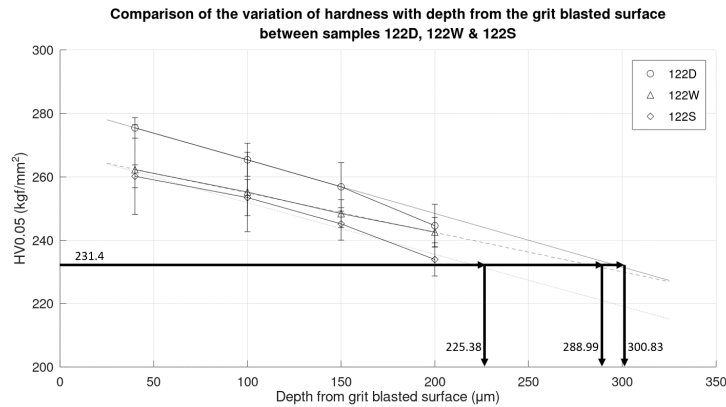


FIGURE 4.37: Comparison of the variation of microhardness with depth for samples 122D, 122W & 122S

Na & Cl formations is another reason for the lower hardness values reported.

• X-Ray Diffraction (XRD) analysis

The XRD pattern for sample 133S (tested under: grit size=16 mesh, SOD = 100 mm, time = 60 s, environment = saline water) is shown in Fig. 4.38.

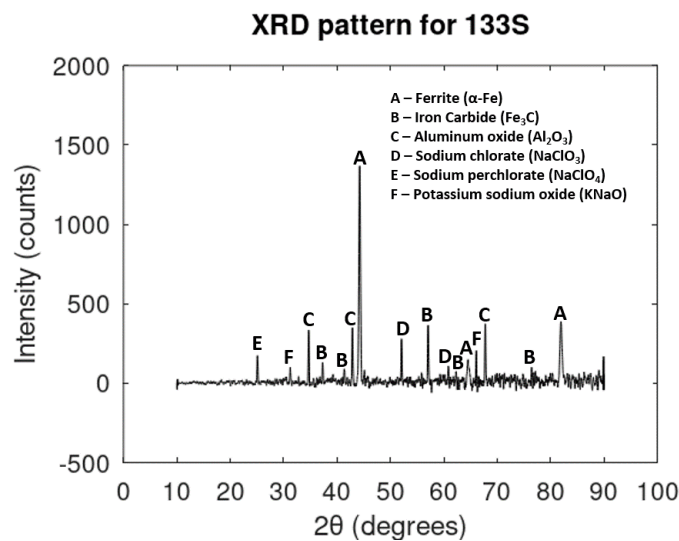


FIGURE 4.38: XRD pattern for 133S

Occurrence of iron carbide (Fe_3C) peaks in the XRD pattern of 133S is most likely due to some specific initial (pre-grit blasting) sub-surface conditions or defects; otherwise, the presence of ferrite ($\alpha\text{-Fe}$) peaks suggests that the nascent surface metallurgy is unchanged. However, the nascent surface undergoes significant contamination in a saline water environment as indicated by the presence of sodium chlorate (NaClO_3), sodium perchlorate (NaClO_4) & potassium sodium oxide (KNaO) peaks in the XRD pattern of 133S. NaClO_3 & NaClO_4

are readily formed in the presence of concentrated sodium chloride solutions. Potassium sodium oxide is basically a pseudo-alkali oxide that is used to represent the combined total of potassium oxide (K_2O) & sodium oxide (Na_2O). K_2O & Na_2O are highly reactive and rarely encountered; instead $KNaO$ is used to represent oxides that contain sodium (Na) & potassium (K) along with some other elements.

The formation of the aforementioned sodium compounds over the grit blasted surface is detrimental for subsequent coating adhesion. Thorough chemical cleaning post grit blasting is required to dissolve these formations. Chemicals used for the purpose must be selectively chosen to only dissolve the aforementioned contaminations and not lead to any other side-effects.

The intensity of Al_2O_3 peaks in the diffraction pattern of sample 133S is much higher than those observed for samples 133D & 133W. It is possible that the other phases detected over the grit blasted surface of sample 133S also have some of their peaks at the same locations as Al_2O_3 and as the XRD pattern of a mixture of phases is a simple sum of the XRD patterns of the individual phases, the resulting intensity of at these overlapping locations is higher. However, in case of overlapping peaks, priority is given to the phase with the highest score. As a result, it is still reasonable to argue that the entrapment of grit residue is higher for 133S than that observed for samples 133D & 133W. This can be explained considering the fact that the structural integrity of the substrate is hampered by the surface contamination resulting from Na & Cl formations. This results in an increase in brittleness of the surface & sub-surface regions which leads to a higher number of surface & sub-surface cracks within which the grit residues can be entrapped.

- **Sub-surface microstructure study using optical microscopy, FESEM & EDS**

Fig. 4.39 shows the surface & sub-surface regions of sample 133S. These images were captured at 1000X magnification using Leica DM IL LED inverted microscope.

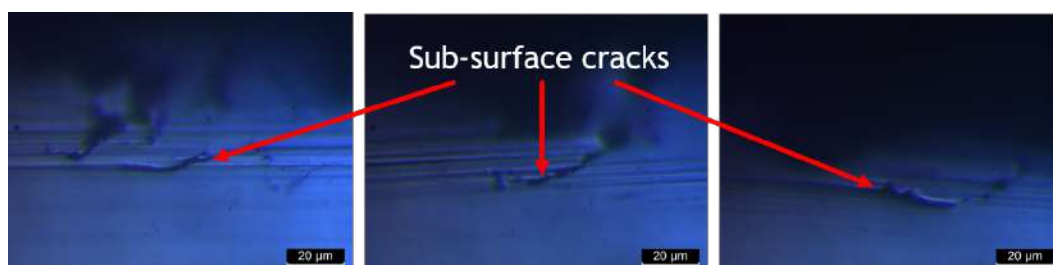


FIGURE 4.39: Sub-surface cracks near the grit-blasted surface of sample 133S

Sub-surface cracks are visible in Fig. 4.39 & also in the SEM micrograph presented as Fig. 4.40i. Sub-surface damage is quite substantial, comparable to that observed under dry conditions. On one hand, there is a reduction in the thermal stress levels due to better heat

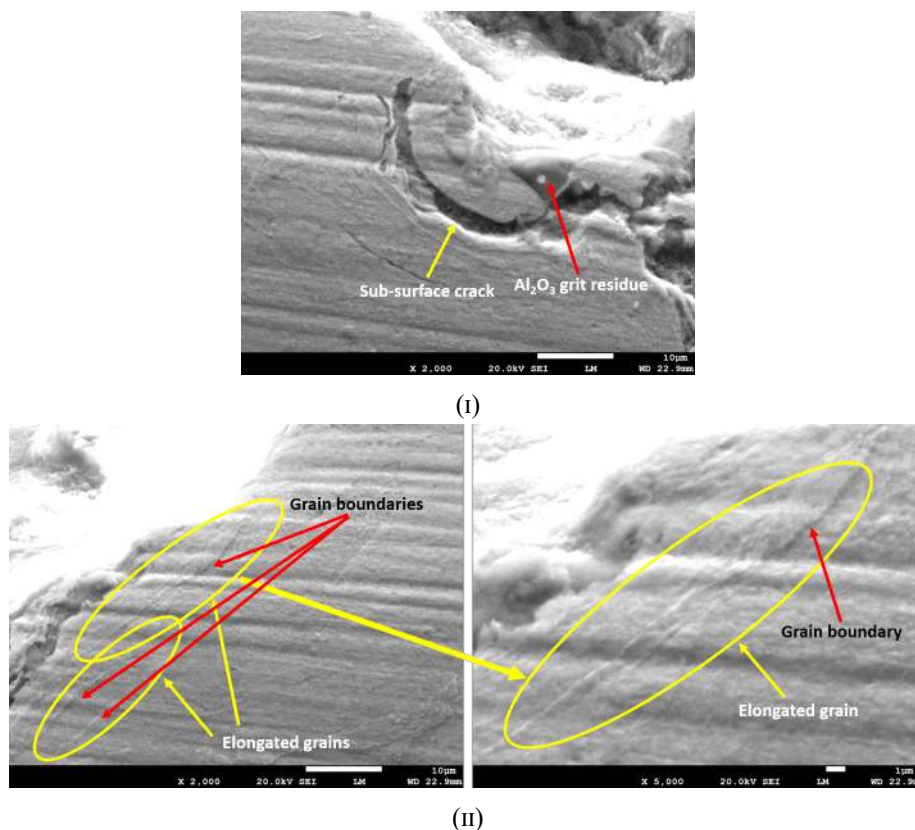


FIGURE 4.40: SEM micrographs of a sub-surface region of sample 133S

dissipation through the saline water medium but on the other hand, there is an increase in brittleness resulting from loss of structural integrity due to surface contamination by formation of Na & Cl compounds. Grain elongation near the grit-blasted surface is visible in Fig. 4.40ii. Some Al_2O_3 grit residue is also visible in the sub-surface region captured in Fig. 4.40i. The EDS layered image of the same region shown in Fig. 4.41 makes it easier to identify the surface contamination in the region. The elements corresponding to the contaminated zone are detected to be Na, Cl & O which is consistent with the XRD results that suggest formation of sodium chlorate (NaClO_3) & sodium perchlorate (NaClO_4) over the surface.

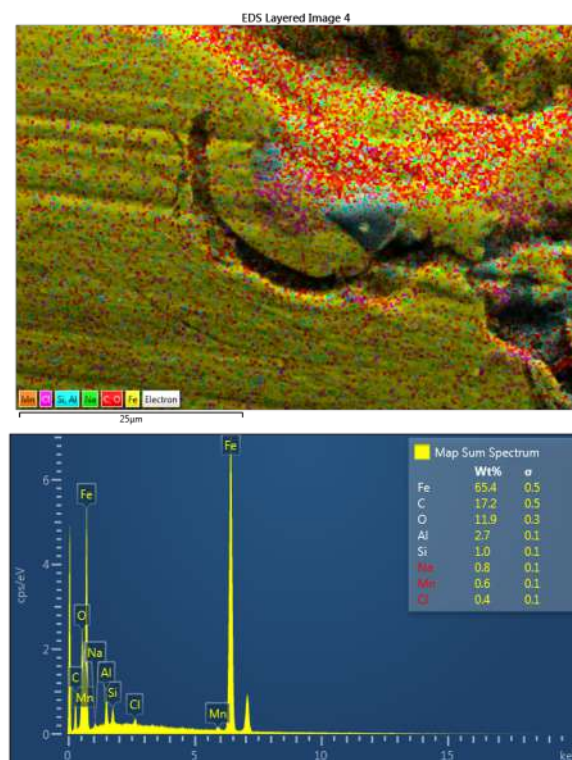


FIGURE 4.41: EDS layered image of a sub-surface region of sample 133S & its corresponding spectrum

4.1.4 Alcohol

As mentioned earlier, experiments in saline water & alcoholic environments are performed for 16 mesh only.

The final profilometric results for 16 mesh experiments carried in a wet environment of 50% diluted ethyl alcohol are tabulated in Table 4.22.

TABLE 4.22: Final profilometric results for 16 mesh trials carried out in a wet environment of alcohol

| Trial | CODE | Ra | RPc |
|-------|------|---------------|------|
| - | - | μm | 1/mm |
| 1 | 111A | 6.74 | 32.1 |
| 2 | 122A | 7.22 | 46.5 |
| 3 | 133A | 7.15 | 33.4 |
| 4 | 144A | 6.91 | 38.4 |

A one-to-one comparison of results in terms of Ra obtained for each 16 mesh trial performed in dry, water, saline water & alcoholic environments is visualized in the Fig. 4.42.

Ra values obtained in the alcoholic environment fall in between those obtained under dry conditions and those obtained under wet (water) conditions. Ra values vary in the order: Dry

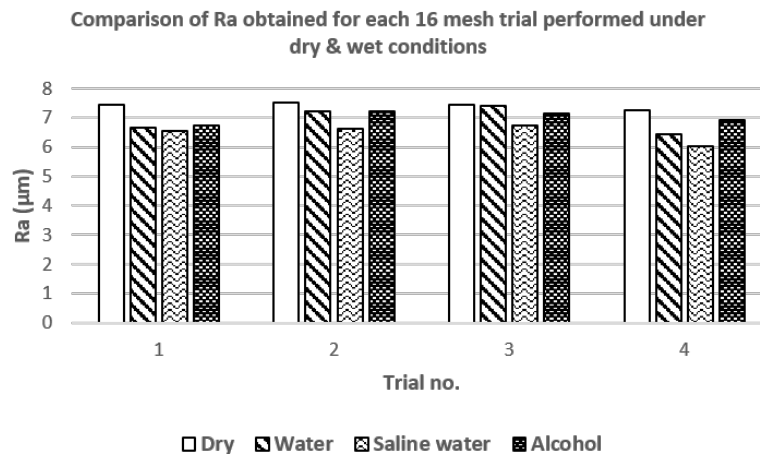


FIGURE 4.42: Comparison of results obtained for each 16 mesh trial performed in dry, water, saline water & alcohol environments in terms of Ra

> Alcohol > Water > Saline water. Further, the variation of Ra with each trial in the alcoholic environment closely reciprocates the variation obtained under dry conditions. This is as per the expectations. The density of 50% diluted ethyl alcohol is lower than the density of water, resulting in less hindrance in the motion of the impinging grits. Plus, higher volatility of ethyl alcohol reduces the overall boiling point of the solution as well, some of which vaporises into the atmosphere during blasting, leading to slightly drier conditions than other wet environments.

• Estimation of increment in contact area due to roughening

The increment in contact area per unit reference area is calculated for each of the four 16 mesh grit experiments performed in an alcoholic environment, based on the Ra and RPc data finalised for the same. The results are tabulated in Table 4.23.

TABLE 4.23: Increment in contact area for 16 mesh trials carried out in a wet environment of alcohol

| Trial | CODE | Ra | RPc | ICA |
|-------|------|---------------|---------------|---------------------------|
| - | - | μm | $1/\text{mm}$ | mm^2/mm^2 |
| 1 | 111A | 6.72 | 32.1 | 0.2533 |
| 2 | 122A | 7.22 | 46.5 | 0.5296 |
| 3 | 133A | 7.15 | 33.4 | 0.3007 |
| 4 | 144A | 6.91 | 38.4 | 0.3599 |

• Optimal set of process parameter levels

The final results for the grit blasting experiments performed in an alcoholic environment are tabulated in Table 4.24. In this case, maximum Ra and maximum contact area are both obtained for **trial 122A: grit size = 16 mesh, SOD = 80 mm, time = 45 s, environment = alcohol**. Consequently, the optimal set of parameter levels for grit blasting trials performed in the alcoholic environment is: **grit size = 16 mesh, SOD = 80 mm, time = 45 s**. A scatter plot showing the variation of ICA with Ra & RPc for grit blasting trials performed in the alcoholic environment is shown in Fig.4.43. Fig. 4.44 shows the 3D surface profile of sample 122A.

TABLE 4.24: Optimal set of process parameters (alcohol)

| Trial | CODE | Ra | RPc | ICA |
|-------|------|---------------|------|---------------------------|
| - | - | μm | 1/mm | mm^2/mm^2 |
| 1 | 111A | 6.72 | 32.1 | 0.2533 |
| 2 | 122A | 7.22 | 46.5 | 0.5296 |
| 3 | 133A | 6.63 | 33.4 | 0.3007 |
| 4 | 144S | 6.04 | 38.4 | 0.3599 |

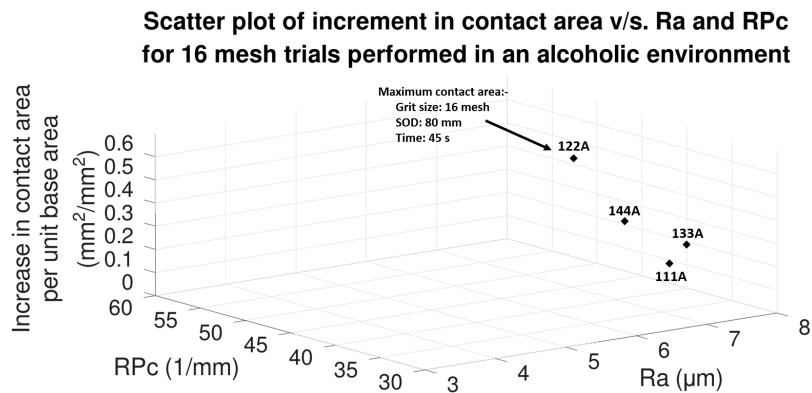


FIGURE 4.43: Scatter plot showing the variation of ICA with Ra and RPc for 16 mesh experiments performed in an alcoholic environment

Comparative visualization of the optimal sets of parameter levels

The optimal sets of process parameter levels determined for each environment and the corresponding Ra & ICA values are tabulated in Table 4.25. The 3D surface profiles of the samples grit blasted under the optimal sets of parameter levels determined for each environment are visualized for comparison in Fig. 4.45.

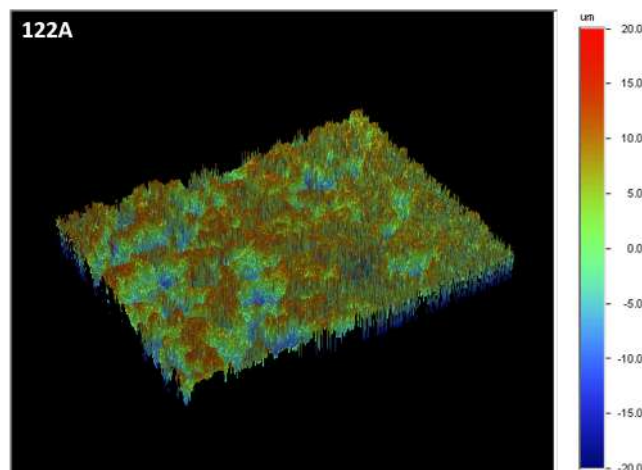


FIGURE 4.44: 3D surface profile of sample 122A

TABLE 4.25: Optimal set of process parameter levels and corresponding Ra & ICA values under each environment

| Environment | Parameter levels | | | Ra | ICA |
|--------------|------------------|-------------------|------------------|---------------|---------------------------|
| - | Grit size (mesh) | SOD (mm) | Time (s) | μm | mm^2/mm^2 |
| Dry | 16 | 60 | 30 | 7.44 | 0.5765 |
| Water | 16 | 80 | 45 | 7.22 | 0.5387 |
| Saline water | 16 | 100 | 60 | 6.72 | 0.4554 |
| Alcohol | 16 | 100 80 | 70 45 | 7.22 | 0.5296 |

The proportion of regions with darker shades in the 3D surface profiles gives an estimation of the surface roughness. Higher the proportion of these regions, greater is the roughness. The 3D surface profiles collaged in Fig. 4.45 are consistent in this regard with the roughness values tabulated in Table 4.25.

It can be inferred from Table 4.25 that contact area increases with Ra which is certainly true. But this inference does not convey the entire picture. Contact area depends not only on the average surface deviation created due to roughening (measured in terms of Ra) but also on the number of surface asperities generated. Previous researchers have not considered the interpretation of roughness in terms of the number of surface asperities or peak density. As mentioned earlier, in addition to influencing the coating-substrate contact area, the surface asperities also act as activation sites for chemisorption & physisorption reactions crucial for coating adhesion. Research work on the factors influencing peak density needs to be undertaken so that the maximum possible contact area can be generated by optimally controlling those factors.

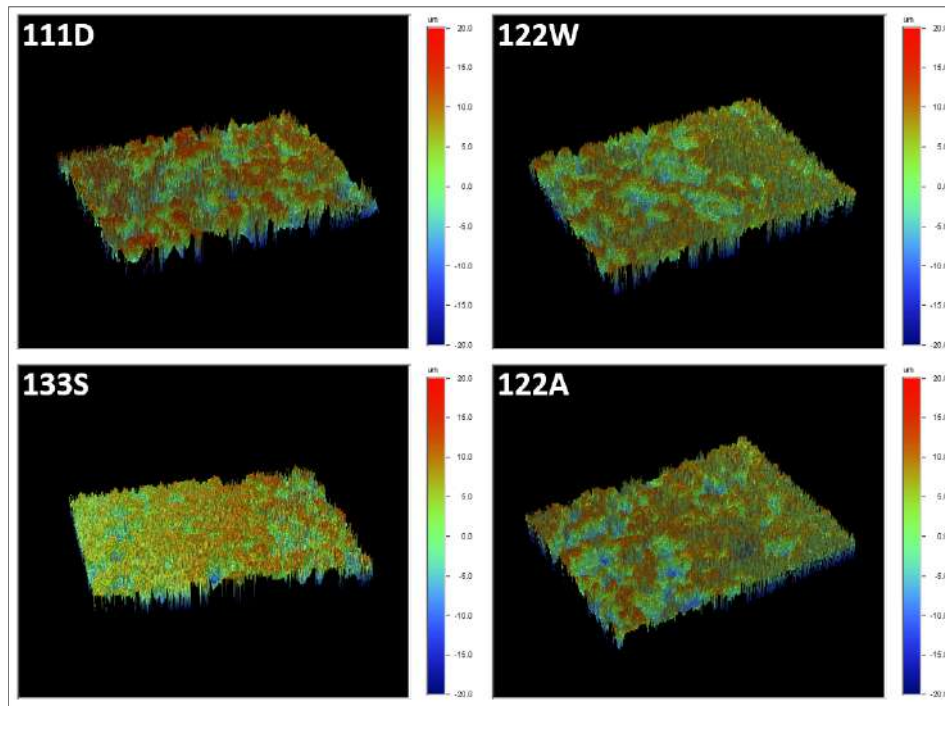


FIGURE 4.45: 3D surface profiles of samples 111D, 122W, 133S & 122A

• Microhardness evaluation

Vickers hardness measurements were carried out at a load of 50 gf (dwell time: 10 s) and at depths of 40, 100, 150 & 200 μm from the grit blasted surface of sample 122A. The Vickers indentations made at various depths on sample 122A are visible in Fig. 4.46. The final results showing the variation of average Vickers hardness with depth for sample 122A (grit size: 16 mesh, SOD: 80 mm, time: 45 s, environment: alcohol) are summarized in Table 4.26.

TABLE 4.26: Variation of Vickers hardness with depth from grit blasted surface for 122A

| Depth from grit blasted surface | Avg. HV0.05 | Std. dev. HV0.05 |
|---------------------------------|-------------------|------------------|
| μm | kgf/mm^2 | |
| 40 | 248.8 | 5.6 |
| 100 | 237.2 | 14.7 |
| 150 | 235.4 | 6.7 |
| 200 | 235.2 | 7.0 |

The variation of average cross-section Vickers hardness with depth from the grit blasted surface for sample 122A is shown in Fig. 4.47.

The comparison of the variation of microhardness with depth between samples 122D, 122W, 122S & 122A is shown in Fig. 4.48.

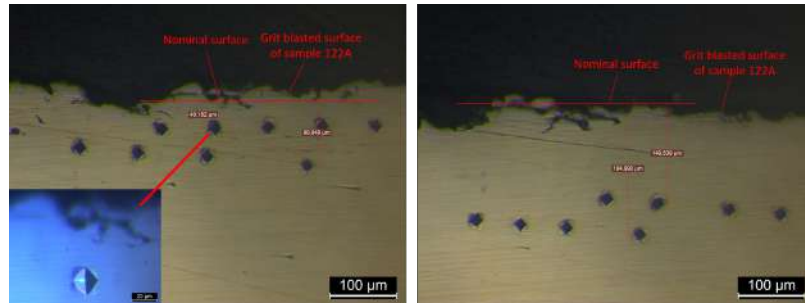


FIGURE 4.46: Vickers indentations on the cross-section of 122A at depths of 40, 100, 150 & 200 μm from the grit blasted surface

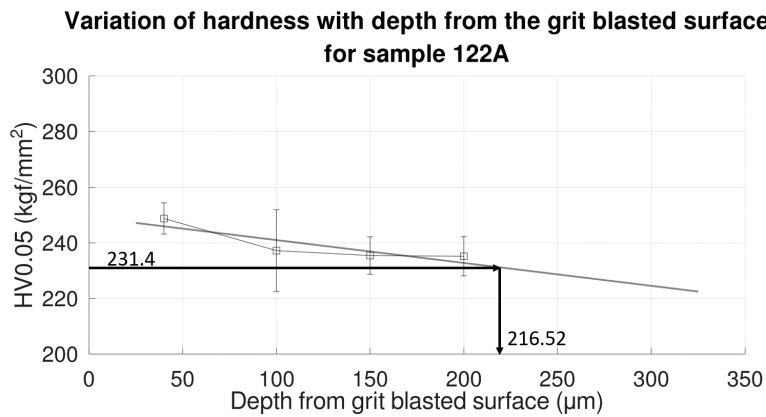


FIGURE 4.47: Variation of cross-section Vickers hardness with depth from the grit blasted surface for sample 122A

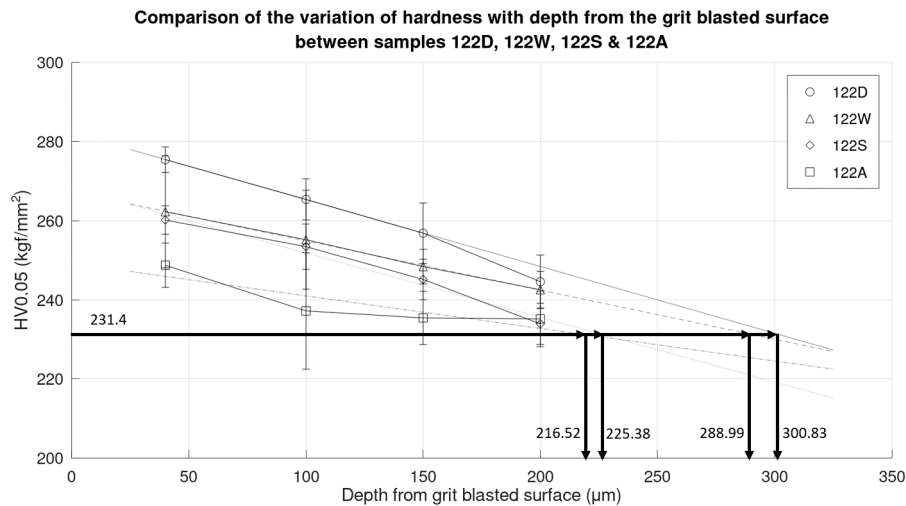


FIGURE 4.48: Comparison of the variation of microhardness with depth for samples 122D, 122W, 122S & 122A

Extrapolation using the best fit line ($R^2 = 0.7591$) suggests that bulk hardness would be achieved at a depth of approximately $216.52 \mu\text{m}$; consequently, the depth of the affected

layer is around 216.52 μm .

The density effects of alcohol are lower than water & saline water. One would expect the impinging grits to create greater impact on the surface as suggested by the higher Ra values obtained in an alcoholic environment. This is expected to lead greater work hardening than that reported under water & saline water environments. However, this has not been the case observed. It can be argued that greater volatility of alcohol results in better heat dissipation than other media, which significantly lowers the susceptibility of substrate surface to deformation, leading to brittle conditions. Higher Ra values reported in an alcoholic environment suggest better material removal by crack propagation near the surface. Further, crack propagation being more localized, work hardening is expected to be lower.

Comparative study of hardness data and its correlation with roughness

The Vickers hardness values for samples 122D, 122W, 122S & 122A at a depth of 40 μm from the grit blasted surface, corresponding depths of the affected layers and Ra values are tabulated in Table 4.27.

TABLE 4.27: Correlation between hardness and roughness

| Sample | Ra | HV0.05 at 40 μm | Depth of affected layer |
|--------|---------------|----------------------------|-------------------------|
| - | μm | kgf/mm^2 | μm |
| 122D | 7.5 | 275.5 | 300.83 |
| 122W | 7.22 | 262.3 | 288.99 |
| 122S | 6.63 | 260.2 | 225.38 |
| 122A | 7.22 | 248.8 | 216.52 |

The maximum hardness values for each sample (obtained at 40 μm) serve as an estimate of the level of work hardening that has taken place during grit blasting. Higher the hardness, higher the work hardening & consequently, higher is the depth of the affected layer, as is being reflected in the results. The correlation between hardness near the grit blasted surface and the depth of the affected layer can be seen in Fig. 4.49.

The correlation between work hardening and roughness induced by grit blasting is visualized in Fig. 4.50.

More or less, it can be concluded that higher the roughness induced, higher is the level of work hardening taking place at the surface, which is as per the expectations. The alcoholic environment is clearly an outlier in this trend as can also be seen in Fig. 4.50. The reasons for the same have been mentioned earlier.

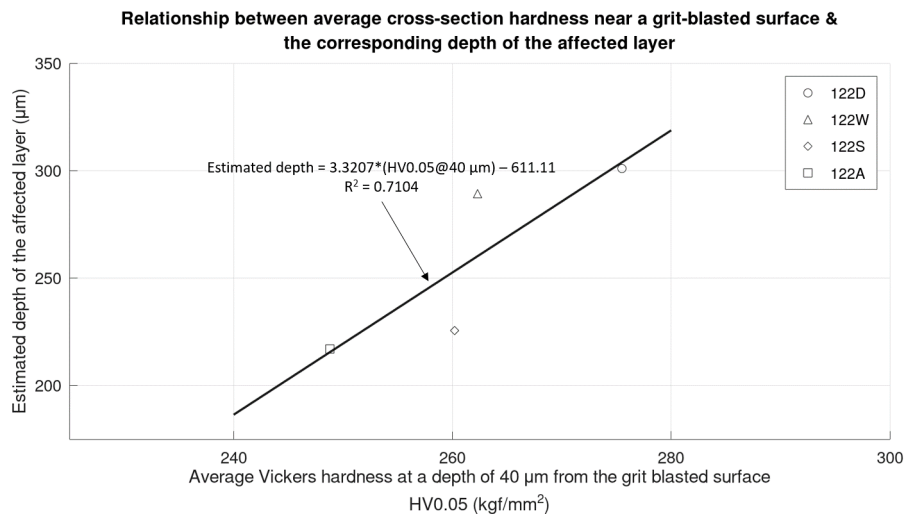


FIGURE 4.49: Relationship between average cross-section hardness near a grit blasted surface & corresponding depth of the affected layer

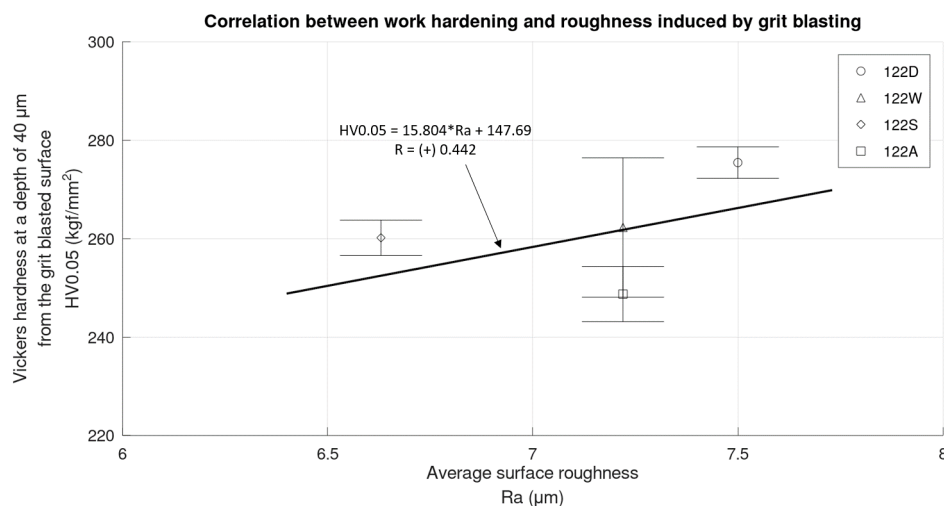


FIGURE 4.50: Correlation between work hardening and roughness induced by grit blasting

• X-Ray Diffraction (XRD) analysis

The XRD pattern for sample 133A (tested under: grit size=16 mesh, SOD = 100 mm, time = 60 s, environment = alcohol) is shown in Fig. 4.51.

The presence of ferrite (α -Fe) peaks in the XRD pattern of sample 133A suggests that there is once again no change in nascent surface metallurgy following grit blasting in an alcoholic environment. Occurrence of Al_2O_3 peaks can be attributed to alumina grit residues entrapped over the surface. Al_2O_3 peaks are, however, the least prominent among all the diffraction patterns of samples grit blasted in different environments. This suggests the least level of grit residue entrapment over the surface. Material removal by crack propagation

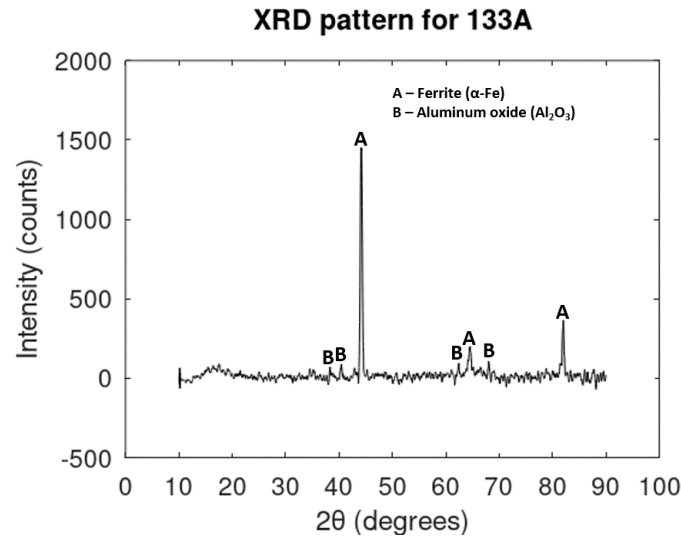


FIGURE 4.51: XRD pattern for 133A

is dominant in an alcoholic environment due to better heat dissipation owing to its greater volatility. One would expect grits to entrap within these surface cracks & resulting grit residue on the surface to be higher. However, higher volatility of alcohol leading to its vaporisation would result in creating a negative pressure that helps in driving out the grit residues from the surface cracks. This action is expected to result in a cleaner surface with a lower proportion of grit residue.

Comparative study of XRD data

The XRD patterns of samples 133D, 133W, 133S & 133A are collaged in Fig. 4.52. Nascent surface metallurgy remains unchanged under all environments - ferrite (α -Fe) is the dominant phase occurring over the nascent grit blasted surface under all environments. No surface contamination due to in-situ chemical formations is observed under environments of water & alcohol. However, significant surface contamination is reported to take place in the saline water environment. Further, on the basis of the relative intensity of Al_2O_3 peaks in the diffraction patterns of the samples 133D, 133W, 133S & 133A, it has been suggested that the entrapment of grit residue over the grit blasted surfaces is the lowest for sample 133A. It has been argued that the negative pressure generated due to vaporisation of alcohol helps to drive out some of the grit residues entrapped within the surface cracks/craters, resulting in a cleaning action. The as-received surfaces of substrates grit blasted in the alcoholic environment also appear to be cleaner to the naked eye as compared to the substrates grit blasted under other environments. However, further research is necessary to validate this cleaning action claimed to be taking place under the alcoholic environment.

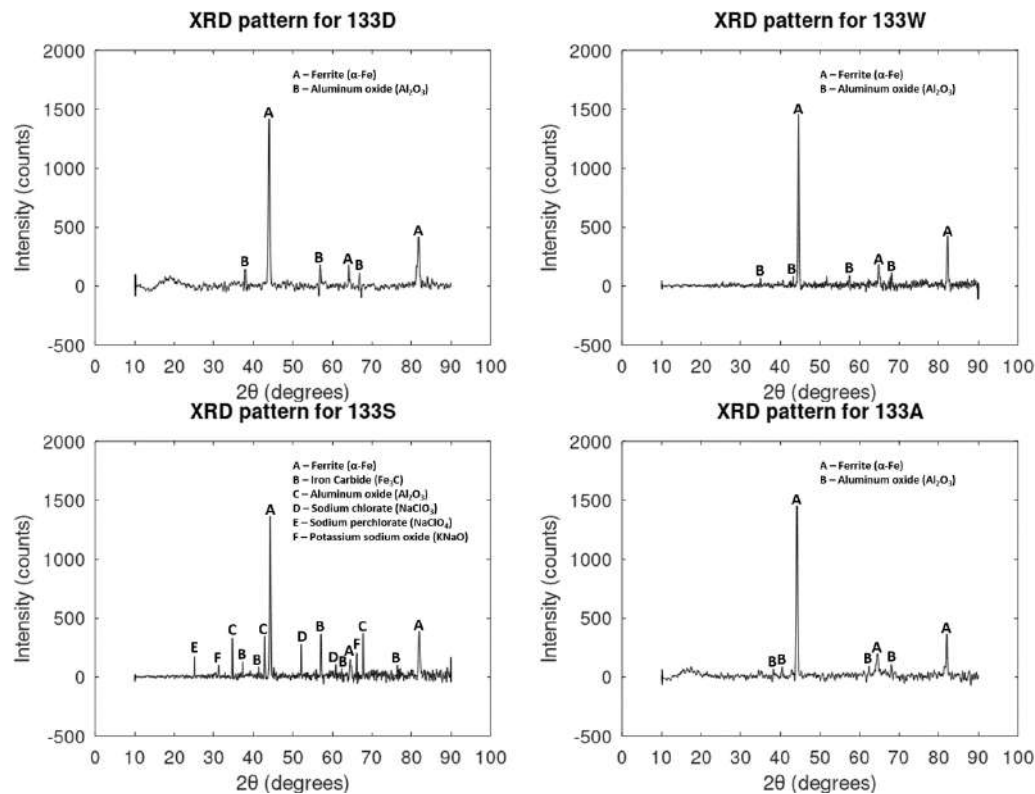


FIGURE 4.52: Comparison of the XRD patterns of samples 133D, 133W, 133S & 133A

• Sub-surface microstructure study using optical microscopy, FESEM & EDS

Fig. 4.53 shows the surface & sub-surface regions of sample 122A. These images were captured at 1000X magnification using Leica DM IL LED inverted microscope.

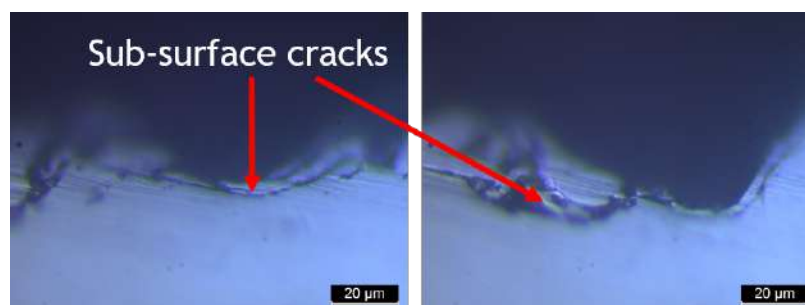


FIGURE 4.53: Sub-surface cracks near the grit-blasted surface of sample 122A

Sub-surface cracks can be noted in Fig. 4.53. The level of sub-surface damage is appreciably lower than that observed under dry conditions. Earlier, it was argued that higher R_a values obtained in the alcoholic environment are due to crack propagation being the dominant material removal mechanism. Lower level of sub-surface damage suggests that the cracks attributed to simulation of brittle conditions due to better heat dissipation are restricted to

the surface regions only. Level of thermal stresses generating in the sub-surface regions would again be lower due to better heat dissipation. Overall, optical examination reveals that sub-surface damage in samples grit blasted in an alcoholic environment is lower than that observed under dry conditions.

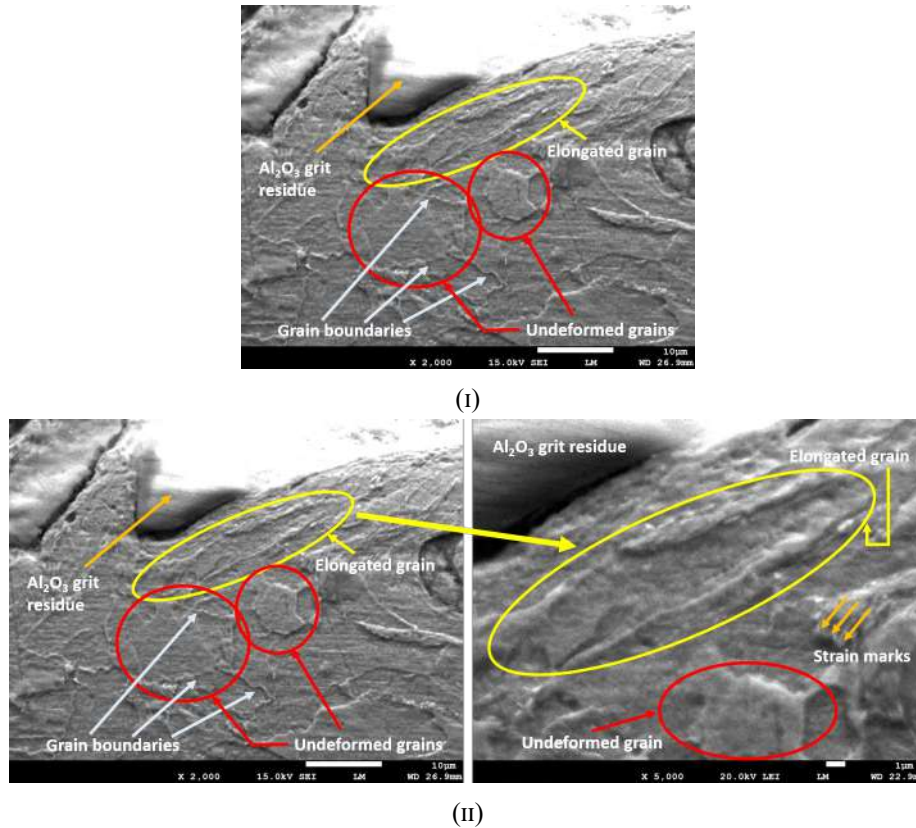


FIGURE 4.54: SEM micrographs of a sub-surface region of sample 122A

Fig. 4.54 depicts the SEM micrographs of a sub-surface region of sample 122A while Fig. 4.55 shows the EDS layered image & corresponding spectrum of the same region. Al₂O₃ grit residue entrapped near the surface is visible in the micrographs. The grains in the vicinity of the grit blasted surface have undergone significant deformation leading to their elongation. Deformation effects of grit-blasting on the microstructure fade out as one moves away from the surface, which is validated by the undeformed grains visible in the SEM micrographs at higher depths from the grit blasted surface. The distinction between the elongated & undeformed grains is easily noticeable in the micrographs. While explaining the lower level of work hardening taking place in an alcoholic environment despite the higher Ra values obtained for the same, it was argued that the deformation effects of grit blasting under alcoholic environment would be highly localized & restricted to the surface regions due to the brittle conditions simulated by better heat dissipation. The SEM micrographs stand in validation of the reasoning used earlier.

EDS results are in agreement with the XRD results, in that, only the elements corresponding to the phases detected by XRD (ferrite (α -Fe) & Al_2O_3) have been detected by EDS.

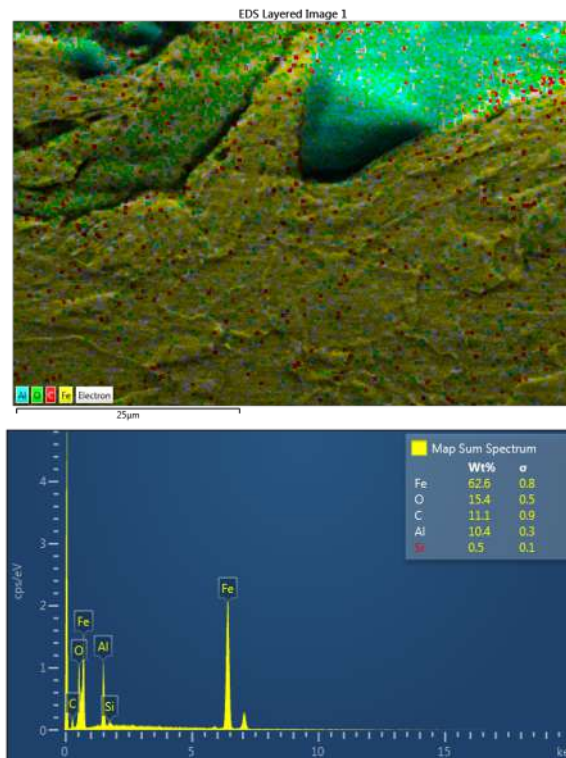


FIGURE 4.55: EDS layered image of a sub-surface region of sample 122A & its corresponding spectrum

Chapter 5

Conclusions & future scope

5.1 Conclusions

The conclusions derived from the research work presented in this thesis are summarized in this chapter under the following headings.

5.1.1 Variation of mean response with process parameters under dry & wet conditions

Ra increases with grit size. The variation of Ra with SOD is initially increasing, reaches a maximum & then decreases. With time, the variation was slightly decreasing. Very high roughness can be achieved within a short time span. Increasing the blasting time is effective only up to a certain limit. Overblasting is detrimental to roughness. ANOVA analysis suggests grit size is the most significant factor influencing Ra. The aforementioned results are consistent with those reported in the existing literature on dry blasting. The nature of the variation of mean response with process parameters remains the same under wet conditions as well; however, the maxima with respect to SOD & time shift to higher SODs & time periods respectively. Deceleration & deflection of the impinging grits is higher when grit blasting is carried out in a wet environment. The hindrance to the motion of the impinging grits increases when the medium used to simulate a wet environment has a higher density. Splashing of the medium & other density effects creating a hindrance in the motion of the impinging grits are higher at lower SODs. The presence of a medium over the substrate surface is expected to reduce the effective SOD, leading to a maximum Ra being achieved at higher SODs than that for dry conditions. Further, the continuous presence of a medium over the substrate surface delays the initiation of the roughening process; as a result, the blasting time period for achieving the maximum Ra is higher than that observed under dry conditions.

5.1.2 Relationship between Ra & RPc

Peak density of roughness profiles (RPc) was found to vary independently of roughness (Ra).

5.1.3 Optimal set of process parameter levels under each environment

The optimal set of process parameter levels under each environment, the corresponding roughness values & increment in contact area (ICA) are tabulated in Table 5.1.

TABLE 5.1: Optimal set of process parameter levels and corresponding Ra & ICA values under each environment

| Environment | Parameter levels | | | Ra | ICA |
|--------------|------------------|-------------------|------------------|---------------|---------------------------|
| | Grit size (mesh) | SOD (mm) | Time (s) | μm | mm^2/mm^2 |
| - | | | | | |
| Dry | 16 | 60 | 30 | 7.44 | 0.5765 |
| Water | 16 | 80 | 45 | 7.22 | 0.5387 |
| Saline water | 16 | 100 | 60 | 6.72 | 0.4554 |
| Alcohol | 16 | 100 80 | 70 45 | 7.22 | 0.5296 |

The optimal parameter levels of SOD & time in wet environments are shifted to higher SODs & time periods respectively. With regards to SOD, in general, it is expected that higher Ra and ICA would be achieved at lower SODs when grit blasting is carried out in wet environments because the flaring of the air-abrasive jet stream would be lower and the energy of the impinging grits would be higher when they strike the layer of medium maintained over the substrate surface. But the observations are not in agreement with the general expectations. Optimal surface conditions under wet environments are achieved at higher SODs than that in dry environments. As mentioned earlier, the impinging grits are decelerated and deflected to some extent by the medium used for simulating wet environments. Denser the medium, greater is the hindrance to the motion of the impinging grits. The splashing of the medium and other density effects are expected to be higher at lower SODs. As a result, the impinging grits are expected to be decelerated and deflected to a greater extent at lower SODs, due to which the optimal SOD levels corresponding to wet environments are higher than those observed under dry conditions. The continuous presence of a medium over the substrate surface delays the initiation of roughening. As a result, optimal conditions in wet environments are expected to arrive at higher time periods.

The increment in contact area was estimated according to the mathematical model developed for approximating an actual roughened surface described in previous chapters. For each environment, the parameter levels corresponding to maximum ICA were selected to be the optimal process parameter levels. According to the mathematical model developed, ICA was found to be dependent on both Ra as well as RPc. Further, it was concluded that RPc varies independently of Ra. As a result, different sets of parameter levels corresponding to maximum Ra & maximum ICA were obtained for some environments.

It is easy to infer from Table 5.1 that contact area increases with Ra which is beyond any doubt. But as said earlier, this inference does not convey the entire picture - contact area depends on Ra as well as RPc. The existing literature has so far interpreted surface roughness in terms of Ra only while the interpretation of surface roughness in terms of the number of surface asperities has mostly been ignored. As ICA depends on both Ra & RPc and as RPc was found to vary independently of Ra, it is possible to achieve maximum Ra & maximum ICA under different sets of parameter levels. This discrepancy highlights the need for future work on determining the factors influencing the number of surface asperities, which in addition to contributing to contact area, also act as potential activation sites for chemisorption & physisorption interactions responsible for coating adhesion.

5.1.4 Hardness analysis

Work hardening due to grit blasting is maximum near the surface. The influence of grit blasting on substrate hardness declines with depth. Further, work hardening due to grit blasting is higher under dry conditions vis-à-vis wet conditions. Hardness values measured at different depths consistently vary in the order: Dry > Water > Saline water > Alcohol. Higher the hardness values induced near the surface, greater is the depth of the affected layer. Further, work hardening due to grit blasting can, more or less, be correlated to roughness - higher the roughness, higher is the work hardening. The alcoholic environment stands as a clear outlier in this trend. Higher Ra values are reported for substrates grit blasted in the alcoholic environment; yet the level of work hardening was observed to be lower. The higher Ra values were attributed to the brittle material conditions established due to better heat dissipation owing to greater volatility of the alcoholic solution. This resulted in better material removal via crack propagation at the surface. These cracks being restricted to the surface & near surface regions, the sub-surface damage was observed to be lower. The deformation effects of grit blasting are localized near the surface, especially in the vicinity of the surface cracks. Further, the level of thermal stresses generating in the sub-surface regions was also lower due to better heat dissipation. Lower susceptibility of surface towards deformation, material removal by crack propagation at the surface & reduction in thermal stress levels generating in the sub-surface regions - together result in a unique condition characterized by higher roughness but lower work hardening and depth of the affected layer for the substrates blasted in the alcoholic environment.

5.1.5 XRD analysis

Nascent surface metallurgy remains unchanged under both dry & wet conditions - ferrite (α -Fe) is the dominant phase occurring on grit blasted surfaces under both dry & wet conditions. Entrapment of grit residues over the surface under each environment is validated by

the occurrence of Al_2O_3 peaks in their respective XRD patterns. In wet environments, while no surface contamination was detected for samples grit blasted in the presence of water & alcohol, significant contamination of surface takes place in the saline water environment as suggested by occurrence of peaks corresponding to some Na & Cl formations in the XRD pattern of sample 133S. Based on the relative intensity of Al_2O_3 peaks in the diffraction patterns of the samples grit blasted in different environments, it can be argued that the proportion of grit residues over the grit blasted surface is the lowest for the sample blasted in the alcoholic environment. On similar lines, it can be argued that the proportion of grit residues is appreciably higher for the sample grit blasted in the saline water environment. Surface contamination by formation of Na & Cl compounds over the surface in the saline water environment results in a slight loss of structural integrity of the surface & sub-surface regions. This leads to brittle conditions where a number of cracks originate at the contaminated locations, within which the grit residues can entrap. However, conclusions made on the basis of relative intensity of diffraction peaks need further validation.

5.1.6 Evaluation of sub-surface microstructure

Indentation & corresponding extrusion of material peripheral to the indentation area are the dominant mechanisms of material removal & roughness generation at an impingement angle of 80° , which is consistent with the existing literature. Sub-surface cracks generated due to compressive residual stresses & thermal stresses are substantial for samples blasted under dry conditions. Sub-surface damage is also substantial for samples blasted in a saline water environment; this can be attributed to a slight loss of structural integrity of the surface & sub-surface regions of those samples owing to the contamination caused by Na & Cl formations. For samples blasted under wet environments of water & alcohol, sub-surface damage was appreciably lower which can be mainly attributed to density effects & reduction in the thermal stress levels by better heat dissipation respectively. Grain elongation near the grit blasted surface was revealed in the SEM micrographs by etching of the samples. Grain deformation is restricted to regions close to the grit-blasted surface. As one moves away from the grit blasted surface, the deformation effects of grit blasting die out & the grains are mostly undeformed. The distinction between deformed & undeformed grains is clearly visible in the SEM micrographs. Deformation effects are especially localized for samples blasted in the alcoholic environment. Other signatures of surface & sub-surface regions of grit blasted samples such as Al_2O_3 grit residues, sub-surface cracks & strain marks were also identified in the SEM micrographs. EDS analysis of surface & sub-surface regions was found to be consistent with the XRD results i.e. the elements corresponding to the phases detected by XRD were also detected by EDS.

5.2 Future scope

- A proper pumping setup can be developed for continuously supplying different liquid media in order to simulate different wet environments. The setup must be equipped with a facility to vary the angle at which the medium is supplied to ensure that the medium is always directed towards the substrate surface as the SOD is varied. A valve-like arrangement can be appended to the setup in order to achieve variable flow rates. The setup must be enclosed in a protective casing in order to prevent any damage by grit blasting. Further, the substrate holding setup can be provided with a tall side-enclosure from four sides to avoid splashing of liquid media into the blasting cabinet. A facility for disposal of wet grits can also be thought of.
- The existing literature on grit blasting has so far interpreted surface roughness in terms of Ra only. The interpretation of roughness in terms of the number of surface asperities or peak density has mostly been ignored. However, as highlighted by this research, contact area depends on both the average surface deviation (Ra) as well as the number of surface asperities (RPc). In addition to influencing contact area, surface asperities also act as potential sites for chemisorption & physisorption reactions that are crucial to subsequent coating adhesion. This makes a case for further research on peak density to determine the factors affecting it.
- Based on the relative intensity of Al_2O_3 peaks in the diffraction patterns of the samples grit blasted under different environments, it has been suggested that the proportion of Al_2O_3 grit residues entrapped over a grit blasted surface is the lowest when grit blasting is carried out in the alcoholic environment. It has been argued that the negative pressure resulting from vaporisation of alcohol is beneficial in driving out some of the grit residues entrapped in the surface cracks/crevices, resulting in a cleaner nascent surface. However, further research is necessary to validate the aforementioned claim. Image analysis techniques have been used by previous researchers for determining the variation of grit residue proportion with process parameters. Similar techniques can be used to compare the surface contamination by grit residues under dry vis-à-vis wet conditions.
- The surfaces of samples grit blasted under different environments can be coated with a suitable coating material using any of the available plasma spray techniques. The bond strength of the coatings can then be tested & the optimal grit blasting process parameter levels corresponding to the maximum coating bond strength can be determined. These sets of parameter levels can be compared with those obtained using the mathematical model developed in this thesis to either validate or disprove the model. In case of a disagreement, attempts can be made to develop a more precise mathematical model taking into account the contact area as

well as other surface topographical features.

References

- Asl, S. K. & Sohi, M. H. (2010), 'Effect of grit-blasting parameters on the surface roughness and adhesion strength of sprayed coating', *Surface and Interface Analysis* pp. 551–554.
- ASM International Handbook Committee (1994), *ASM Handbook*, ASM International.
- Begg, H., Riley, M. & de Villiers Lovelock, H. (2015), 'Mechanization of the grit blasting process for thermal spray coating applications: A parameter study', *Journal of Thermal Spray Technology* .
- Black, J. T. & Kohser, R. A. (2008), *DeGarmo's Materials & Processes in Manufacturing*, 10th edn, John Wiley & Sons, Inc.
- Bobzin, K., Öte, M., Linke, T. F., Sommer, J. & Liao, X. (2015), 'Influence of process parameter on grit blasting as a pretreatment process for thermal spraying', *Journal of Thermal Spray Technology* .
- Chander, K. P., Vashista, M., Sabiruddin, K., Paul, S. & Bandopadhyay, P. P. (2009), 'Effect of grit blasting on surface properties of steel substrates', *Materials and Design* **30**, 2895–2902.
- Enviro-Managament & Research, Inc. (1976), *Abrasive Blasting Operations - Engineering Control and Work Practices Manual*.
- Ghara, T., Paul, S. & Bandopadhyay, P. P. (2020), 'Effect of grit blasting parameters on surface and near-surface properties of different metal alloys', *Journal of Thermal Spray Technology* .
- Griffiths, B. J., Gawne, D. T. & Dong, G. (1996), 'The erosion of steel surfaces by grit-blasting as a preparation for plasma spraying', *Journal of Thermal Spray Technology* pp. 95–102.
- Groover, M. P. (2010), *Fundamentals of Modern Manufacturing*, 4th edn, John Wiley & Sons, Inc.
- Kalpakjian, S. & Schmid, S. R. (2010), *Manufacturing Engineering and Technology*, 6th edn, Prentice Hall.

- Mellali, M., Grimaud, A., Leger, A. C., Fauchais, P. & Lu, J. (1997), 'Alumina grit blasting parameters for surface preparation in the plasma spraying operation', *Journal of Thermal Spray Technology* **6**, 217–227.
- Muslimin, Muhamad, A. M., Triawan, F. & Nandiyanto, A. B. D. (2020), 'Surface characteristics of low carbon steel jis g3101 ss400 after sandblasting process by steel grit g25', *Journal of Engineering Research* .
- Sen, D., Chavan, N. M., Rao, D. S. & Sundararajan, G. (2010), 'Influence of grit blasting on the roughness and the bond strength of detonation sprayed coating', *Journal of Thermal Spray Technology* **19**, 805–815.
- Varacalle, D. J., Guillen, D. P., Deason, D. M., Rhodaberger, W. & Sampson, E. (2006), 'Effect of grit-blasting on substrate roughness and coating adhesion', *Journal of Thermal Spray Technology* **15**, 348–355.